Use of ultrasonic Rayleigh-Lamb waves to detect defects in metal and rubber composites

HONEY, THOMAS,JACK

Use of ultrasonic Rayleigh-Lamb waves to detect defects in metal and rubber composites

Thomas Jack Honey

Submitted in accordance with the requirements
for the degree of
Master of Science by Research

Department of Physics

Durham University

2019

CONTENTS

LIST OF FIGURES

LIST OF TABLES

STATEMENT OF COPYRIGHT

ACKNOWLEDGEMENTS

I would like to thank my supervisors Douglas Halliday and Paula Chadwick for their incredible support and guidance throughout the project, including soothing my panic in the last few months. I would also like to thank the Engineering and Electronics Workshop for their incredible work and success at meeting my (sometimes odd) requests.

I would like to extend my unending thanks to the entire Coltraco family, including Dr. Carl Hunter for their inspiring words and support, George Hunter and Daniel Dobrowolski for mainting my spirits, and Adrian Saw for maintaining my focus.

I would like to thank my family; my mam Ann, my brothers Bob, David, and Simon, and my sister Laura for their lifelong support of my journey into (among other things) academia. Finally, I would like to thank my undergraduate and postgraduate coffee buddy Ra'ad Mahmoud, my very patient partner Danielle Oliver for the love and tea that she has provided throughout this project, along with my irreplaceable friends Kai Shepherd, Kyle Mason, and Jacob Viles for joining me in regularly escaping to Eämbar in our D&D games.

"Shy bairns get nowt."

ABSTRACT

An investigation into the use of constant coupled ultrasonic non-modal Rayleigh-Lamb waveforms to detect defects within hatch seals was conducted to improve the current generation of ultrasonic leak detection devices.

An anechoic chamber was first constructed in order to isolate the emitted ultrasonic signal from the environment. The chamber walls reduced reflected 40 kHz signals emitted by ultrasonic transducers by 34.3 dB. Subsequently, an investigation was conducted into how effectively a varying hole size within metal plates, designed to mimic a non weather-tight seal, could be detected using 40 kHz ultrasonic signals. It was found that even at small distances from a hatch seal, using ultrasonic detection becomes unreliable. The decay rates of 40 kHz and 400 kHz ultrasonic signals were measured as they travelled through homogenous aluminium and steel plates in order to recommend a suitable number of emitters and receivers that would be required for consistent signal intensity. It was shown that 35 cm from the emitter, the signal did not decay significantly, suggesting that the maximum distance allowed between each subsequent receiver and emitter is greater than 35 cm. An investigation into how 40 kHz and 400 kHz ultrasonic waveforms traverse aluminium-rubber and steel-rubber non-adhered composites was then conducted and compared to composites with a varying number of air spacers present (which represent a non-defective and defective seal respectively). Although no statistically significant evidence showed that it is possible to distinguish between differing numbers of air spacers, it was established that a 400 kHz signal provides more consistent measurements than 40 kHz.

Finite element analysis (FEA) was conducted and compared to experimental results. In some cases, the analysis showed qualitative agreement with the findings. FEA was then used to guide preliminary experiments using artifically degraded rubber, showing strong indication that Rayleigh-Lamb waves could be used to measure the degradation of rubber within hatch seals.

1. INTRODUCTION

1.1 Context

Ultrasonics concerns sound waves of any frequencies higher than the range of human hearing [1]. These mechanical sound waves have a myriad of uses from industrial detection [2] to imaging used in medical diagnostics [3]. Ultrasonic detection is currently being used as a leak detection system within hatch seals on board ships, which offers advantages over the traditional method of chalk testing [4]. Chalk testing uses chalk to cover all points of compression on one edge of a hatch seal, which is then fully closed and reopened. As the hatch is closed, the chalked edge should imprint onto the corresponding edge of the hatch leading to an unbroken chalk mark across the unchalked edge. Any gaps in this would indicate a poor seal [4]. Chalk testing is favoured over more sophisticated methods of leak detection as no experienced or specialist operator is required to interpret measurements [4] (see ultrasonic detection below).

This project focusses on the analysis of detected ultrasonic waves attenuated within a physically simulated hatch seal to refine the current leak detection process. It is the intention to enhance the understanding of the underlying physics of ultrasonic defect detection using a current model developed by a leading provider of ultrasonic measurement devices; Coltraco. The results of this investigation will enable more reliable instruments to be developed which can detect leaks more accurately.

Coltraco, a world-leading developer of ultrasonic technologies for use on board seafaring vessels [5], provided a brief to investigate the possibility of using a permanent ultrasonic device to test whether hatches on seafaring vessels are weather- and water-tight, to replace their current Portascanner^{TM} instrument [6]. The Portascanner^{TM} is a watertight integrity testing device that emits ultrasonic signals at 40 kHz to be read by a receiver on the other side of a

sealed hatch or hold. This is currently achieved by placing the emitter inside a hold, 5 metres from an entrance or access hatch [7]. The device is turned on to emit the signal and the hatch is shut and secured. Although there is a range of hatch cover styles, the fundamental design element remains the same: a steel covering that sits on the hull opening. Between the cover and hull rests a rubber gasket that is compressed when the cover is secured (typically by dogs, as shown in Fig. 1.1, cleats (Fig. 1.2), or wingnuts (Fig. 1.3)). If the hold is properly secure, the ultrasonic signal will not escape the hold. However, in a defective seal, the signal may escape through any air gaps that are present, whether through fractures and wear in the materials, or improper resting of the rubber. The signal is not within the audible frequency range, but can be picked up by the receiver, which translates the signal into a decibel measurement and displays the digital result. The receiver detects audio frequencies at 40kHz only and therefore any readings registered notify the user that a leak is present at the entrance or access hatch.

Fig. 1.1: Dogs used to secure hatch cover in place. These would feature inside the hatch covering and, when closed into position, would be turned by hand. The curved square end (left most section of the handle on the figure) will be pivoted to lock into a protruding metal lip. After BenFrantzDale [8].

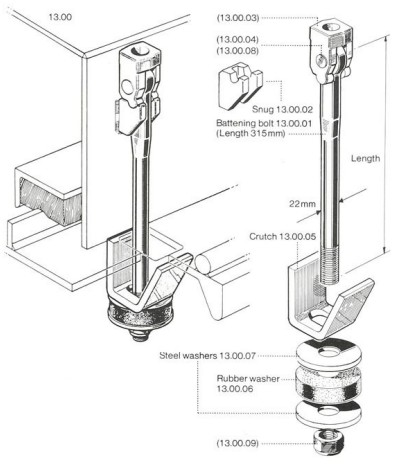

Fig. 1.2: Cleats (left to right) constructed, and deconstructed, use a screw to secure the hatch covering to the ship hull. A T-shape bar would be positioned inside a socket (shown at the top of the figure), and turned until secure. Whilst a rubber washer is compressed below the screw to ensure a good fit, this also occurs inside the hatch lining to ensure weather- and water-tightness. After Pacific Marine & Industrial [9].

Fig. 1.3: Wingnuts are similar to those seen in Fig. 1.2; these are hand tightened thumbscrews which attach to hinged threaded rods and lock onto the hook-like protrusions from the hatch covering. After Zhiyou Marine [10].

1.2 Aims and Objectives

Within the scope of this project, a discussion and investigation will be conducted into the feasibility of using a permanently fitted ultrasonic waveform emitting device and corresponding receiver to detect defects present within the hatch seal.

First, in Section 2.1, the importance of weather- and water-tightness in hatch covers on board ships is discussed as well as the current tightness tests that are conducted and their particular advantages or disadvantages. In Sections 2.2 and 2.3, the underlying physics of ultrasonic detection will be covered, including ultrasonic theory, and how an emitted ultrasonic waveform interacts with the environment and materials. This will then link to how the ultrasonic waveform traverses through a material using Rayleigh and Lamb Waves, in Section 2.4.

As the waveform is received, a review of current detection methodologies is covered in Section 2.5, before finally discussing noise and the filters and computations that can be utilised in order to obtain a more accurate signal in Section 2.6.

Second, in Section 3, an overview of the current generation of computer simulation software that can be utilised to both model an environment and qualitatively compare experimental data to theory will be given. This will lead to a demonstration of how a typical environment is computationally simulated in Section 3.2, before showing the process of simulating a simple 2D ultrasonic waveform in Section 3.3.

Third, based on the conclusions of the review in Section 2 of the investigation, appropriate experiments will be carried out. This will feature the construction and evaluation of a suitable echo-less chamber in Section 4.1, before investigating how a varying hole size within an aluminium plate can be detected using ultrasonic waveforms in Section 4.2. In Section 4.4, an experiment will be conducted to measure how an ultrasonic signal intensity decays with distance, providing an indication of the suitable number of emitters and receivers that are required over a given distance for consistent signal intensity. Finally, in Section 4.5, a metal-rubber layered composite will be created and defects will be introduced using air spacers simulating a non-defected and defected hatch seal. This will then undergo the proposed method of ultrasonic leak detection

to conclude whether a fixed ultrasonic system is able to detect defects within a hatch seal.

Fourth, using the COMSOL software discussed in Section 3, simulations of experimentations will be carried out and qualitatively compared in Section 4.6.

Fifth, once agreement has been established between experimental and simulated results, COMSOL simulations will be used to guide further experiments in Section 4.6.3, and these will be preliminarily carried out in Section 5.

In Section 6, these findings will be discussed and recommendations towards a permanent leak detection system will be given. In addition, possible further routes of investigation will be offered, and points of interest will be provided which were noted throughout experimentation and would improve the quality of data taken.

Finally, in Section 7, a summary of the work will be given and closing remarks on the investigation will be offered.

2. LITERATURE REVIEW

This chapter presents an overview of the current literature available, starting with the importance of ultrasonic detection within the context of the field, then covering the theory of ultrasonic sound waves and their interactions with materials. Finally, detection methodologies will be covered. Each section will include a review of the current literature and how this builds a framework for the final experimental process.

2.1 Importance of Hatch Security

The purpose of a hatch cover on board ships is to provide a barrier at any access points on board ship in order to prevent the passage of water into the interior of a ship [4]. As mentioned in Section 1.1, a secure hatch works as the rubber gasket is compressed between the cover and the hull. Over time the rubber gasket will deteriorate gradually. This can occur through repeated compression, damage from both sea water and the detritus that the water moves, ultraviolet (UV) radiation, and oxygen [11]. This deterioration appears as softening or hardening (depending on the structure of the rubber), cracking, or charring [11].

From 2005-2014, Protection and Indemnity Insurance (P&I) reported that leaking hatch covers accounted for 4.39% of the total number of claims for cargo damage, and 4.56% of the total payout of claims recorded at values between 5,000 and 3,000,000 (USD) [12]. Although not the primary cause of cargo damage, it still provides a substantial risk factor that can be greatly reduced through proper maintenance and thorough inspection. However, proper maintenance and thorough inspection are not considered a priority, and often done without consideration of established practices [13].

Whilst visual inspections of the hatch covers should always be advised in addition to any hatch cover test [13], in addition to chalk testing there are

currently two widely-used methods to detecting leaks within hatch seals: water hose and ultrasonic tests [4]. These two methods shall be described briefly below.

2.1.1 Water Hose Testing

Water hose testing is performed using a spray hose that simulates rainfall and assesses the ingress of water. To do this, the hatch is closed and a water jet placed outside of the ship directed towards the seal at a 45° angle (shown in Fig. 2.1). After a period of 3 minutes, the ingress of water below the hatch shall not exceed between 0.05 L and 0.5 L, depending on the weather conditions and degree of watertightness. The recommended degree of watertightness of the seal is a scale from 1 to 4 that is noted for the vessel type, design and hatch type [14], and is shown in Table 2.1.

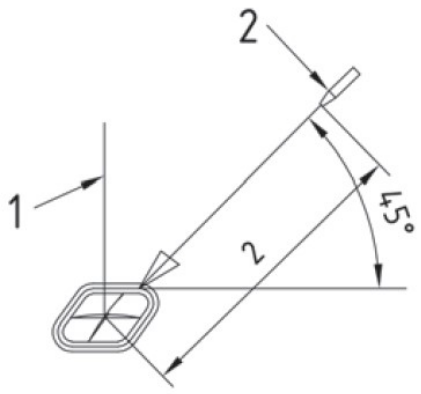

Fig. 2.1: Test arrangement for water hose testing. Note the nozzle (2) should be 45° from the horizontal, (1) shows the perpendicular. After British Standards [14].

Table 2.1: Minimum degree of watertightness required for hatches on board ship from 1 to 4 relating to increasing levels of watertightness. Each degree of watertightness has a separate experimental setup according to standards. The Type of Boat refers to the method of propulsion and hull type. Appliance location area is split into 4 areas; Area I is hull area above waterline, Area II is areas where those on board are likely to traverse, Area III includes areas not covered by Areas I and II, and Area IV refers to parts of Area III "protected from the direct impact of sea or slamming waves" [14]. Note that areas below the waterline are not covered by this standard. Table borrowed from BSI Standards [14].

Type of Boat	**Appliance location Area**	**Type of Appliance**	**Design Category**			
			A	**B**	**C**	**D**
Any	Area I	Any	2	2	2	2
Any	Area II	Any	2	2	3	4
Any	Area II	Sliding companionway hatch	3	3	3	4
Any	Area III	Any	3	3	3	4
Sailing monohull	Area IV	Any	3	3	3	4
Motor and Multihull	Area IV	Any	3	3	4	4

For example, for a degree of weathertightness 4, heavy rain will be simulated and assessed with the requirement that there should be an ingress of water no greater than 0.5 L. Rainfall is typically measured over a metre square sample size with the total being expressed as a depth in mm. Should it be assumed that all water from heavy rainfall is incident on the hatch, this would imply that the total amount of rainfall in 3 minutes, using the definition of heavy rainfall as being 4 mm per hour [15], would be 0.2 mm. Substituting $h = 0.2$ mm into

$$r = \sqrt{\frac{V}{\pi\sqrt{2gh}A}}, \tag{2.1}$$

where V is the total volume, r is the radius of the hole, g is the acceleration due to gravity, taken as 9.81 m·s^2, and A is a constant that translates litres per second to total volume in 3 minutes, which is equal to 180,000. The ship hatch would therefore be considered watertight should the cumulative area of any number of holes not exceed an area of 0.05 mm^2. Similarly, for a weathertightness degree of 2, there would be a flow of at least 10 L/min for 3 minutes and the ingress of water should not exceed 0.05 L. From above, this would equal a rainfall, h, of 130 mm and therefore, from Equation 2.1, a cumulative area of any number of holes not exceeding $2{\cdot}10^{-4}$ mm^2 would be considered watertight.

Clearly, depending on the degree of weathertightness required, the allowable ingress of water and associated hole size varies greatly.

2.1.2 Ultrasonic Testing

Ultrasonic testing is performed using an emitter and receiver which measure the output sound level in decibels (dB) and are calibrated to a certain frequency within the ultrasonic range [16]. Although there is no specific frequency noted in the guidance [16], the sound levels recorded from a closed hatch should be measured in dB and may also be compared to a percentage of the Open Hatch Value (OHV). The OHV is the sound level measured (in dB) at the receiver from the emitter when the hatch is fully open [17]. A received sound level of between 1 dB and 10% of the measured OHV is considered a weathertight hatch; above this would be considered not weather- or water-tight [16]. For example, for an OHV of 40 dB, a hatch would be considered weathertight for a sound level measured between 1 and 4 dB.

This is not directly comparable to the standards discussed in Section 2.1.1, as a watertight hatch would allow less ingress of water than a weathertight one. For example, an Open Hatch Value of 30 L (100%) in ultrasonic testing would be considered a degree of watertightness 3 in water hose testing. Therefore, should 10% of this value ingress the hatch (the maximum allowed value to still be considered weathertight), this would imply a total ingress of 3 L; far greater than 0.05 L found in water hose testing. Whilst this may be a reflection of watertightness decaying into weathertightness, this same process cannot be applied at 1dB as this is a constant.

No further guidance on the manufacturing standards is given for an ultrasonic testing device, aside from being approved by the Det Norske Veritas Society [16].

2.1.3 Comparison of testing methods

Firstly, it is noted that ultrasonic testing offers an easier operation and interpretation of results than water hose testing as the leak measurement is given as a percentage of OHV, rather than a volume for a given flow rate and a given degree of watertightness. In addition, ultrasonic hatch testing can be performed when holds are loaded. This offers advantages over water hose testing which could cause cargo damage should ingress of water occur [4]. This advantage means that ultrasonic testing can also be done during transit and offers a much shorter required time to operate, giving results immediately should a leak be present [17].

However, due to the limitations of the manufacturing standards, it may be considered that the water hose test is a more consistent method of testing hatch tightness. It is not within the scope of this investigation to define such standards of manufacture or testing, but instead, from experimentation, to make recommendations for the parameters of ultrasonic testing.

Using the information from Section 2.1.1, there is an allowable total gap size which, when using ultrasonic testing, could be factored into any measurements (i.e. a cumulative gap size of 0.2 mm, which is allowable for a degree of weathertightness 4, will have an associated dB measurement in an ultrasonic test. Any dB measurement below this would therefore be an acceptable degree

of weathertightness).

Similarly, from Section 2.1.2, extending the principle from Section 2.1.2 that an OHV would be 100% of the intensity, a fully sealed hatch (i.e. weathertight) would have a value (as a percentage of the OHV) of 0%. This is often not the case, as intensity measurements have been noted for an otherwise weathertight seal (A. Saw, personal communication, April 2019).

2.2 Ultrasound Theory

A mechanical sound wave of a frequency equal to or greater than 20 kHz resides in the ultrasonic range (hereafter, such a sound wave will be referred to as an ultrasonic signal) [19, 20]. Classically these have been generated using a piezoelectric crystalline structure that oscillate at one of their natural frequencies when an alternating current is applied across their axes [19]. In their infancy, these were produced using quartz and Rochelle Salt [19, 21], although in the modern era these crystalline structures take on a more diverse range, such as synthetic crystalline structures and piezoelectric ceramics [21].

2.3 Propagation of waves through media

As ultrasonic signals travel through a given material they are attenuated by it. This will lead to an exponential decay of the form

$$I = I_0 e^{-\alpha z}, \tag{2.2}$$

where I_0 and I are the original intensity and intensity at a distance z respectively, and α is the attenuation coefficient, assuming the material is homogenous. The attenuation coefficient is dependent on both the properties and phase of the material. For example, in a fluid, the attenuation coefficient is defined by the viscosity, thermal conductivity, molecular weight, molar specific heat at constant volume, and the ratio of specific heat at constant pressure to that at constant volume [22]. In solids, the attenuation coefficient of a waveform is related to the logarithmic decrement, given by δ , defined as:

$$\delta = \alpha z, \tag{2.3}$$

where z is the total length of the material.

Further, attenuation in a solid is an umbrella term used for *scattering* and *true absorption*. Scattering of a wave occurs due to inhomogeneity of the material; at boundaries between often differently orientated grains, the abrupt change can cause the wave to scatter at angles to the plane [23]. This effect is more pronounced when these grains are of different materials such as alloys where the material properties (such as densities) are also distinct [23].

True absorption removes energy from the wave by creating various excited states (e.g optical or electrical). For ultrasound, as the wave is incident on the material, the energy is transferred to the lattice structure, causing the lattice to vibrate and deform due to the force of the wave. This wave travels through the material as a quantised excitation of lattice vibrational energy (known as phonons), which excite electrons from their equilibrium state within the Fermi surface (the surface that separates electron space from unoccupied lattice space) to pre-defined energy levels. The excess energy (i.e. energy insufficient to excite an electron to the subsequent energy level) is converted into heat [24].

Metals have further complications, where the magnetism [22], cast structure [23], and how the structure is worked [23] all contribute to the way in which the mechanical wave is attenuated. Ultrasonic waves travelling through a material subject to a magnetic field have higher attenuation when compared to an absence of the magnetic field [24]. If molten metal is poured into a mould, this would be considered "as-cast", which has shown to prevent ultrasonic penetration at small thicknesses, however after being "worked" (e.g. rolled), ultrasonic penetration becomes far easier [23]. Attenuation also occurs through dislocations within the crystal structure and impurity within the metal, causing strain as waveform stresses are applied [25]. Although dislocations have been noted from kHz frequencies and above, these dislocations are suggested to contribute to hysteretic losses which disappear at higher frequencies where the stress of a signal occurs too quickly to cause a response from the dislocation [1]. Hysteretic losses here refer to the stress-strain curve that takes the form a hysteresis loop, the area of this giving the energy absorbed per half-cycle [1].

Returning to Eqn 2.2, an exponentially decaying curve will rapidly decay over relatively short distances, and sufficiently low amplitudes of ultrasound would

be unable to traverse the material, decaying before reaching the receiver. To counteract that, the initial amplitude, I_0 could obviously be increased. However the material is also affected by the ultrasonic wave, which causes non-elastic deformation. Indeed, it has been shown that both low [26] and high [1] amplitudes cause plastic deformation in the structure of a material. For ultrasonic waves at high enough energies (when the stress and resultant strain relationship is no longer linear [1]), plastic deformation will occur within the structure with each cycle, eventually causing breakages [1], whereas low amplitude waves will fatigue the material through hardening and softening (see Section 2.1 on changes in rubber) [26]. The fatigue life of a material is measured by the number of repeated loading cycles before breakage occurs provided that the load is above a threshold that will cause deformation in the material. For example copper has a fatigue life of $1{\cdot}10^8$ cycles with a threshold load of 24 ksi [27], whereas steel has a fatigue life of $5{\cdot}10^8$ cycles with a threshold load of 70 ksi [28], therefore steel is able to withstand an infinite number of cycles at 24 ksi.

Further, at amplitudes between these extremes, both fatigue and cracking has been shown over prolonged exposure to ultrasonic stresses [29]. Whilst all amplitudes will cause stresses and strains to a material, lower amplitudes appear to cause less damage than the higher ranges.

2.3.1 Discussion

It is noted that the effects of metals in particular are difficult to accurately predict as many indeterminate variables can have varying effects [23]. For example, the pore volume within a structure increases in proportion to the structure's specific gravity which, for cast copper, is between 8.3 and 8.9, but increases to between 8.9 and 9.0 if the copper is hammered [23]. Similarly, the Vickers Hardness Value (HV) was found to gradually increase in stainless steel when cold rolled (i.e. compressed between two rollers) from 188 to 419 HV with successive passes through the rollers [30]. This variation in structure discussed would imply that each hatch and seal should be considered as a unique system. It is therefore necessary to establish benchmark parameters for each hatch, deviations from which indicating degradation of hatch seal integrity.

It has been shown that all amplitudes of ultrasound have caused long-term

degradation on the measured material, but nonetheless the amplitude should be at least sufficient to fully penetrate any measured material. Regarding the frequencies of the ultrasound, as there is evidence that attenuation losses occur through various process, as discussed, and that sufficiently high frequency could reduce this, two high frequency signals shall be used to see if any conclusions can be quantitatively drawn to confirm this effect.

2.4 Rayleigh and Lamb Waves

As discussed previously, as the ultrasonic signal travels through a medium, it undergoes attenuation. Similarly, losses can occur at boundaries between media (e.g. between gases and solid), where the waveform is partially reflected back into the first, and refracted into the second. Whilst ultrasonic signals obey the same physical laws governing other mechanical waves, they do change their mode of propagation [31]. Below, the concepts of how the wave undergoes change in media are discussed as well as the practical utility of waveforms when used to assess hatch integrity.

2.4.1 Rayleigh Waves

First discussed theoretically in 1885, Rayleigh waves, their names taken from the discoverer Lord Rayleigh, are analogous to deep-water waves [32]. They are defined as waves that travel across the surface of a plate or plane boundary [33]. Taking a mechanical wave propagating from the origin (Fig. 2.2), the waves will travel outwards in a combination of two modes; longitudinal waves displacing in the same direction of wave propagation, denoted by ϕ, and transverse waves displacing perpendicular to the direction of wave propagation, denoted by ψ, as given by the equations:

$$\phi = -Ae^{i(kx-\omega t)-qz}, \tag{2.4}$$

$$\psi = iA\frac{2kq}{k^2+s^2}e^{i(kx-\omega t)-sz}. \tag{2.5}$$

Here, A is an arbitrary amplitude constant, ω is the angular frequency, $q^2 = k^2 - {k_l}^2$, $s^2 = k^2 - {k_t}^2$, and k, is the wave number, with k_l and k_t the

wave numbers for longitudinal and transverse waveforms respectively [34]. For highly symmetric crystal systems, the modulus of longitudinal and transverse waveforms will be equal, however refer to different directional waveforms. The material undergoes displacements and stresses as a result along the path of the waveform, which travels radially from the point of penetration at a velocity and depth from the surface that is dependent on the properties of the material, in this case, Poisson's Ratio, ν:

$$\nu = -\frac{\epsilon_{transverse}}{\epsilon_{longitudinal}}, \tag{2.6}$$

where the strain, $\epsilon = \frac{\Delta L}{L}$, and L is the length of material under strain in the corresponding orientation. As the Rayleigh wave travels through the material, energy is absorbed and scattered through the surface leading to a decay in amplitude of the wave, and is proportional to $\frac{1}{R^2}$ [34], where R is the distance from the source.

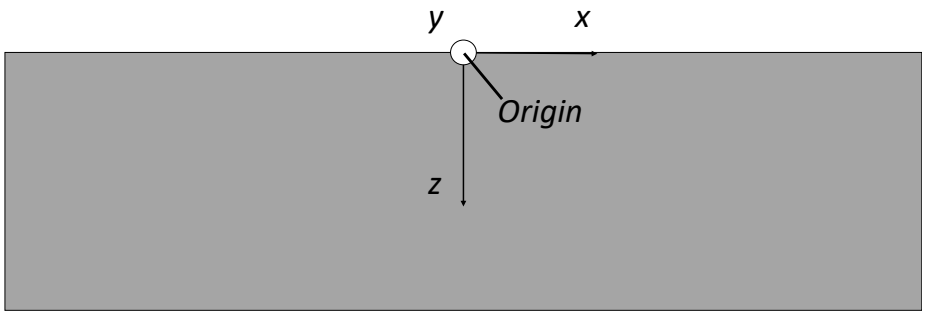

Fig. 2.2: Half Space Boundary between the material (grey) and space. Here the origin is at the centre (0 on all axes), with the waveforms travelling radially in the x and y direction. Note that the y-axis is orientated pointing out of the page. After Viktorov [34]

2.4.2 Lamb Waves

As the thickness of a material increases perpendicular to the incident surface, Rayleigh Waves will become Lamb Waves [23], which are surface phenomena that occur both in the direction of, and perpendicular to wave propogation [34]. These were first discussed in 1917 when Horace Lamb further examined vibrational waves within a material in response to the growing number of questions arising through seisomological studies [35]. If a mechanical wave travels across a plate of thickness $2d$ (across the x direction in Fig. 2.3), as in Rayleigh Waves, there are two characteristic wave equations for the longitudinal, ϕ, and transverse, ψ, waves, given by

$$\phi = A_s \cosh(qz) e^{i(kx-\omega t)} + B_a \sinh(qz) e^{i(kx-\omega t)}, \tag{2.7}$$

$$\psi = D_s \sinh(sz) e^{i(kx-\omega t)}) + C_a \cosh(sz) e^{i(kx-\omega t)}, \tag{2.8}$$

where A_s, B_a, C_a, and D_s are arbitrary constants, k is the Lamb wave number, x and z are the respective axes, $q = \sqrt{k^2 - k_l^2}$, $s = \sqrt{k^2 - k_t^2}$ where k_l and k_t are the transverse and longitudinal wave numbers respectively [34].

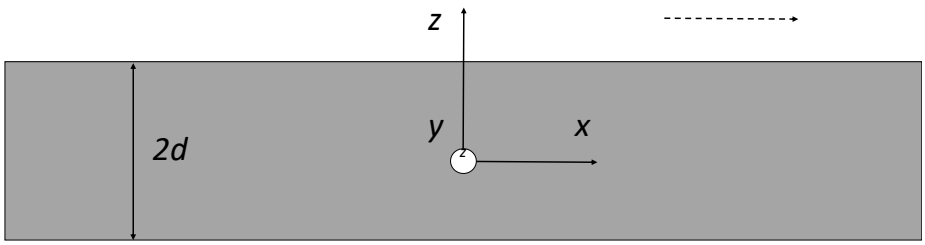

Fig. 2.3: A layer of material of width $2d$, where the direction of propagation for a mechanical wave is shown as the dashed line (x direction). Note that the y-axis is orientated out of the page. After Viktorov [34].

The combination of longitudinal and transverse waveforms leads to two characteristic equations for symmetric and anti-symmetric modes (given by Eqn. 2.9 and 2.10 and respectively)

$$\frac{\tan(\frac{qd}{2})}{\tan(\frac{pd}{2})} = \frac{-4k^2pq}{(q^2-k^2)^2}, \tag{2.9}$$

$$\frac{\tan(\frac{qd}{2})}{\tan(\frac{pd}{2})} = \frac{-(q^2-k^2)^2}{4k^2pq}, \tag{2.10}$$

where $p^2 = (\frac{\omega^2}{k_l} - k^2)$, and $q^2 = (\frac{\omega^2}{k_t} - k^2)$ [36]. These modes are dependent on the wavelength, λ, of the source, and have been utilised in high ultrasonic frequency Non-Destructive Testing (NDT), of 1 MHz or higher [37].

To characterise Lamb Waves, it is important to know the phase velocity of the wave, $v_p = \frac{\omega}{k}$, which can be used to determine the wave number, and calculate stresses and displacements throughout the plate. In cases where a pulse is used, this would create a wave packet with multiple frequency components, therefore the group velocity should be considered when calculating frequency, given by $v_g = \frac{d\omega}{dk}$.

2.4.3 Rayleigh and Lamb waves in defect detection

Both penetrative waveforms have diverse applications within the emerging technologies of ultrasonics. For example, Rayleigh waves undergo perturbations, which can be measured and analysed to identify defects within the surface of a structure, and are regularly used in the field of seismology [38]. However, as the measured material becomes more complex (e.g. an anisotropic, inhomogenous one), Rayleigh waves are generally considered to have little practical use at the ultrasonic frequency range [34].

Like Rayleigh waves, Lamb waves are used in ultrasonic flaw detection to measure the elastic and thermoelastic characteristics of sheet samples [34]. The classical generation and subsequent detection of such waves has been discussed at length, for example the wedge method [34, 39] or water coupling [2, 37]; however novel techniques are being utilised using laser-generated Lamb Waves to achieve higher degrees of accuracy in flaw detection [40, 41]. For example, an

investigation into laser-generated Lamb Waves by Kim et al. found that defects as small as 0.3 mm in diameter were detectable, as opposed to the conventional defect detection which was unable to find defects smaller than 1 mm in diameter [41].

The current well-investigated method of Lamb wave generation and detection utilises symmetric and anti-symmetric modes as discussed in Section 2.4.2. Whilst both modes offer sufficient defect detection [42], it was later argued that both are not equally sensitive to defects, and that symmetric Lamb waves measure centrally located defects (i.e. defects located approximately equidistant from the incident and opposite surface) with greater precision [37]. At higher modes, the wave becomes a more complex problem to solve [34], however they have been noted to be more sensitive to defects [37]. The versatility of defect detection using Lamb waves is well documented [43, 44] in both continuous and pulsed [45] waveforms, which are capable of travelling over greater distances than conventional ultrasonic testing [46], and through small gaps between plates [39].

2.4.4 Discussion

Ultrasonic Rayleigh and Lamb waves have been shown to have varying sensitivity to defect detection, dependent on coupling type, frequency, and in the case of Lamb waves, mode. The suggested increasing sensitivity at higher frequencies [46] has led to the investigation in this project of two different frequencies in the ultrasonic range, 40 kHz and 400 kHz, in order to quantitatively and qualitatively analyse the efficacy of changing frequencies for detecting defects.

Whilst Lamb wave modes offer greater accuracy than conventional ultrasonic testing, these use comparatively thin plates of known thickness, where a hatch is a thicker, multi-layered composite structure that is particularly varied. As at greater thicknesses Rayleigh waves will become Lamb waves, an ultrasonic wave at normal transmission (i.e. zero order modes, hereafter referred to as non-modal) will be measured through composite plates of mimicking a hatch cross section with and without defects and will be referred to as Rayleigh-Lamb waves (Section 4.5). Due to the shorter distances covered by non-modal ultrasonic waves, additional transducers should be used and these signals will

therefore be parameterised in order to advise on suitable number of transducers for a given distance (Section 4.4).

2.5 Detection Methodologies and Post-Processing

Each mechanical wave that travels through a material holds valuable information regarding the internal structure, such as attenuation coefficients and material thickness, that can be calculated. Comparative studies can always draw further conclusions regarding the change in structure between the different points in time in which they were measured. The more common detection methods will be discussed as well as their advantages and limitations both within and without the scope of the project. In addition, the ways in which the received signal can be interpreted will also be covered.

2.5.1 The Pulse-Echo Method

The pulse-echo method uses an ultrasonic pulse that traverses the material structure, reflecting off any defect present [1]. Depending on the specimen, these may have rear boundary walls where the return signal will be unimpeded (aside from the natural attenuation due to the material). A defect can be located by summing over multiple point sources and analysing the scatter from each defect [47].

This offers advantages where access to the measured structure is only available from one side, for example pipes or panels [48]. However, defects may be overlooked should smaller defects become hidden in the "shadow" of a larger one [1]. Complications may also arise as scattered waveforms that are reflected back may bury the intended echo within the "noise" of the signal (see "Noise" in Section 2.6) [23], hence multiple measurement points are necessary.

2.5.2 The Transit-Time Method

This methodology uses a pulsed ultrasonic signal across a material, and measures the time intervals between two markers: the original pulse, and the far boundary wall echo [23]. These find their uses in non-invasively measuring wall thickness [23], and flow rates within pipelines [49]. However, should an initial

measurement be made for a boundary wall, any changes in subsequent measurements could highlight defects or flaws within a structure.

2.5.3 The Shadow Method

The shadow method (or intensity-measurement) uses a transmitter and receiver placed on the specimen in-line and face-to-face with one another. Intensity measurements are taken across the length of the specimen and compared. Should a defect be present, it will attenuate the ultrasonic signal and therefore the received intensity will be lower [23]. These are useful as they monitor the intensity changed within a specimen, and have found increasing accuracy with increasing frequency (below 1 MHz) [50].

Similarly to the pulse-echo method mentioned in Section. 2.5.1, complications could arise from smaller defects within the transmitter-receiver line of sight, overlooking additional defects within the system. This method also requires access to the entire boundary of the specimen which could present further issues in restricted spaces.

2.5.4 Post-Processing: Fast Fourier Transformations

It is well established that the received waveform has additional information stored within the frequency spectrum. When utilising Lamb waves in particular, due to their dispersive nature [51], Fourier Transforms (and the particular algorithms to calculate Fourier Transforms known as Fast Fourier Transforms; FFT) are used to convert the received signal into a magnitude-frequency spectrum [44, 46], which has shown excellent agreement with finite element analysis of a simulated specimen [52] (see Section 3 for further information on finite element analysis).

To calculate a FFT, for a signal received at $x = 0$, the function $f(0,t)$, where t is time, the function in the Fourier domain would be

$$f(0,\omega) = \int_{-\infty}^{+\infty} f(0,t)e^{-i\omega t}dt, \tag{2.11}$$

where ω is the angular frequency [51]. The output is a frequency spectrum, and is widely used in other areas of study involving frequency measurements.

2.5.5 Discussion

In the context of multi-layered composite defect detection, algorithms have been written that account for reflection from layer boundaries to a high level of accuracy [48], and defect detection can also be assessed through guided waves [47]. However at the boundaries between layers, a form of bonding occurs (e.g. adhesive layer between two plates, or a paint layer atop a plate), therefore this approach has not been found to be currently studied on non-adhered composite layers. Although all detection methodologies mentioned are viable options, each comes with practical advantages and disadvantages which need to be considered on a case by case basis. Within the project, a direct plane emitter to receiver waveform as used for the Shadow Method in Section. 2.5.3 will be used.

In addition, where appropriate, a FFT will be conducted on the received signal, as it has provided high degrees of accuracy in previous experiments. Although these are used for received modal Lamb wave signals, the principle can be used for non-modal Lamb waves, with the compromise of a lower detection area [52]

2.6 Noise

It is well established that "noise" can greatly affect or "corrupt" sound measurements [53, 54, 55]. After the ultrasonic signal is incident upon the receiver (regardless of the methodologies used as outlined in Section 2.5), the signal can be affected by noise; a term used to describe any factor which distorts the desired signal. Here, the "desired signal" would be the signal received along the straight line path from source to receiver. Incoherent noise can be caused by mechanical or electrical waves present in the environment, from low frequencies such as the 50 Hz hum emitted from electrical applicances or bird song, to high frequencies emitted from fluorescent lights and monitors. Noise can also come about through echoes of the desired signal that reflect from chamber walls resulting in interference, referred to as "coherent noise". Noise does not come from just the environment, but also from the output of the desired signal as no function generator outputs a perfect signal; this can also be true for transducers, which could corrupt both the emitted and received signals.

The limitations of an inherently flawed receiver and emitter appear universally, with some of greater quality of manufacture than others. Noise from interactions with the receiver can be reduced through methods discussed in Section 2.7, but the quality of manufacture is a priority over noise reduction techniques.

2.7 Noise Cancellation

Due to problems caused by noise discussed in Section 2.6, techniques need to be considered both internally by a measurement device and externally by altering the environment in which the device is situated. Both of these reduce the noise from external incident signals.

2.7.1 Anechoic Chambers

Whilst practical limitations may prevent the removal of all external sources of noise an isolating environment, or chamber, can be introduced in which both the emitter and receiver are enclosed, free from external sources. Anechoic (free from echo) materials have the property of absorbing incident mechanical waves and all internal surfaces of the chamber should be lined with this suitably sound absorbent material [54]. The chamber should also be sufficiently large to ensure that the ratio of energy density of reflected sound, E_R, to direct sound, E_D, is kept to a minimum [54].

Although standards have been published regarding the absorbative properties of sound, this does not extend into the ultrasonic frequency range [53], typically not exceeding 6 kHz. This is important, as absorption coefficients are dependent on frequency (see Fig. 2.4 for an example absorbative material). Garner III et. al [56] constructed and evaluated an anechoic chamber for ultrasonic acoustics, and showed that a chamber could be made from thick layers of acoustically absorbent high-density material that reduced the acoustic intensity by 100 dB for insertion loss [56], IL, given by;

$$IL = 10\log_{10}(\frac{P_o}{P_i}), \tag{2.12}$$

where P_o is the measured power of acoustic signal reflected from a chamber

wall, and P_i is the initial power of the acoustic signal.

Further, Anderson suggests that higher frequencies are easier to absorb than lower and audible frequencies due to their comparatively small wavelength (B. E. Anderson, personal communication, 03 November 2017).

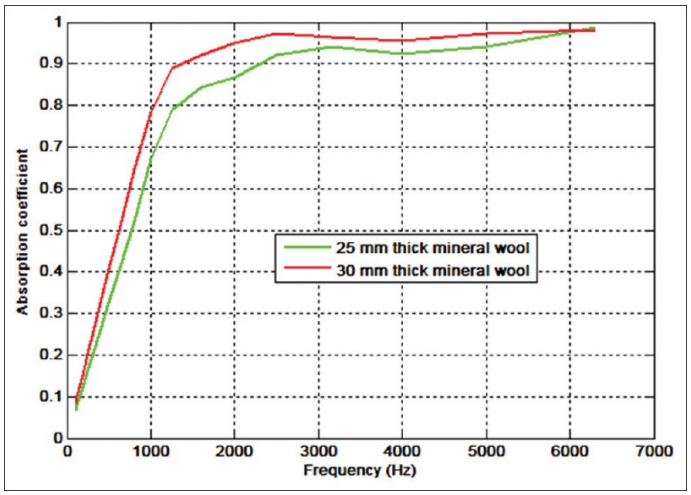

Fig. 2.4: Absorption coefficient of 25 and 30 mm mineral wool. After Forouharmajd [57].

2.7.2 Signal Processing

When it is not possible to alter the environment when measuring a signal, techniques must instead be incorporated to alter the incoming signal. Although there is a wealth of literature on the subject of filters and signal processing techniques [58, 59], suitable techniques for use on board ships are detailed below.

2.7.2.1 Phase-Locking

Phase-locking synchronizes an oscillator with a secondary input signal (known as the "reference") so that a single frequency is output [60]. Practically, an output signal from a Voltage Controlled Oscillator (VCO in Fig. 2.5) is used when an ultrasonic measurement is taken. This output is also fed separately into a phase detector. This phase detector is receiving an input from a static reference frequency ("reference frequency" in Fig. 2.5). These VCO and reference signals

may not be the same frequency[1], and will likely be out of phase with each other. This difference in phase is transferred to the loop filter, which changes the input voltage to the VCO. When it cannot reduce the error any further (i.e. Error Voltage in Fig. 2.5 is equal to 0) the loop is locked [61].

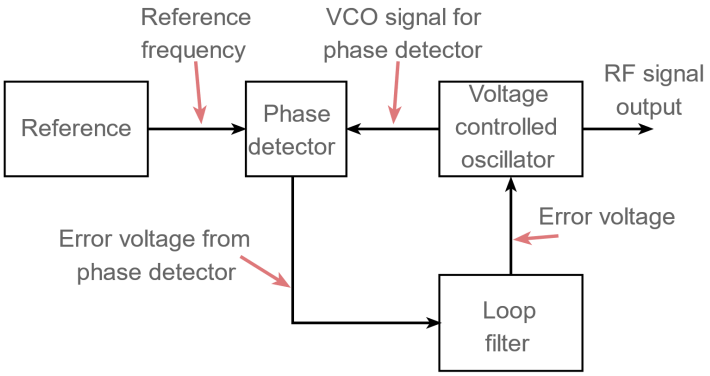

Fig. 2.5: A generic Phase-Lock block diagram, where the VCO is shifted in phase equal to the error detected by the phase detector. After Electronics Notes [61].

A phase-lock circuit incorporated into the Portascanner^{TM} device will not only provide a consistent signal, but also improve the accuracy of the output signal by reducing the noise in the system and decreasing the frequency error [60, 61]. However, due to the time constraints within the scope of this investigation, phase-locking has not been used.

2.7.2.2 Adaptive Filters

Typical filter units remove explicit frequency bandwidths, depending on the input boundary conditions. For example, high-pass filters (and their counterpart low-pass filters), remove all frequency components below (or above) a predetermined value [62]. Each design of filter has certain practical functionality; as an example, comb filters are able to discriminate between a repeated pulse and background continuous noise and are particularly useful when tracking passing objects such as aircraft [62].

[1] When the VCO and reference frequencies are not equal, it is found that the phase difference will not be consistent, and will always be at some point out of phase [61].

Whilst filters such as the above could be incorporated into an ultrasonic measurement device to reduce noise, the limitations of these systems become apparent should one consider attempting to discriminate a desired variable signal from variable noise. Variable filtration units, known broadly as adaptive filters should therefore be incorporated. Adaptive filters take an initial signal (*s(n)* in Fig. 2.6) which is filtered based on a secondary input (*y(n)* in Fig. 2.6). The summing tool then feeds back into the system and changes the filter accordingly to reduce the error output of the system [59].

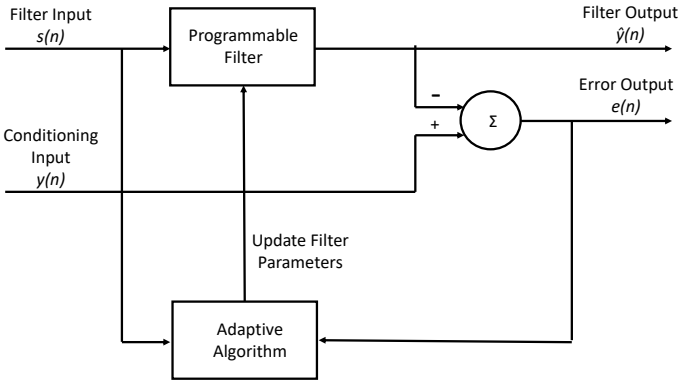

Fig. 2.6: A standard adaptive filter block diagram, where the input signal, *s(n)* undergoes a weighted filter based on a secondary input, *y(n)*. After Cowan and Grant [59].

This method of adaptive filtration can be applied whenever a suitable reference input is available [55], which requires little to no a priori knowledge of the desired signal [55, 59]. These offer advantages over fixed filters when the input signal or surrounding noise fluctuates [55]. Adaptive filters have seen more medical applications such as discriminating between a mother's heart beat and the fetal heart beat [55] and are also used in telecommunications [59]. With the variable noise present on board ships (for example, the noise caused by the vibrations of ship engines, or of footfall near the measurement location), adaptive filters would offer excellent reduction of noise on the measured signal.

2.7.3 Discussion

Fixed filtration units are still a viable form of signal processing; for example window functions have been employed in NDT for data discrimination [43] and damage detection [63]; however adaptive filtration offers a more robust approach as it can be used within an acoustically varied environment.

Signal processing techniques should be used in measurement devices where practical considerations allow (e.g. the addition of filtration units could conflict with the constraints of the overall dimensions of a measurement device). Within the scope of this investigation, filtration systems will not be used as the intention is to assess the full spectrum of the received signal, however as multiple measurements will be taken and averaged, this will reduce incoherent noise present. An environment will be created in such a way as to reduce echoes (see Section 4.1) and numerical and statistical analysis (e.g. FFT in Section 2.5.4) will be performed where appropriate.

2.8 Summary

From the review of the current literature on the focus of the investigation the importance of hatch security on board ships was established in Section 2.1, and of the two weather-tightness tests that are used, ultrasonic testing offers the greatest versatility, but has few standards. Therefore, as the investigation follows a novel approach to ultrasonic testing, a combination of both standards has been utilised here.

In Section 2.2, the underlying physics of ultrasound, and its interaction with the environment was discussed, noting in particular the varied interaction with differently worked or produced metallic structures. This theory moved onto how the ultrasonic waveform traverses through a material using Rayleigh and Lamb Waves, in Section 2.4. It was found that Rayleigh waves have their purpose within seismic investigations, where Lamb waves have been used predominantly in NDT. Whilst modal Lamb waves have been found to measure defects within materials to a greater accuracy, the a priori knowledge required to detect defects is unsuitable for weathertightness tests. Therefore a non-modal Rayleigh-Lamb waveform will be emitted entirely through a solid with and without defects in

an attempt to detect defective specimens.

Finally, in Sections 2.5 and 2.6, the detection of incoming signals and reduction of unwanted signals (noise) was covered. As the investigation is a proof of concept piece, signal processing was covered but unused, instead modifying the environment of the system through the construction of an anechoic chamber to reduce noise through external sources or reflected source signal. Signals will be emitted and obtained through air first within and then outside of the chamber in order to quantify the reduction of noise within the chamber.

3. COMPUTATIONAL ANALYSIS

To compare experimental results to theory, computational modelling is used and validated by experimentation, which is subsequently used to guide future work.

3.1 Finite Element Analysis

Finite Element Analysis (FEA) is a series of calculations that simulate a physical system. FEA first breaks the physical system into a series of connected shapes. These elements collectively are referred to as the "mesh". A numerical approximation of the system (e.g. stress and strain on a physical system) is then derived from the mesh in response to a given parameter (e.g. force applied), which is then used to analyse specific results in relation to the physical experiment. An example of when FEA is used is calculating surface deformations as a result of force applied, or thermal buckling as a result of an increase in temperature [64].

Classically the displacement method (i.e. determining stresses and strains in response to applied forces) is used to establish a series of equations for nodal displacements (i.e. determining stresses and strains at each intersection of the mesh). These equations are then solved using initial conditions and, using the solutions, other quantities of the system can be calculated (e.g. curvature, slopes etc.) [65].

As an example, for a displacement to a two dimensional system, the system would be split into a series of square elements, joined at nodes, each with displacement, rotation, and stiffness matrices [65]; this series of elements forms the mesh (see Fig. 3.1). To solve this, the stiffness matrix is first derived, and the displacements experienced at these nodes are calculated for the forces applied [65]. These stiffness matrices are then applied to the elements before adding boundary conditions [65]. This allows the solution of the equations, and the

subsequent calculation of stresses, bending moments etc. [65]. The equations become more complex to solve in higher dimensions and require the use of triangular elements as opposed to square elements as the mesh allows the modelling of irregular shapes more easily; however, the principle remains the same [65]. These elements can be of any dimensions, however care must be taken as, whilst smaller elements lead to a more refined analysis, this would come at the cost of larger computational timescales.

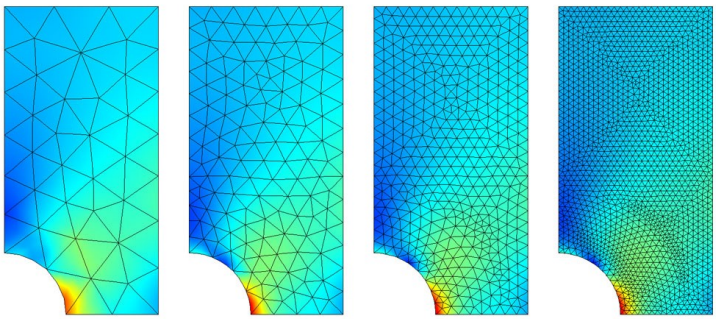

Fig. 3.1: An example of a 2D mesh for a geometry from (Left to Right) largest ("coarse") to smallest ("fine") element size. After COMSOL [66].

FEA has found many applications in modelling the static, dynamic, and modal responses of aerospace and civil engineering [67]. With the increase in efficiency of computational processes, the applications grow more diverse with the complexity of calculations required.

A FEA platform developed by COMSOL, COMSOL Multiphysics [68], is a software package which allows for a comprehensive toolset for analysing a physical problem [69]. Although there are a number of different applications, or modules (for example, electromagnetics, fluid flow, and heat transfer), the acoustics module will be the focus of this study.

3.2 Simulating an environment

Firstly, when creating the initial environment, dimensions of the simulation must be chosen, followed by the desired area of study (although additional studies may be added throughout the simulation). The parameters of the analysis (or simulation) are then defined; these can be referenceable variables that can be changed in one instance without repetition. For example, the initial acceleration of a plane wave could be defined as A, then, within the parameters, A could be given a quantity, for example -20 m/s^2. After the simulation has been completed, the initial acceleration may change, and having the parameter A in place is both efficient and less prone to being overlooked in later studies.

Next the geometry of the system in which the physical study will be tested is defined. These begin as simple shapes, but more complex geometries may be created to suit the intended purpose with the following operations:

- Extrude: expanding a 2D object into a third axis creating a 3D object,
- Revolve: to extrude an object about an axis, and
- Sweep: to extrude an object into 3D space using a user-defined path [70].

Each geometry can be built separately or grouped together (to create more complex shapes), after which these geometries are defined as "components".

Next, the materials of the simulation are defined which can be added to components separated by application area (e.g. liquids and gases, or nonlinear magnetic materials). Each component has parameters such as density, and conductivity, that are used in calculations. Many materials will be applicable to various studies and will therefore possess numerous parameters within the software's built-in materials. For example, air has electrical conductivity for electromagnetic studies, but also heat capacity at constant pressure for use with fluid flow and heat transfer studies. Each material has associated definitions that would typically be seen in real world materials, such as permittivity and density, with some broader material classes prompting user input (for example, although different types of aluminium are featured, some aluminium materials prompt the user to input the speed of sound within the material which is reflective of the many variations of aluminium available). When a simulation is performed, the

calculations used draw these constants from the tested material. In addition to the built-in materials, the user is also able to create a material by inputting any number of the desired parameters of the material outlined above.

With the geometry constructed and materials applied, boundary conditions are then imposed on the geometry, defined by the physical study. Generally speaking, these definitions are used to set the initial values of the components at rest, then the values of the actions applied to the components, finally defining how the surface interacts with the actions. For example, within the acoustics module, the initial values of a component is pressure. Next, an initial wave is defined, by selecting a face of the component and inputting a value (as above, A could be used as a variable to change in the parameters section). Finally the other faces of the components are defined as to whether they allow the plane waves to pass freely, to be absorbed, or to reflect.

To perform the finite element analysis on the components as discussed earlier, they must first be divided into the mesh of smaller shapes (for example triangles or tetrahedrons), in order to discretise the model allowing for calculations to be performed within each shape [71]. The mesh, whilst variable in geometry, is also variable in mesh coarseness, called the"element size" (see Fig. 3.1). Broadly speaking, element size can be considered the resolution of the simulation.

Once the above steps have been completed, the simulation is run. A variety of dimensional plots can then be drawn in order to potray different elements of these data in the desired format.

Creating a simulation and qualitatively comparing this to experimental data will not only add confidence to the results of experimentations, but will validate the use of FEA to guide future experiments.

3.3 Simulation of a 40kHz Ultrasonic Wave

Here the steps above will be illustrated by working an example of a 2D simulation of a 40kHz waveform within two separate media: water and air.

A 2D simulation was created within the Pressure Acoustics, Frequency Domain.

The "global definitions" were then defined which, for this example, consist of the frequency, *f*, equal to 40 kHz. Next, the geometry was created; for this

illustrated example, this is a rectangle of 0.5 x 1 m.

In two separate simulations, water and air are chosen from the built-in materials. This was added directly to the component in each simulation.

The physics of the simulation are then defined. It is noted from Fig. 3.2, that the Pressure Acoustics, Frequency Domain has specific domains, boundaries, pairs, and points. These are outlined below:

- Pressure Acoustics 1: Defined as the area in which acoustic pressure calculations are performed, in this case the entire area.
- Sound Hard Boundary (Wall) 1: Defined as a boundary condition that halts the travel of the incident wave.
- Initial Values 1: Before the waveform is transferred through the material, this defines the system at time is zero. For this reason, 0 Pa was used for the pressure.
- Plane Wave (Incident Pressure Field 1): This is the pressure amplitude at which the wave is transferred. For simple calculations, a standard plane wave of amplitude 1 Pa was used.
- Bounadies: Boundaries is a placeholder and contains no parameters for the simulation.

Fig. 3.2: A screenshot of the COMSOL interface showing Pressure Acoustics, Frequency Domain boundary parameters.

The Component is discretised into a mesh which, as previously mentioned (see Fig. 3.1), can be loosely considered the resolution of the results. For this example, Extra Fine Mesh was used.

As an example of the results, the intensity of the pressure was plotted by bisecting the geometry. Here a line was defined, and the sound pressure evaluated across this. In Figs. 3.3 and 3.4, the waveform "snapshots" show distinct difference in both initial intensity and decay of the curve in air and water respectively. The waveform through air shows rapid decay, as expected and therefore, although a "real" signal will travel through air in experimentation (as water submersion is not feasible in practice), water shall be used in comparative simulations due the excellent illustrative purposes.

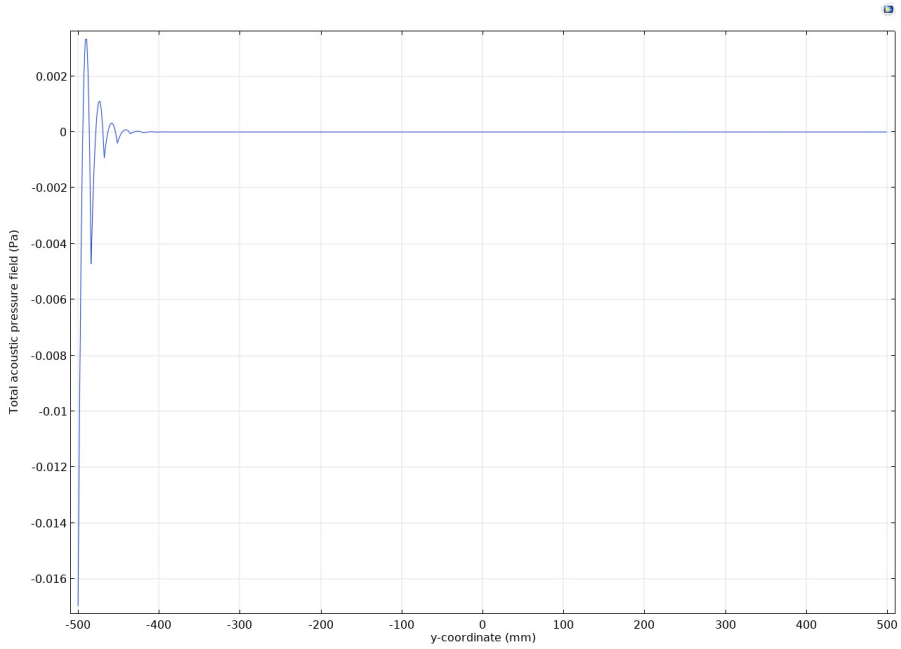

Fig. 3.3: Total acoustic pressure in Pa of a 40 kHz ultrasonic signal travelling from left to right in air.

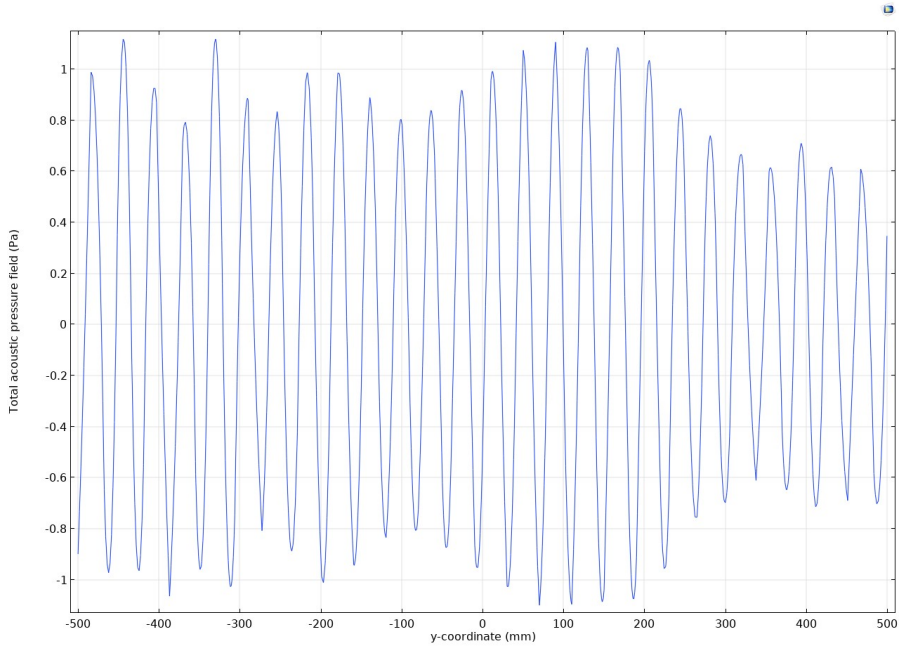

Fig. 3.4: Total acoustic pressure in Pa of a 40 kHz ultrasonic signal travelling from left to right in water.

A colour map of this can be found in Fig. 3.5 or a link to an animation of the colour map can be found in Fig. 3.6.

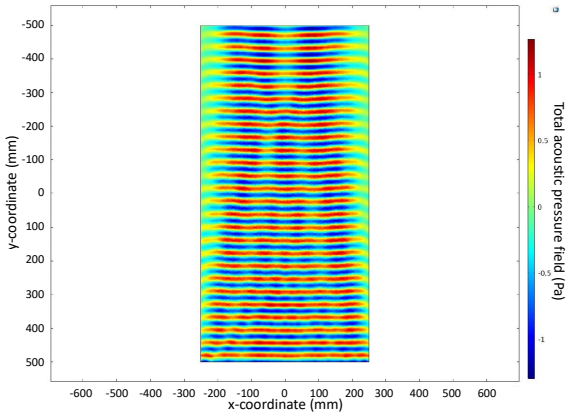

Fig. 3.5: A colour map of a 40 kHz wave travelling through water. The wave is emitted from the lowest edge. The colour scale gives the pressure in Pa.

Fig. 3.6: A QR Code that shows animation of Fig. 3.5.

Here a simple simulation shows how a 40 kHz wave behaves in a medium. Using this principle, experimental results will be qualitatively compared to theory using a virtually simulated geometry within COMSOL (Section 4.6). Once it has been established that a virtual environment can be effectively simulated, subsequent simulations will be used to guide future experimentation.

4. EXPERIMENTATION

With the lab environment being both saturated in environmental noise and one that reflects signals easily, it is important that an environment is created that removes noise as far as possible, as discussed in Section 2.7.1, to measure accurate and reproducible findings. The reduction of noise can then be quantified, before seeing how the ultrasonic signal passes through varying hole sizes within plate metal, in order to quantify the efficacy of using ultrasonic signals to calculate the hole size and subsequent ingress of water in line with standards outlined in Section 2.1. Thirdly, an investigation shall be conducted into how an ultrasonic signal tranverses common metals such as aluminium and steel that would usually be found on board ships to quantify the traversable distance when using two different ultrasonic frequencies. Finally, investigation into how Rayleigh-Lamb Waves traverse composite layers that would simulate a standard hatch seal shall then be conducted at two frequencies to conclude whether or not ultrasonic signals passing through a hatch seal would be an effective method of defect detection, and how changing frequencies affect the accuracy of these measurements, as discussed in Section 2.4.

Each ultrasonic emitter and receiver will be surface coupled (i.e. where the emitter and receiver are placed against the surface of the measured specimen but have no medium between them, for example water), as the purpose of the investigation is a proof of concept, although other coupling medium could be considered, such as a gel, which would improve the accuracy of wave response. In addition, methods such as water submersion would not be considered as, in practice, given the location of ship hatches and the risk to stored cargo in hold, this methodology is inappropriate.

4.1 Testing Environment: Anechoic Chamber

The following will discuss how ultrasound signal reflection can saturate a room and dilute a signal, and how an appropriate environment can be constructed in such a way as to absorb any reflected soundwaves. This will allow a clearer direct signal from source to receiver.

As discussed in Section 2.7.1, it is clear that the higher the frequency and hence the lower the wavelength, the smaller the pore size, or "pockets", required to trap unwanted reflections. In theory, although not discussed in the literature [53, 54, 56], any sufficiently porous material would act as a suitable absorption boundary.

Previous studies on ultrasonic devices have found difficulty in making accurate measurements in laboratory environments, which are small spaces when compared to a typical ship hold, where the ultrasound intensity 'saturates' the laboratory room and effective readings cannot be made. The reflections, or echoes, that occur are linked to the absorption coefficients of the materials with which a signal interacts. Absorption coefficients are intrinsically linked to a material, and are a measure of their ability to attenuate ultrasound in proportion to the incident frequency. Here a sufficiently high absorption coefficient would be required in any chamber construction.

The boundary walls of a laboratory space are typically made from plaster or plasterboard, which would have a low absorption coefficient (μ in Equation 4.1) of 0.04 [72], which results in a decibel reduction (R in Equation 4.1) of 0.35 dB, using

$$\mu = 1 - 10^{-\frac{R}{20}}, \tag{4.1}$$

after Bannon et al. [73]. As a soundproofing material, this would fall below the minimum reduction of 40 dB required by industry regulations to be considered sufficiently soundproof [74]. Therefore a dB reduction of at least 40 dB would deem any soundproofing material sufficient for use in further experiments, which any regulation conforming soundproofing material should possess.

Although the interior structure of an isolated anechoic chamber will absorb much of the incoming waveform intensity, precautions should be taken to avoid

acoustic leakage from the boundary or external sources. For this reason, the exterior of the chamber was also considered. From the outset, there are a few different broad categories of materials to choose from: metals, wood, and plastic. These were chosen for their accessibility and their common usage in construction.

Metal has highly reflective properties [72] and, due to the crystalline structure, it transmits sound easily and at high velocity. Therefore metal would be an unsuitable material. Both wood and plastic are porous materials, however the porosity of plastic depends on the manufacturing style. As both wood and plastic are considered suitable, wood was chosen for the exterior of the chamber as this was readily available. Wassilief [75] discusses the range of sound absorbing wood based materials, suggesting that medium-density fibreboard (MDF) is highly reflective. This is due the increased density of compressed wooden fibres within a binding agent medium [75]. Wassilief proceeds to analyse the effect of incident sound on test samples manufactured from loose wood fibres. This is not ideal as it would require a binding agent and a manufacturing process that is not appropriate for the time constraints. It was found, however, that an exposed piece of fibreboard (a fibreboard with the panel on the side that would be considered the incident plane removed, exposing a surface that differs from the surrounding fibreboard) has a consistently high absorption coefficient at normal incidence, which is improved when using a binding agent [75]. Whilst it was also found that porosity does not have much bearing on the absorption of the incident sound wave [75], a smooth, often laminated surface such as the front panel of an MDF board provides a homogenous plane that is highly reflective.

How this compares with natural wood is not mentioned, however there are many sound absorbing wall panels [76, 77] which have small slots within them akin to the soundproofing foam used by Jenny and Anderson [53]. Additionally, United Kingdom Government Building Regulations do not specify any particular wood or plasterboard porosity, only a mass per unit area of 10 kg/m^2 [74], which aligns with Wassilieff's conclusions regarding high-density materials, but overlooks the surface of the material, which have shown to have a significant effect on the aborption of the material [75]. What is required is not necessarily porous but may mostly rely on density and surface finish. For these

reasons, any type of wood structure that has a non-smoothed/laminated surface would provide sufficient precautionary dampening, and therefore the most readily available wood was chosen.

4.1.1 Construction

MDF with a non-smooth, unlaminated surface was used as a suitable chamber frame (dimensions 1120 x 300 x 375 mm), with a hinged side for access. This hinged side was affixed with small clasp locks in order to seal and secure the chamber. On the smaller two surfaces, a small access port (dimensions 30 x 30 mm) was placed 50 mm from a lower corner to allow for the passage of connecting cables.

As discussed, soundproofing foam that reduces waveforms in the audible frequency range would also achieve the same effect for ultrasonic signals, therefore readily available self-adhesive soundproofing foam was purchased and cut to length to fit the interior dimension. The edges were then chamfered at an angle of 45 degrees on the boundary edges of the foam to allow for well fitted edges and corners. When attaching the foam, the self-adhesive secured well to the MDF surface, and care was taken to ensure that the backing of the self-adhesive layer was left intact in areas such as the access ports, where regular movement of the foam would be required.

Fig. 4.1: The constructed MDF chamber with appropriate soundproofing inserts; each soundproofing insert has a self-adhesive backing.

4.1.2 Measurement

To quantify the efficacy of the anechoic chamber in comparison to the laboratory environment, the current generation of Portascanner was used, which emits a 40 kHz frequency through three piezoelectric crystals mounted at different angles, covering a wide arc (although the exact angular dependence is not available). The centre beam line of the emitter was placed facing the largest chamber wall side, at a distance of 5 cm, whilst the accompanying receiver was placed a distance 10 cm from the emitter at 10 degree intervals for the 180 degrees about the rear of the device (see Fig. 4.2). To ensure a parallel orientation, a parallel line was drawn 5cm away from the chamber wall with a centre point in order to align the edge and centre of the device consistently. This was then repeated in laboratory space, using a boundary wall. The receiver was connected to an oscilloscope due to the versatility of the measurement outputs (discussed further in Section 4.1.3) and 3 measurements were taken for both peak-to-peak voltage, V_{pp}, and root-mean-square voltage, V_{rms}. A background measurement was also conducted in the laboratory space and within the anechoic chamber, without an operating emitter. This was used to reduce the systematic error introduced by environmental noise by subtracting the average value from the average measurements.

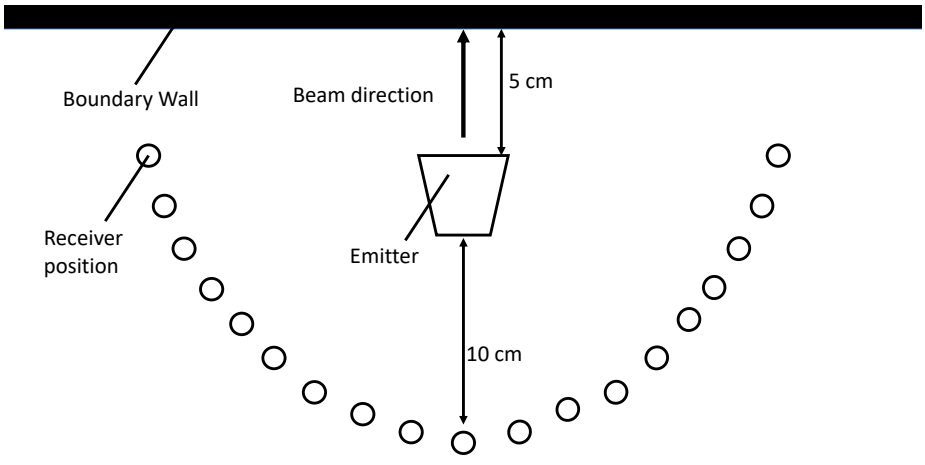

Fig. 4.2: Top-down view of emitter and receiver position for both laboratory and chamber experiments.

4.1.3 Results and Discussion

The Portascanner measurement device that accompanied the receiver converts received signals to decibels using the pressure/power ratio of 20 μPa. However these measurements saturated at 76.06 dB, and would not increase further. As the device is designed for use in large spaces, such as vessel storage spaces, comparatively small lab spaces can reflect the sound across the room creating a constant standing wave of high intensity. To overcome this, the receiver was instead connected to an oscilloscope which was able to give a linear output above the 76.06 dB limit.

The peak-to-peak voltage, V_{pp}, received from the device in both the anechoic chamber and the laboratory space were plotted (Fig. 4.3). In comparison with open space, the anechoic chamber dampened the noise by 2240 $\pm$ 4 mV (the uncertainty was calculated by adding in quadrature [78]).

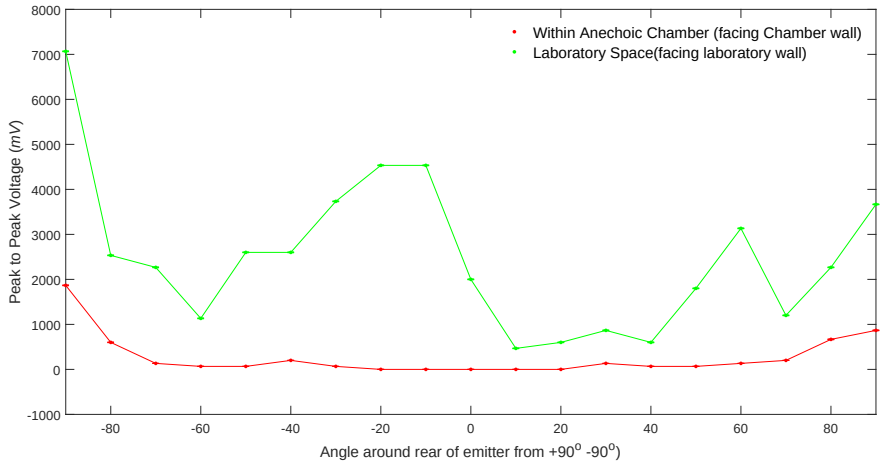

Fig. 4.3: Peak to Peak Voltages measured over a 180 degree range around rear of the device. Error bars present but too small to be seen. Note that background has been removed from both data sets.

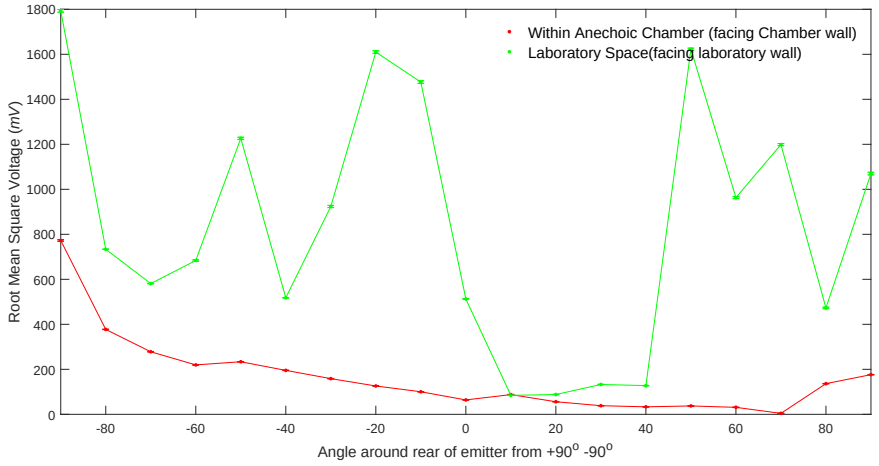

Fig. 4.4: Root Mean Square Voltages measured over a 180 degree range around rear of the device. Error bars present but too small to be seen. Note that background has been removed from both data sets.

This shows an overall improvement in the dampening of the ultrasound signal in the anechoic chamber, also observed in V_{rms}, which showed a similar improvement with an average difference of 668 $\pm$ 6 mV.

The decibel reduction was calculated using

$$\mathrm{dB} = 20\log_{10}(\frac{V_2}{V_1}), \tag{4.2}$$

where V_2 is the measured intensity, and V_1 is the reference intensity, 8500 $\pm$ 800 mV, which was taken from an unimpeded signal measured at a distance of 10 cm between source and receiver. Here, the average voltage measured (V_2) in open space is 832 mV, a dB reduction of 20.2 dB compared with the output signal. For the anechoic chamber, with an average voltage measured of 165 mV, the reduction is 34.3 dB, which is greater than in the laboratory space, however would not comply with soundproofing regulations [74].

From Fig. 4.3 and 4.4, the anechoic chamber shows a large decrease in unwanted acoustic signals from the environment. It is also noted that using a

laboratory wall as a reflective surface provides a non-uniform response, which supports the theory that an incident waveform will reflect off a flat surface in all directions. Anomalous peaks are seen (see Fig. 4.4 at -20° for laboratory space) which could be due to the imperfections present at a chamber wall, causing inconsistent angles of incident and reflections. However, as reasonable symmetry could be seen from 25°, this may also be due to placement of transducers within the device, as alignment accuracy is not paramount for the intentions of the device (i.e. as it is intended only to saturate a hold), asymmetric transducer placement could cause these anomalous peaks. This may also have caused the apparent bias towards the left-most side (-90° on all figures), where unaligned ultrasonic emitting piezoelectric crystals cause a beam angle shift towards one side.

Two peaks can be seen at left and right-most sides (-90° and +90° respectively on all figures), which may be side lobes created from the reflection from the wall. Repeating these measurements at greater distances could verify this in future studies.

4.2 Ultrasonic Waves through different hole sizes

The current leak detection method relies on detecting ultrasonic signals passing through small holes in the spacings between the hatch cover, the rubber gasket, and the hull of a ship, whether through rubber gasket deterioration or steel deformation, as discussed in Section 2.1. Therefore the effect of a variable hole size on the ultrasonic signal was analysed, to find out whether the hole size could be determined and therefore whether the rate at which the ingress of water occurs through a vessel hatch could be calculated.

4.2.1 Method

An open top hollow aluminium box (165 mm x 165 mm x 160 mm) was constructed, with one face allowing for several interchangeable plates of variable hole sizes drilled in the centre to be inserted. To overcome the offset directionality issues discussed in Section 4.1.3, a single piezoelectric 40 kHz emitter and receiver was constructed, placed in the centre of the cube with the direction of the beam orientated towards the interchangeable side, and connected to an

analogue function generator set to a 40 kHz sinusoidal waveform. Both cube and the receiver were placed inside the anechoic chamber at set distances ("Distance" in Fig. 4.5); 10, 30, and 50 cm away from, and on the same plane as, each other. As different plates with centered holes varying from 0.5 mm to 10 mm (see Table 4.1) in diameter were placed in the open face of the metal cube ("Hole Size" in Fig. 4.1), the intensity was measured three times through an oscilloscope measuring the V_{rms}.

Table 4.1: Measured gap sizes with centred holes in aluminium plates. The uncertainty on all measurements was ± 0.018 mm.

Hole Size Diameter (mm)
0.553
0.963
1.463
3.943
5.863
7.880
9.923

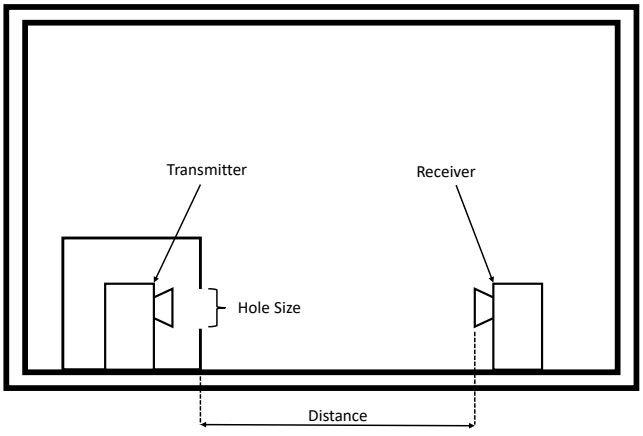

Fig. 4.5: Hole size experimentation setup of the transmitter housed within the metal container and receiver, both housed within the anechoic chamber to reduce reflective noise.

4.2.2 Results and Discussion

A boxplot (Fig. 4.6) shows the signal recorded versus hole size with the mean, 25th and 75th percentile, and maximum and minimum values recorded.

As can be seen from the results, there is a steady rise in intensity as the hole size becomes greater. In addition, a steady increase in the uncertainty is seen with each increase in hole size diameter for 40 kHz at 10 cm (Fig. 4.6a), whereas at 30 cm (Fig. 4.6b) and 50 cm (Fig. 4.6c) the signal intensity is consistently much smaller and therefore have expected smaller and more consistent uncertainty. The intensity of the wavefront is expected to decay over distance, however for smaller hole sizes as seen in Fig. 4.6 and more explicitly in the example for a hole size of 1.463 mm in Fig. 4.7, the intensity appears to increase over distance. To characterise the fit, a curve proportional to $\frac{1}{r^2}$, where r is the receiver distance, was fitted to the data as this would be the expectation for a sound travelling radially outwards.

To test the goodness of fit of Fig. 4.7, a reduced chi-squared analysis was conducted with a value of 0.008, suggesting an error dominated fit (i.e. due to the large errors, various best fit curves could be used, all with equal validity).

The smaller intensity ranges measured at further distances as seen in Fig. 4.6c, suggests that detection of the source energy is difficult even at small distances. The conclusion inferred from these data is that, even at small distances from the seal, using ultrasonic detection would be unreliable.

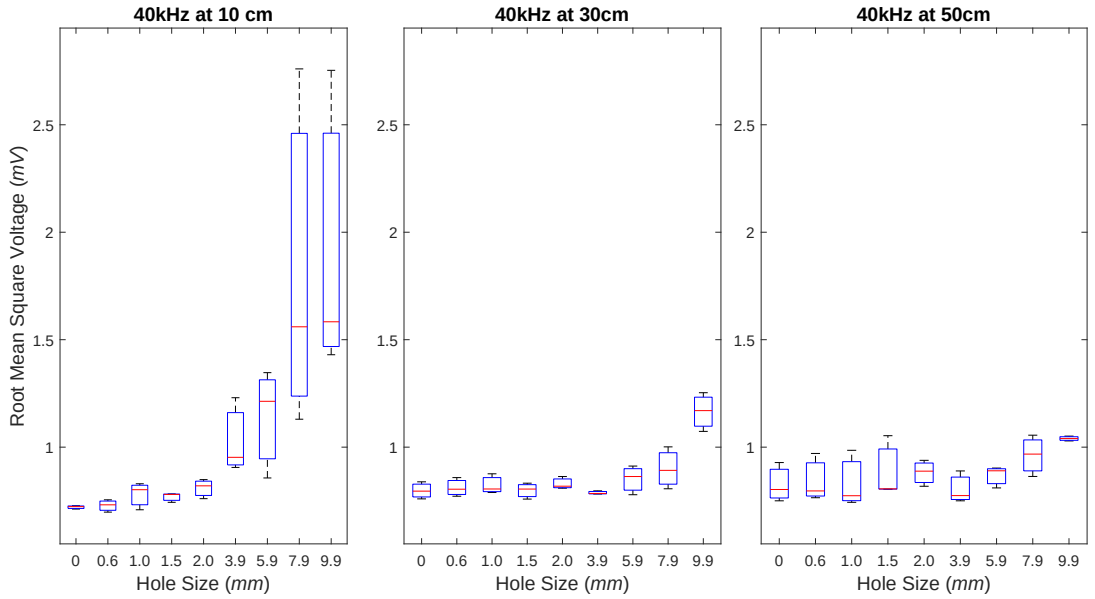

Fig. 4.6: A boxplot of a 40 kHz incident wave intensity received through different hole size diameters at a) 10 cm, b) 30 cm, and c) 50 cm.

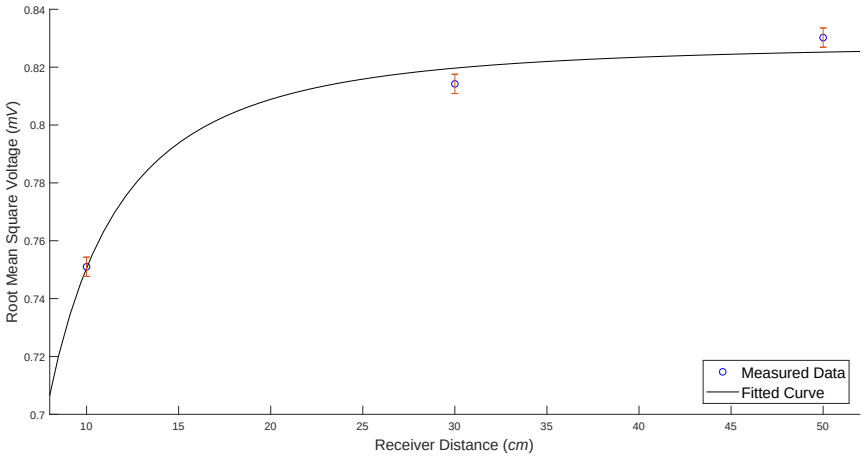

Fig. 4.7: 40kHz incident wave intensity received through a hole size of 1.463mm with fitted curve.

4.3 Use of the Picoscope 6 and Fast Fourier Transform

A Picoscope [79] was used for further experimentation as opposed to a live oscilloscope reading as it allows for a greater number of repeat measurements over a shorter time interval. In addition, Fourier transform techniques were implemented to gain further insight into the individual frequency behaviour of the system.

The Picoscope was set to measure 1000 data sets (known as "buffers"). Each buffer contained 5000 data points at a rate of $50{\cdot}10^6$ measurements per second.

A Fast Fourier Transform, the methodology of which was discussed in Section 2.5.4, was performed on these data using a module within MATLAB; a computer software package developed by MathWorks used for data analysis [80].

4.4 Ultrasonic Waves through homogenous materials

As the ultrasonic wave is attenuated by the material, the signal intensity will decrease. As a result, the information contained within the signal will become more difficult to measure and, by association, characteristic features of the spectrum will become less pronounced. It is possible to circumvent this problem by introducing additional devices at a certain distance from the first device in order to maintain the intensity of the signal.

Initially, it could be theorised that an unlimited number of both generators and detectors could be used, with no space between the devices. However, this would be impractical not only from an economic perspective, but also when considering how one may power such a system. Therefore a suitable distance should be found at which the intensity falls below a certain threshold and, using this distance, be able to specify the number of devices for a given distance (e.g. per metre).

4.4.1 Method

Two experiments to measure the intensity decay parallel and perpendicular to the source were conducted. Should the intensity decay to different orders of magnitude in different directions across and through a material, it would be appropriate to be made aware of this difference and place devices in orientations of lowest rates of decay.

To create a parallel measurement, a rig was crated that was able to hold a series of plates vertically (see Fig. 4.8). Firstly an aluminium stand was created using a three sided rectangle (175 x 150 mm) and supporting struts on one side. On the opposite side, three legs extended out to a greater distance. These were used to support the vertical plates, as a small stopper secured through a hand-tightened screw secured the vertical plates in place. This stopper would sit atop, and be fastened to, the central leg (for distinction, this shall be referred to hereafter as the ‘rail’).

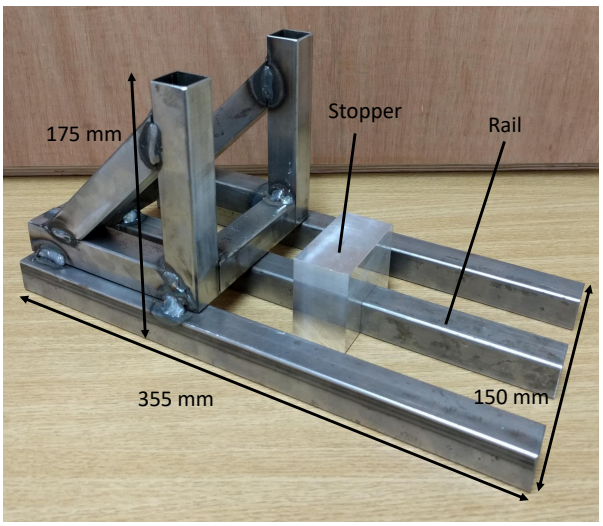

Fig. 4.8: A rig used to support a vertical series of plates. Note the supporting struts on the left, and the extended legs to the right. The hand-tightened screw stopper sits on the central rail.

To measure the attenuation, a single plate was placed vertically in the channel between the three sided square and the stopper (see Fig. 4.8). The stopper was moved to hold the plate firmly and the screw was hand-tightened. The emitting device was placed on one side of the plate, and the receiver was placed on the other side, ensuring both speakers were flush against the plate and secured in placed with reusable adhesive putty (both transducers are now surface coupled to the plates, and hereafter this method shall be referred to as 'surface coupling'). The receiver was connected via a Picoscope to a computer.

The same method was repeated using two, three, and four vertical plates in series, in order to measure the continous waveform at greater distances. As the vertical plates increased, it was found that the stopper was unable to hold high number of plates together from one edge, causing gaps to occur between each plate. This would have a negative impact on measurements taken as the waveform would be travelling through mixed media (i.e. solid and gas), as opposed to homogenous plates. A tool maker's clamp positioned on the opposing edge to the stopper removed the gaps between plates (see Fig. 4.9).

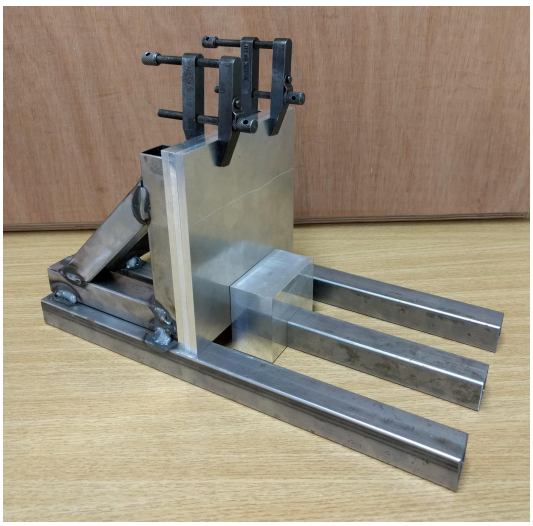

Fig. 4.9: An arrangement of three aluminium plates in rig from Fig. 4.8. Note use of Tool Maker's Clamps.

To create the perpendicular measurement, a solid bar of aluminium and steel was created of 500 mm in length and suspended using stands 200 mm in length located at both sides of their longest edge (see Fig. 4.10). As the width and height of the bar are around 2 cm, Lamb Waves at 40 kHz may occur as a result.

The ultrasonic emitter is then placed on the bar emitting a continuous waveform, with the direction of propagation orientated through the shortest length at the far side of the bar. The receiver is then placed in a similar orientation, a series of 5 cm increments from the source (see Fig. 4.11). Due to the slightly differing sizes of the finished aluminium and steel bars, the cumulative distance for aluminium is over 40 cm, and 35 cm for steel.

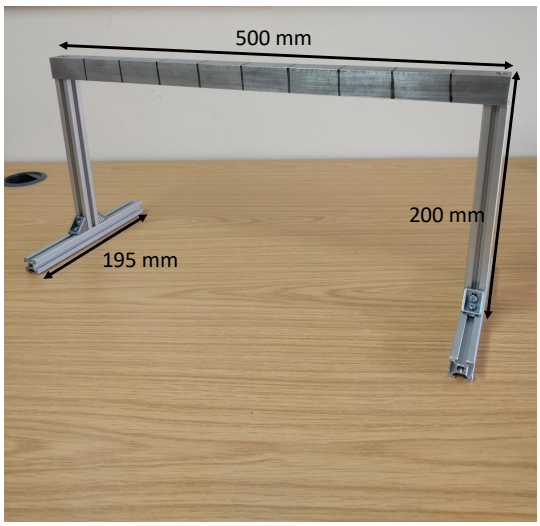

Fig. 4.10: A rig used to measure perpendicular transmissions. Two of these rigs were created, the 500 mm solid bar made from aluminium or steel in each rig.

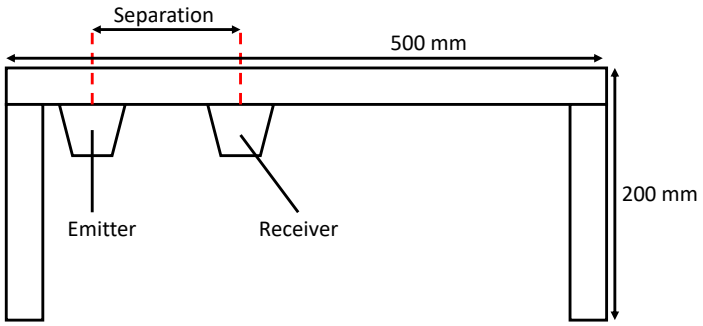

Fig. 4.11: A rig used to measure perpendicular transmissions. The solid bar 500 mm in length is supported by stands 200 mm in length. The emitter was placed at one side and the receiver was moved in 5 cm increments ("Separation").

A background measurement was also recorded using the receiver inside the

anechoic chamber with the emitter switched off. This was removed from the above measurements to reduce systematic error as much as possible.

4.4.2 Results and Discussion

The amplitude of the sinusoidal waveforms was measured in volts and, using a FFT within a MATLAB algorithm, the frequency spectrum was constructed. To translate this into a total power of the system, a trapezium function was employed here. Integrating over the entire spectrum and plotting against the distance from the emitter. Initially 40 kHz in aluminium (Fig. 4.12), the fitted line to the data shows a reduced chi-squared value of $1.1{\cdot}10^{-5}$, when measured parallel to a series of plates, and $1.6{\cdot}10^{-4}$ when measured vertically across a homogenous bar, showing that the fit lines are highly error dominated. In theory, the ultrasonic waveform would spread out from the source equally in all directions, therefore the plot can be mirrored in the negative direction which will increase the number of data points and trends may be identified. The mirrored plot (Fig. 4.13) showed similar reduced chi-squared values of $2.5{\cdot}10^{-6}$ across plates and $2.9{\cdot}10^{-4}$ across a homogenous bar (i.e. still error dominated). This style of plot was repeated for 40 kHz in steel (Fig. 4.14), and 400 kHz in aluminium (Fig. 4.15), and steel (Fig. 4.16).

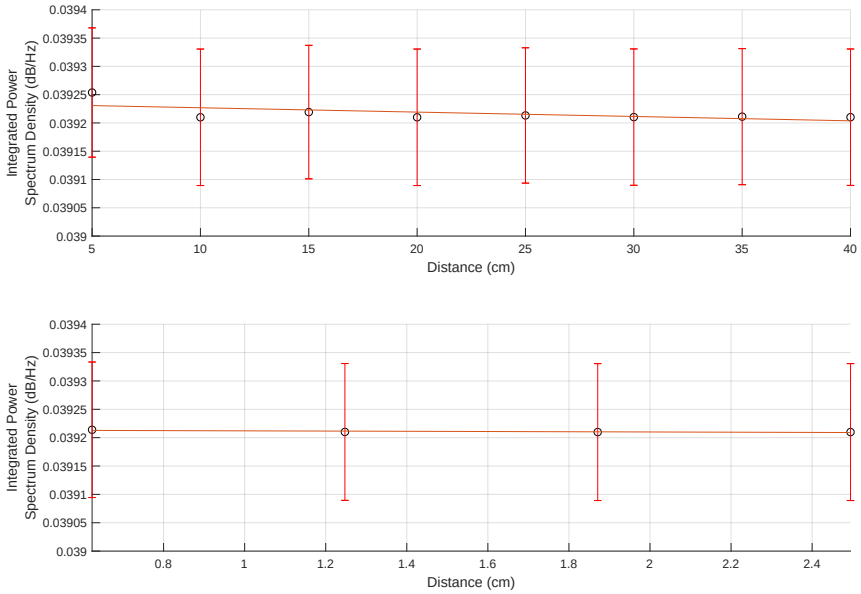

Fig. 4.12: Decay of 40 kHz ultrasonic wave travelling a) perpendicular through a homogenous aluminium beam and; b) parallel to a series of aluminium plates.

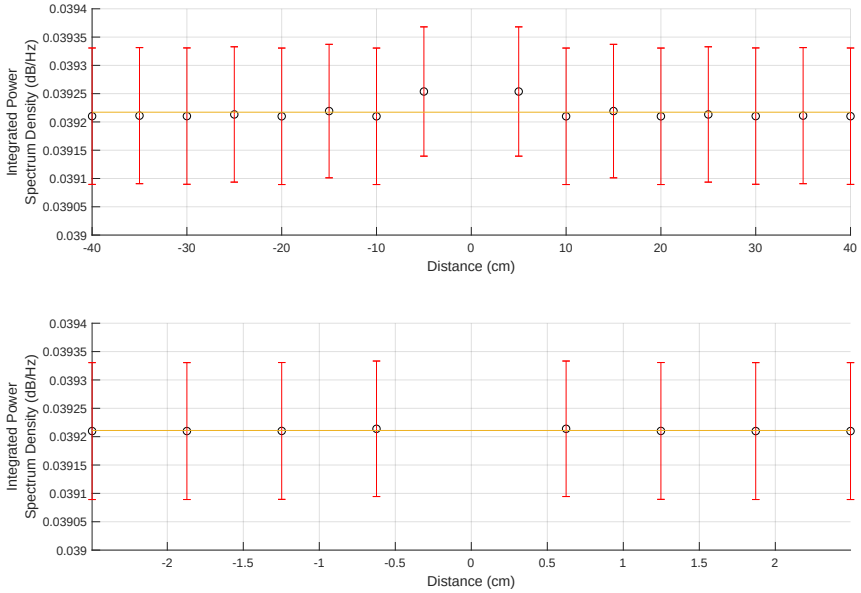

Fig. 4.13: Decay of 40 kHz ultrasonic wave travelling a) perpendicular through a homogenous aluminium beam and; b) parallel to a series of aluminium plates. Plot is mirrored about the x-axis at $x = 0$.

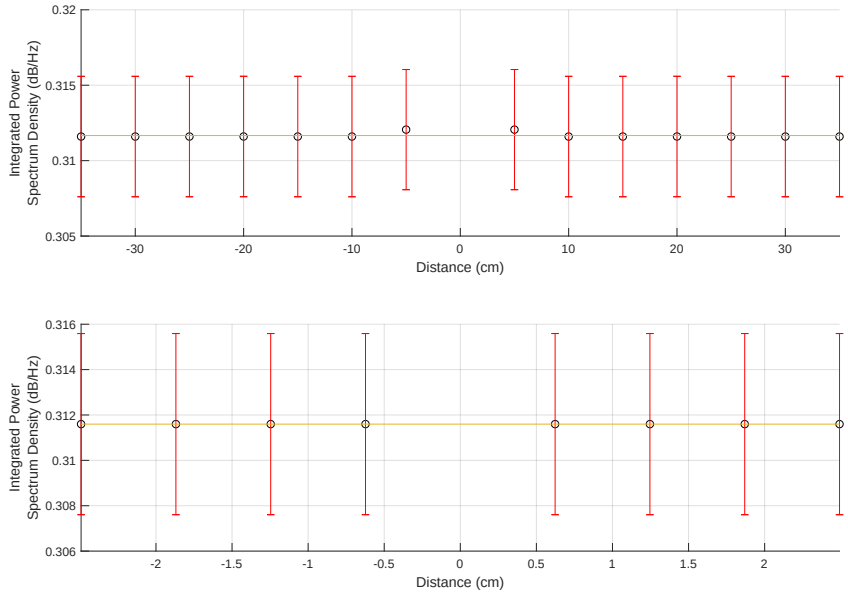

Fig. 4.14: Decay of 40 kHz ultrasonic wave travelling a) perpendicular through a homogenous steel beam and; b) parallel to a series of steel plates. Plot is mirrored about the x-axis at $x = 0$.

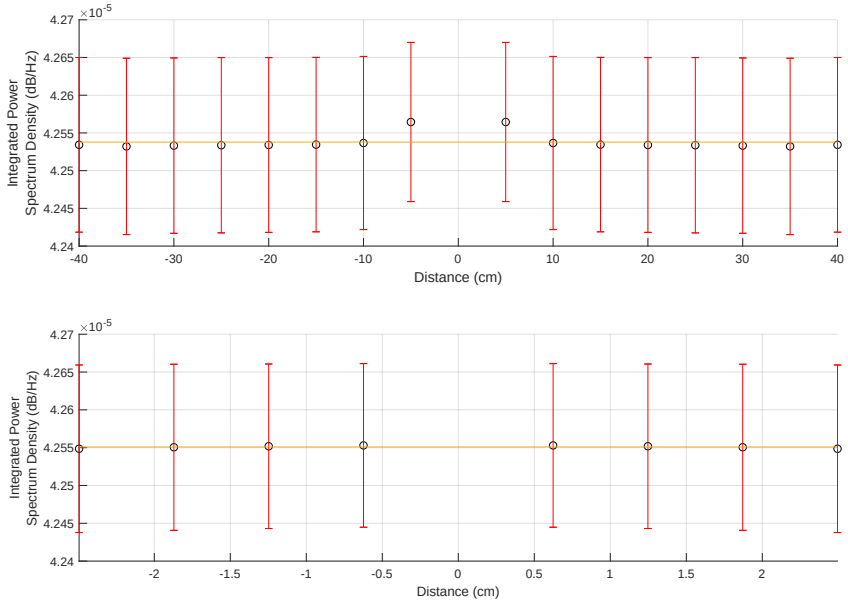

Fig. 4.15: Decay of 400 kHz ultrasonic wave travelling a) perpendicular through a homogenous aluminium beam and; b) parallel to a series of aluminium plates. Plot is mirrored about the x-axis at $x = 0$.

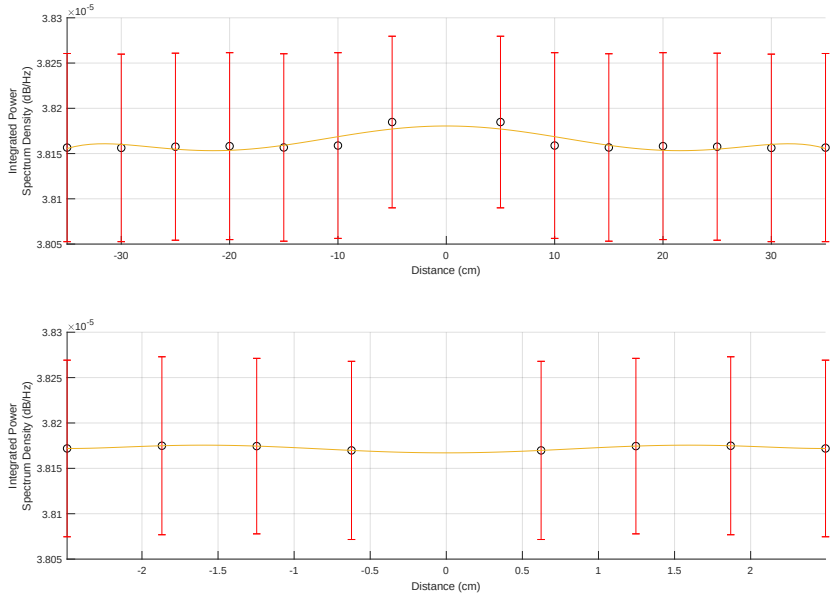

Fig. 4.16: Decay of 400 kHz ultrasonic wave travelling a) perpendicular through a homogenous steel beam and; b) parallel to a series of steel plates. Plot is mirrored about the x-axis at $x = 0$.

Each line of best fit is error-dominated, with the reduced chi-squared analysis found in Table 4.2 being too low to considered a viable best fit. The expectation of the propogation would be a sinusoidal decay, however a test best fit curve for 40 kHz through aluminium showed a worse fit, with reduced chi squared values of $2.4{\cdot}10^{-6}$ when measured parallel to a series of plates, and $9.1{\cdot}10^{-5}$ when measured vertically across a homogenous bar.

Table 4.2: Reduced Chi-Squared values of best fit lines for 40 kHz and 400 kHz frequencies measured parallel to a series of plates and perpendicular to a homogenous beam. Note that all reduced chi-squared values imply an error dominated fit line.

Frequency(kHz)	**Material**	**Orientation**	**Reduced Chi-Squared**
40	Aluminium	Parallel	$3.4{\cdot}10^{-6}$
40	Aluminium	Perpendicular	$0.19{\cdot}10^{-3}$
40	Steel	Parallel	0
40	Steel	Perpendicular	$1.1{\cdot}10^{-3}$
400	Aluminium	Parallel	$4.7{\cdot}10^{-7}$
400	Aluminium	Perpendicular	$6.7{\cdot}10^{-5}$
400	Steel	Parallel	$5.0{\cdot}10^{-5}$
400	Steel	Perpendicular	$6.6{\cdot}10^{-5}$

The standard error was calculated for each data entry, which is larger than the trends shown above. This may be an overestimation of the true errors present in the data, and limits the confidence on any underlying trends and conclusions drawn from the data. Taking this into account, it is not possible to establish agreement between both plate and bar. Although expectations would state that, for a round generator, emission occurs equally in all directions normal to the direction of the emitted waveform, this cannot be stated when travelling through a material. In experimentation using plates, deviation was expected due to the boundaries between plates, however this does not have any statistically significant effect on the overall signal intensity.

It is noted that, although the error bars are large, the data does not deviate from constant. This suggests that the system has a fundamental systematic flaw and therefore repeat measurements would not reduce the errors and would not

increase the accuracy of the best fit.

As a result of this, decay curves are unable to be characterised through the materials and therefore cannot suggest a distance at which the intensity is reduced by half. As a result, this would lead to the conclusion that a standing wave may have been created within both experiments. This does imply that, as similar intensities are recorded up to 40 cm from the source, the distance required between additional devices and the first device is greater than 40 cm for aluminium or 35 cm for steel.

4.5 Rayleigh-Lamb Waves through composites

To test the water- and weather-tightness of a hatch cover, a hatch was simulated by creating a composite structure of hatch components. Taking a typical hinged hatch cover, the ingress of water would occur through the seal between the rubber gasket and coaming, therefore should one bisect the hatch from interior to exterior boundary (as shown by the dashed red line in Fig. 4.17), there are a total of four points that could decay to a sufficient degree to allow the ingress of water.

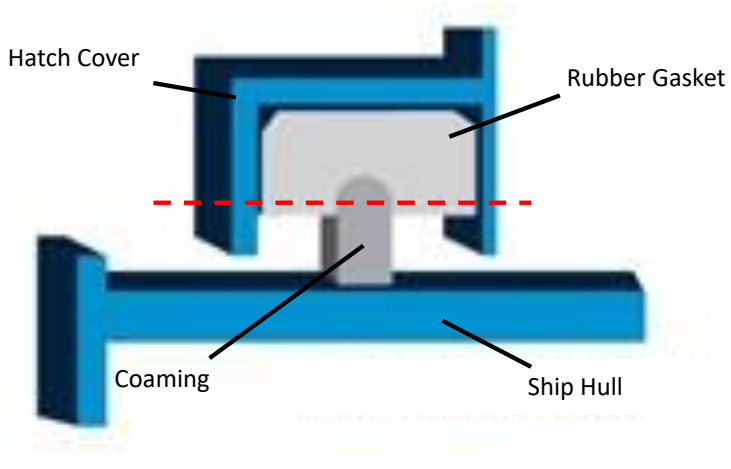

Fig. 4.17: A section of hatch cover. The dashed red line indicates the cutting plane used to create the composite. Image not to scale. After Cargo Care Solutions [81].

As the rubber decays and the metal is warped, small air spaces are created. Placement of an air spacing between rubber and metal in this apparatus was used to simulate this effect.

4.5.1 Method

Using the same vertical plate stand as in Section 4.4.1, a series of rubber plates was created with the same square dimensions as the aluminium and steel plates. These were used in series to create a steel-rubber and an aluminium-rubber non-adhered composite. To simulate a defect, a number of air spacers were created using a plastic C-shape of the same boundary dimensions as the rubber, aluminium, and steel plates, which were then inserted within the composite. As previously, the emitter was surface coupled to one side of the composite, as the receiver was coupled on the other side, taking measurements via the Picoscope system. The emitter was oriented such that the direction of propagation travels through the plates of metal and rubber, and through the air created by the negative space of the plastic C-shape (see Fig. 4.18).

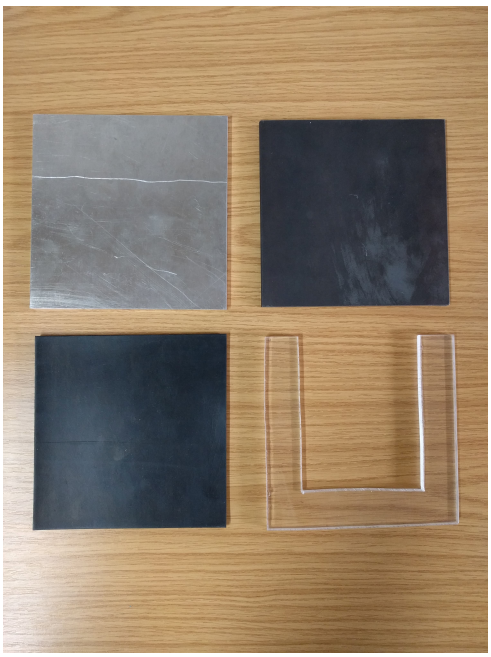

Fig. 4.18: (Top Left to Bottom Right) Aluminium, steel, rubber, and air spacers used in composite material measurements.

Through the cross section shown in Fig. 4.17, when air spaces occur, these would appear between the rubber and metal sections. There are four potential decay sections across the dashed red line in Fig. 4.17, and therefore four air spacers were constructed. Initially, the composite was measured when the air spacer was between the first metal (aluminium or steel) and rubber plate (see Fig. 4.19), meaning that the composite order would be;

Metal-Air-Rubber-Metal-Rubber-Metal.

Once the measurement was taken, the air spacer is moved between the next two plates, and so on, until the final orientation is;

Metal-Rubber-Metal-Rubber-Air-Metal.

This means that, with a single air spacer, there are four possible orientations and four distinct measurements. Similarly, using two air spacers, there are six possible configurations of single air spacers placed between rubber and metal

plates. This was continued for three and four air spacers with four and one orientations respectively. In order to provide a statistically significant measurement with four air spacers, this was repeated three more times. Both steel and aluminium composites were used separately.

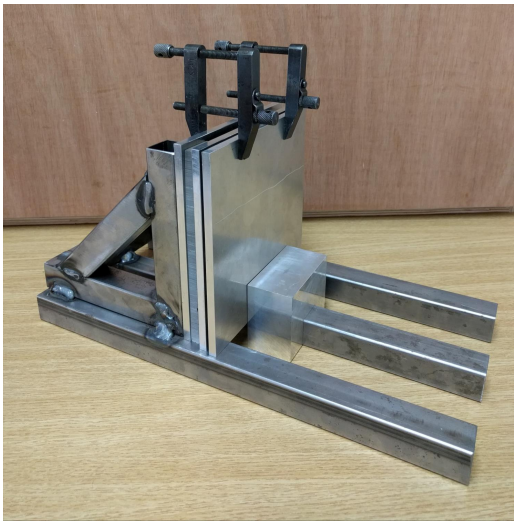

Fig. 4.19: Example composite arrangement. Note air spacer sits between first metal and rubber plate.

4.5.2 Results and Discussion

To quantify the level of decay, each measurement was subtracted from a composite with no air spacers present, representing no air spaces between the rubber and metal, and therefore no decay, i.e;

Metal-Rubber-Metal-Rubber-Metal.

The measurements were integrated using the same trapezium method as seen in Section. 4.4.2. In order to identify trends between measurements, the number of air spacers were grouped together to identify whether the location made an impact on the attenuation of the signal. For example, for 40 kHz in steel for two air spacers, if these values were plotted with uncertainty errors (Table 4.3), it can be clearly seen that the uncertainty overlaps with each measured value.

As a result, it could be suggested that location of air spacers does not significantly impact the overall attenuation of the ultrasonic signal and the number of air spacers can be grouped together and plotted against the integrated power spectrum density.

Table 4.3: Integrated power spectrum density of 40 kHz ultrasonic signal measured through steel-rubber composite with two air spacers present. Note that each uncertainty causes significant overlap with other measurements.

Power Spectrum Density (dB/Hz) ($\cdot 10^{-6}$)	**Uncertainty (dB/Hz) ($\cdot 10^{-6}$)**
20	0.38
21	0.38
21	0.38
21	0.38
21	0.38
22	0.38

An analysis was also conducted to identify any quantative differences between integrated power spectrum density of the full frequency spectrum, and isolated frequency bandwidth (at the emitted frequency of 40 kHz or 400 kHz). As the decay was expected to be exponential, these curves of best fit were added for full frequency spectrum (Fig.4.20) and isolated frequency bandwidth (Fig. 4.21).

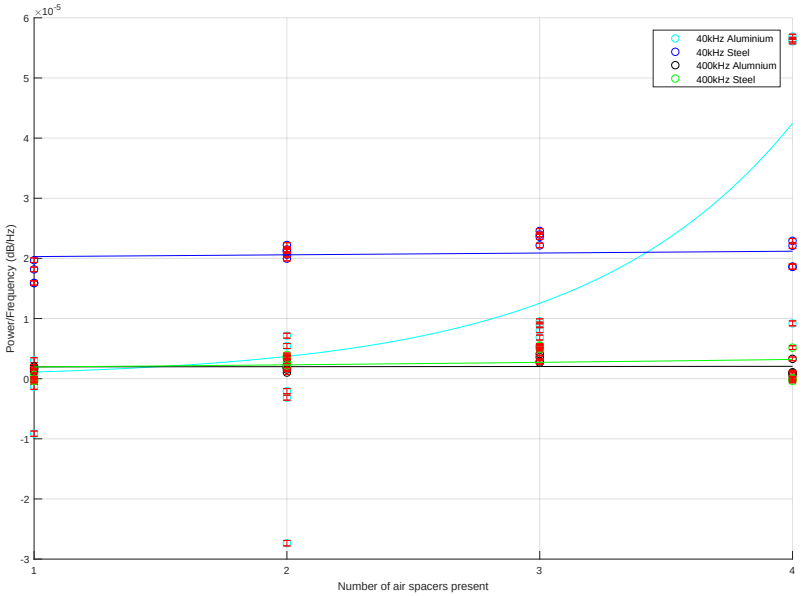

Fig. 4.20: Intensity difference between no air spacers and n spacers present at 40 and 400 kHz through Steel-Rubber and Aluminium-Rubber composites over entire frequency spectrum with exponential line of best fit. Errors bars are present but too small to be seen, shown in red.

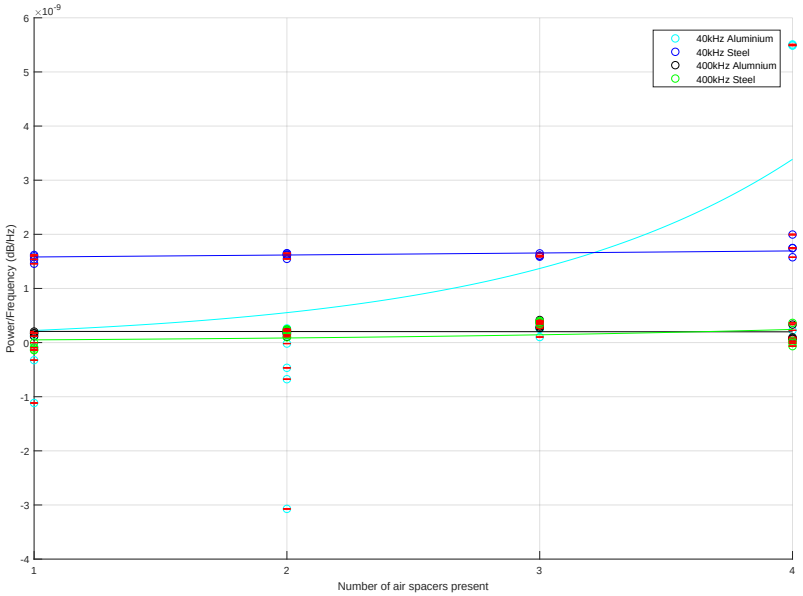

Fig. 4.21: Intensity difference between no air spacers and n spacers present at 40 and 400 kHz through Steel-Rubber and Aluminium-Rubber composites within isolated frequency bandwidth at emitted frequency with exponential line of best fit. Errors bars are present but too small to be seen, shown in red.

The best fit lines are entirely error dominated in both full frequency spectrum and isolated frequency bandwidth, shown in Tables 4.4 and 4.5 respectively. Therefore it cannot be stated whether exponential curves characterise the data, however errors are slightly reduced when the full frequency spectrum is considered as opposed to an isolated frequency bandwidth.

Table 4.4: Chi-Squared and Reduced calculation of best fit in exponential format using whole spectrum calculation alongside average error.

Frequency(kHz)	**Material**	**Chi-Squared**	**Reduced Chi-Squared**	**Average Error**
40	Aluminium	0.000437	0.0209	$1.29{\cdot}10^{-6}$
40	Steel	$4.71{\cdot}10^{-6}$	0.00217	$2.80{\cdot}10^{-6}$
400	Aluminium	$7.85{\cdot}10^{-6}$	0.00280	$4.43{\cdot}10^{-7}$
400	Steel	$3.31{\cdot}10^{-5}$	0.00576	$3.11{\cdot}10^{-7}$

Table 4.5: Chi-Squared and Reduced calculation of best fit in exponential format using single frequency band calculation alongside average error.

Frequency(kHz)	**Material**	**Chi-Squared**	**Reduced Chi-Squared**	**Average Error**
40	Aluminium	$1.02{\cdot}10^{-7}$	0.000319	$2.68{\cdot}10^{-12}$
40	Steel	$1.74{\cdot}10^{-9}$	$4.17{\cdot}10^{-5}$	$9.45{\cdot}10^{-11}$
400	Aluminium	$1.05{\cdot}10^{-9}$	$3.24{\cdot}10^{-5}$	$1.40{\cdot}10^{-11}$
400	Steel	$5.30{\cdot}10^{-9}$	$7.28{\cdot}10^{-5}$	$2.63{\cdot}10^{-12}$

A straight line fit was also fitted to the data, to see if a marked improvement occured, shown for entire spectrum and isolated frequencies in Fig. 4.22 and 4.23 respectively.

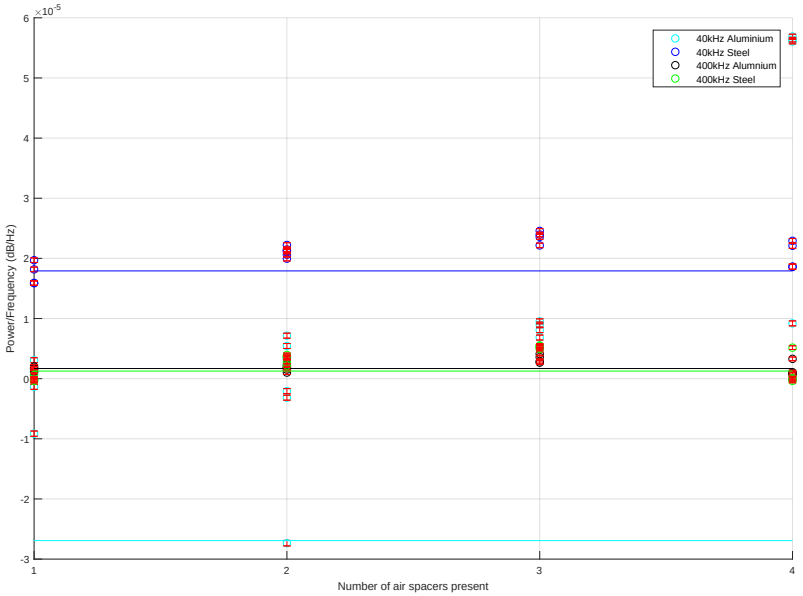

Fig. 4.22: Intensity difference between no air spacers and n spacers present at 40 and 400 kHz through Steel-Rubber and Aluminium-Rubber composites over entire frequency spectrum with straight line of best fit. Errors bars are small, but shown in red.

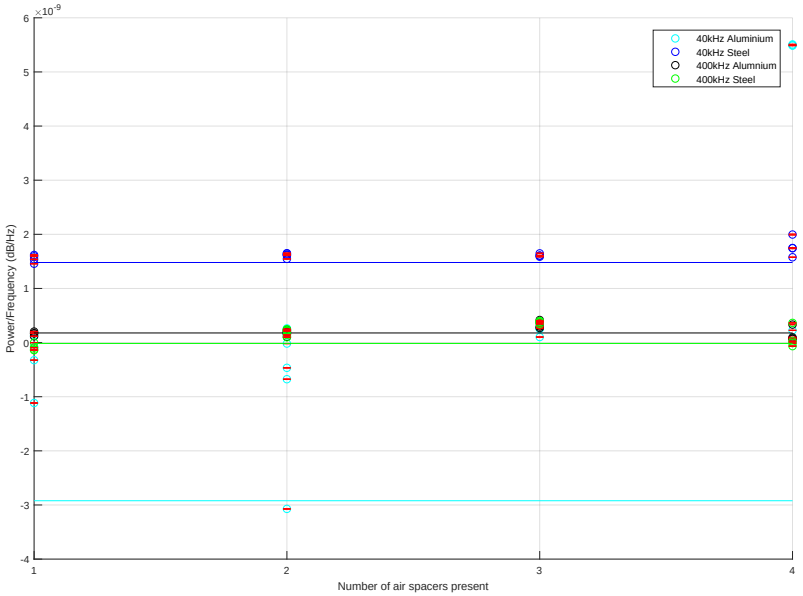

Fig. 4.23: Intensity difference between no air spacers and n spacers present at 40 and 400 kHz through Steel-Rubber and Aluminium-Rubber composites within isolated frequency bandwidth at emitted frequency with straight line of best fit. Errors bars are small, but shown in red.

Plotting best fit lines shows little improvement in the reduced chi-squared analysis for either line or exponential curve, each between 10^{-3} and 10^{-5} in magnitude and therefore error dominated. Although this holds for full frequency spectrum and isolated bandwidth, a slight improvement appears once again when full frequency spectrum is considered, which suggests that this method may provide more accurate results. It is also noted that the grouping together of each air spacer regardless of location is not correct for all cases as previously believed (see Table 4.3), for example, see Fig. 4.20 at 40 kHz in steel for four air spacers, which suggests that the material, or number of air spacers may have a more complicated effect on the ultrasonic signal.

The method of layer attachment through mechanical grips may also have produced inconsistent coupling between plates that may have caused inhomogeneous pressure distribution, thereby varying the ultrasonic signal transmission through the composite.

From this, as there is no statistically significant evidence that the data deviates from a constant value in most cases, it would lead to the conclusion that neither frequency is able to discern between the number of air spacers present and therefore whether a defect is present within the composite. As a result, this method of detecting defects cannot be considered as a viable option.

To show the range of values, each number of air spacers, from one to four (Fig. 4.24, 4.25, 4.26, and 4.27) was separated and a boxplot was created for each frequency and material.

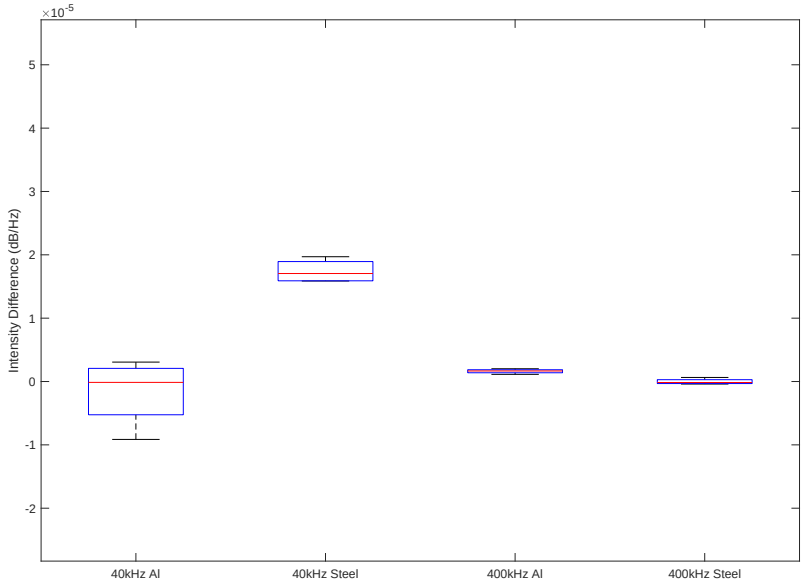

Fig. 4.24: Calculated intensity difference between one air spacer and no air spacers present between composites, separated by frequency and material.

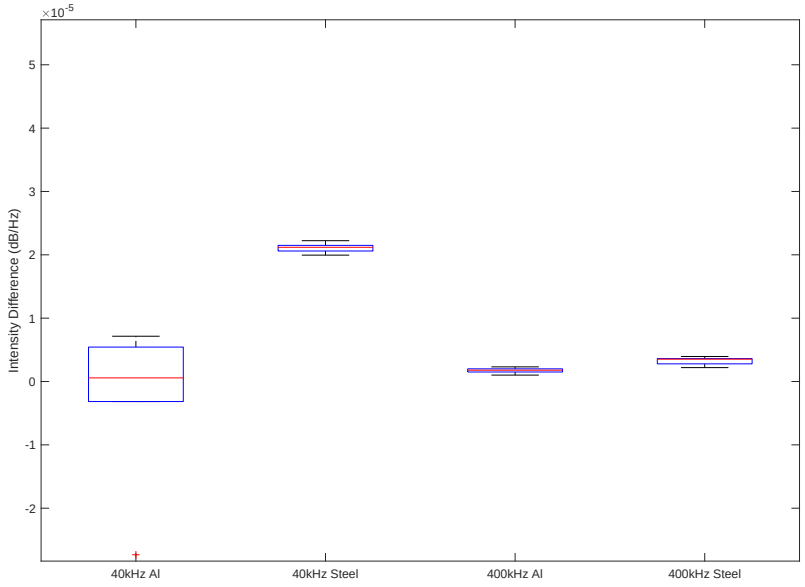

Fig. 4.25: Calculated intensity difference between one air spacer and two air spacers present between composites, separated by frequency and material.

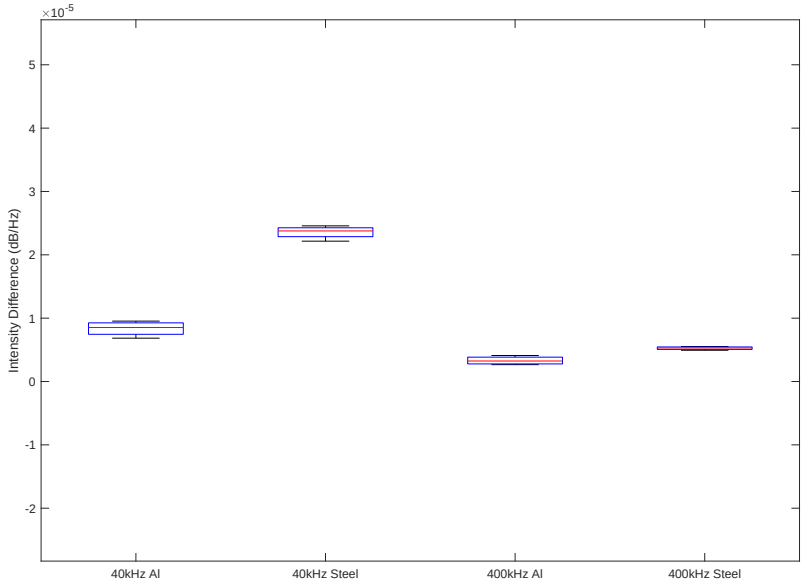

Fig. 4.26: Calculated intensity difference between one air spacer and three air spacers present between composites, separated by frequency and material.

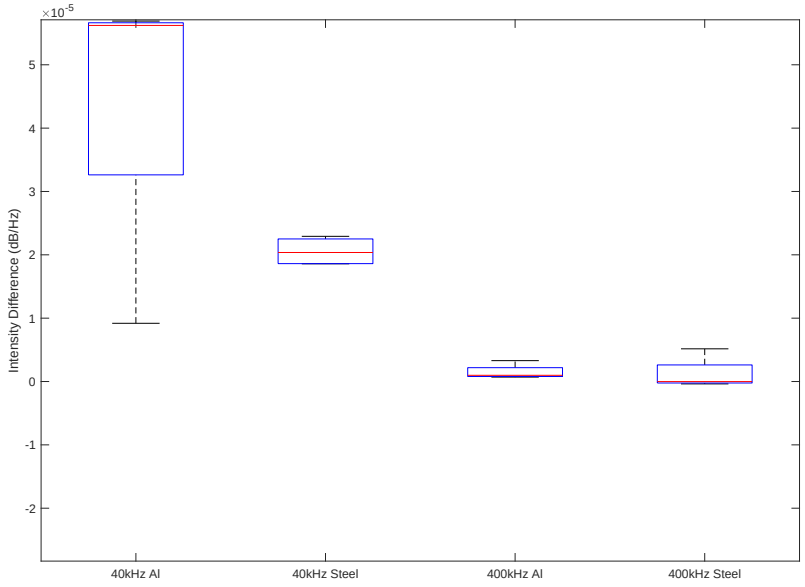

Fig. 4.27: Calculated intensity difference between one air spacer and four air spacers present between composites, separated by frequency and material.

Here, whilst the 40 kHz signal through steel shows consistently positive results, the range of values at 400 kHz in both materials are smaller than 40 kHz. This suggests that using a 400 kHz frequency would provide more consistent results if used in the field, which is in agreement with the literature that suggests that lower frequency signals offer inconsistent measurements [37]. This may be a result of the lower number of very high frequency emissions that occur in the surrounding environment. Although every effort has been made to ensure that background was removed from each measurement, and reduce noise from external sources by taking a background measurement inside the anechoic chamber, as not all measurements could be taken at identical points in time or within a perfectly isolated environment, the fluctuation in environmental frequency may cause sufficient noise to obscure the 40 kHz frequency. This is clearly seen in Fig. 4.20 for 40kHz Aluminium where calculated differences fall below 0 when the background measurement is removed. This effect has also been seen in a small number of 400kHz measurements such as steel in Fig. 4.20.

4.6 COMSOL Simulations

Here FEA is used to quantitatively validate the experimental results from Sections 4.2, 4.4, and 4.5, and then investigate whether following FEA can be used to guide future experiments.

4.6.1 Ultrasonic Waves through hole sizes: Simulation

To simulate the gap size experimentations discussed in Section 4.2.2, a chamber was virtually constructed 600 mm in length and 100 mm wide as shown in Fig. 4.28a, with a small protrusion in the shape of a right angled trapezium with a lower width of 15 mm and and upper width of 10 mm shown at the lower edge at $r = 0$. A variable geometry occurs between 60 and 70 mm of the total length, which will be used to simulate a gap. The variable geometry was w, which would sweep between 0 and 5 mm in length (Fig. 4.28b shows an example geometry where $w = 5$ mm). The revolution was then performed about the r-axis (in Fig. 4.28) to create a cylindrical shape with a circular gap ranging from 0 to 10 mm in width about the centre (Fig. 4.29 shows the example where a revolution occured about the r-axis where $w = 5$ mm), which follows the same

plate size increments as outlined in Section. 4.2.

As in Section 3.3, whilst air showed qualitative alignment with results, water was used as the material of the chamber due to the low attenuation and therefore improved illustrative result for qualitative comparisons.

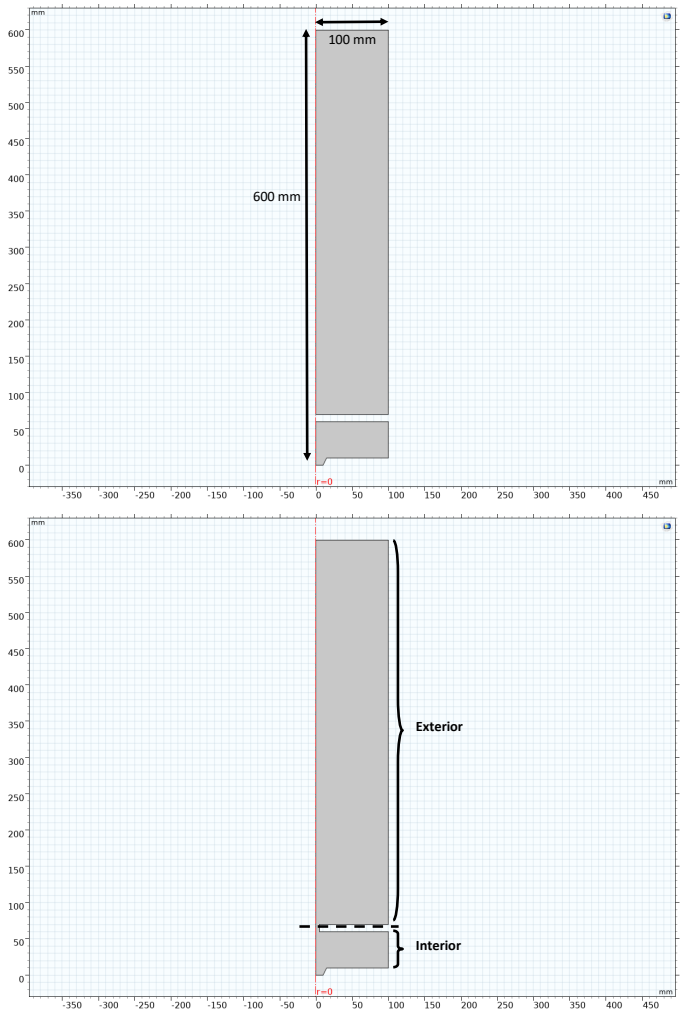

Fig. 4.28: a: Geometry of virtual chamber for a gap size of 0 mm where $w = 0$ mm. Note the separation between the lower chamber between 60 and 70 mm where the ultrasonic signal is emitted and the remainder of the chamber. b: Geometry of virtual chamber for a hole size of 10 mm where $w = 5$ mm. This occurs between 60 and 70 mm. Here the exterior and interior of the hatch space are shown, and the dashed line illustrates the hatch cover.

Fig. 4.29: Revolution about r-axis of the bottom geometry of Fig. 4.28, showing circular hole that would simulate experimental setup. Here the exterior and interior of the hatch space are shown, and the dashed line illustrates the hatch cover. Note that the small red section shows a gap within the hatch cover wherethe ingress of water would occur.

Hard Wall Boundaries are defined along the edges of the trapezium and plate to entirely absorb incident sound waves, which will remove any reflecting waves and prevent standing waves being formed (Fig. 4.30). The initial pressure of the component was set to 0 Pa and a decreasing normal acceleration in all directions was emitted from the shortest width of the trapezium (Fig. 4.31). The mesh chosen was the preset "Extremely Fine"; the smallest preset element size within the software package. Meshing in COMSOL uses a combination of different element types (e.g. tetrahedron or triangular prism) and sizes to effectively mesh the component, and for this reason it is not possible to accurately define the types and sizes of all elements used.

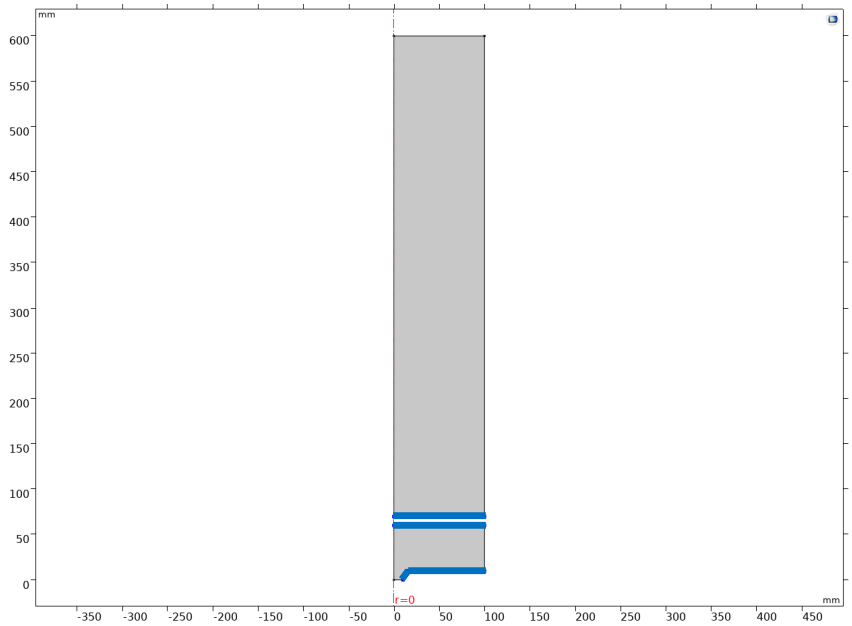

Fig. 4.30: Geometry of hole size 0 mm, highlighting Hard Wall Boundaries in blue.

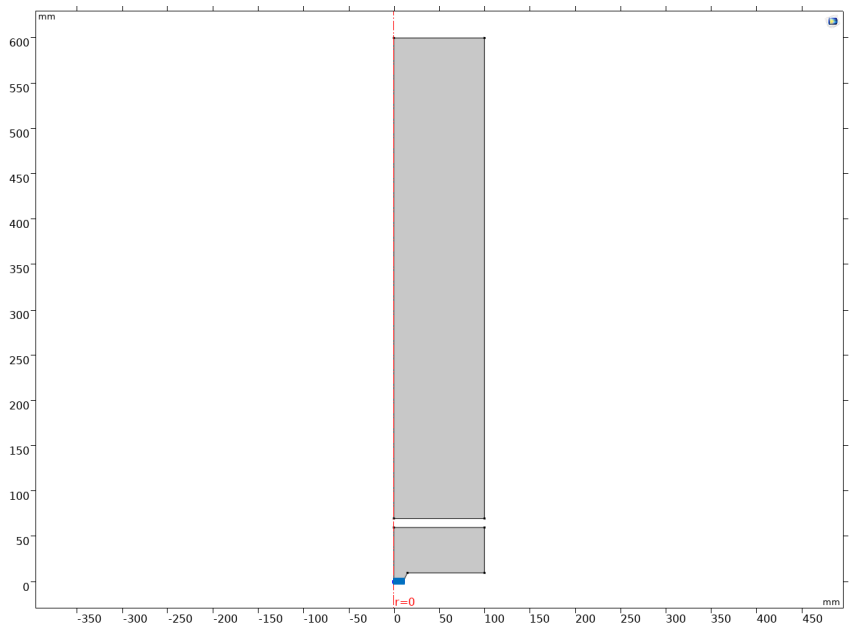

Fig. 4.31: Geometry of hole size 0 mm, highlighting ultrasonic emission boundary in blue. Ultrasonic radiation would be in the positive z-direction.

Computing this in the Frequency Domain outputs a total acoustic pressure field for for all gap sizes (Fig. 4.32 or Fig. 4.33). Each gap size has a natural decay curve plotted in Fig. 4.34, pressure, measured in Pa, is also shown in Fig. 4.35, but it is difficult to distinguish between each waveform.

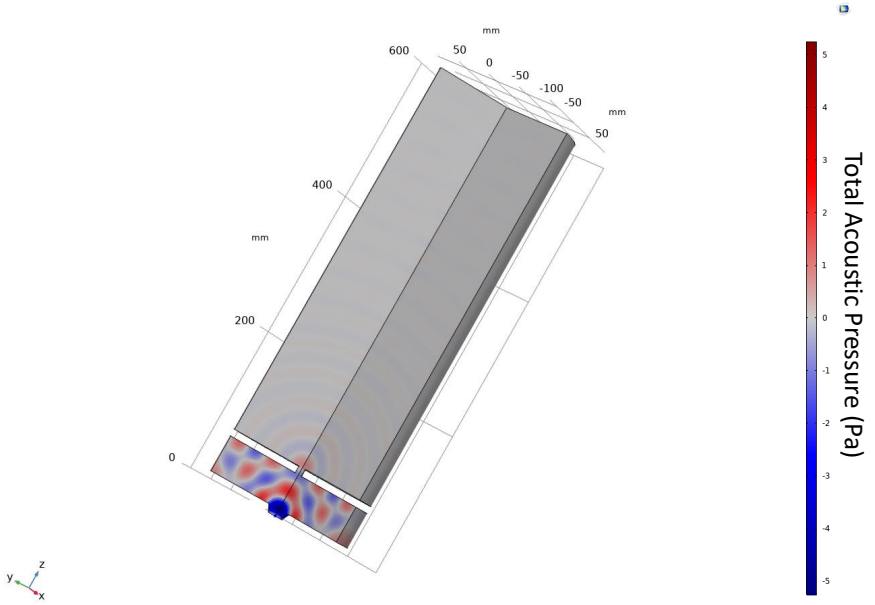

Fig. 4.32: Colour map of total acoustic pressure of 40 kHz signal through a hole of 10 mm.

Fig. 4.33: A QR Code showing animation of Fig. 4.32.

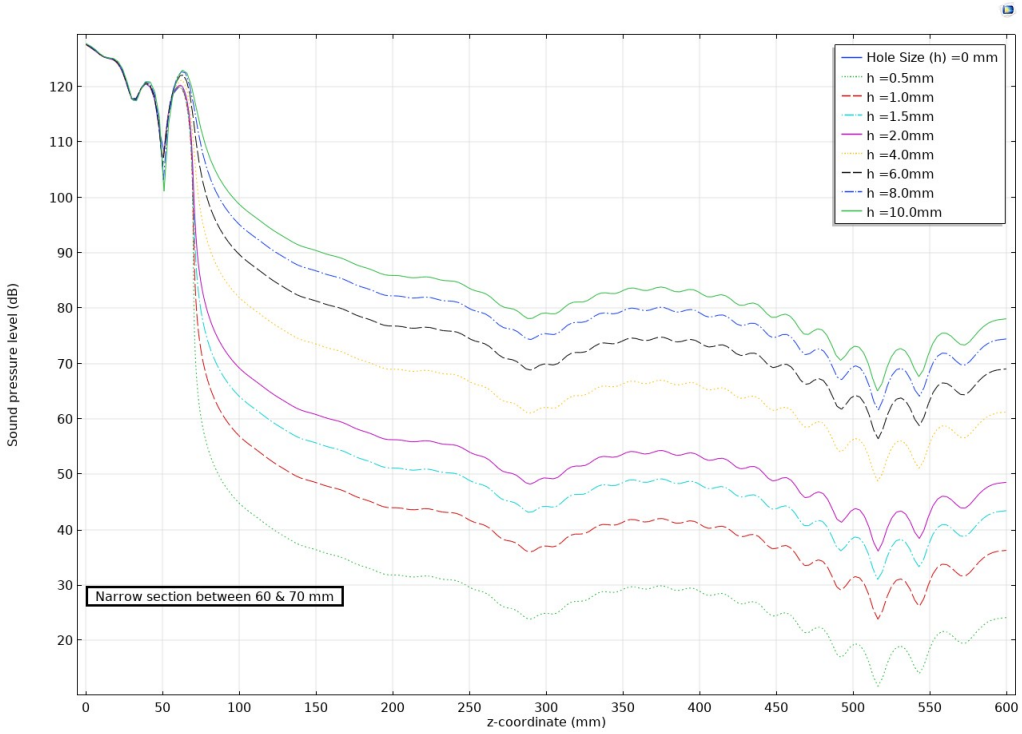

Fig. 4.34: Total acoustic pressure of 40 kHz through gap sizes from 0 to 10 mm in dB.

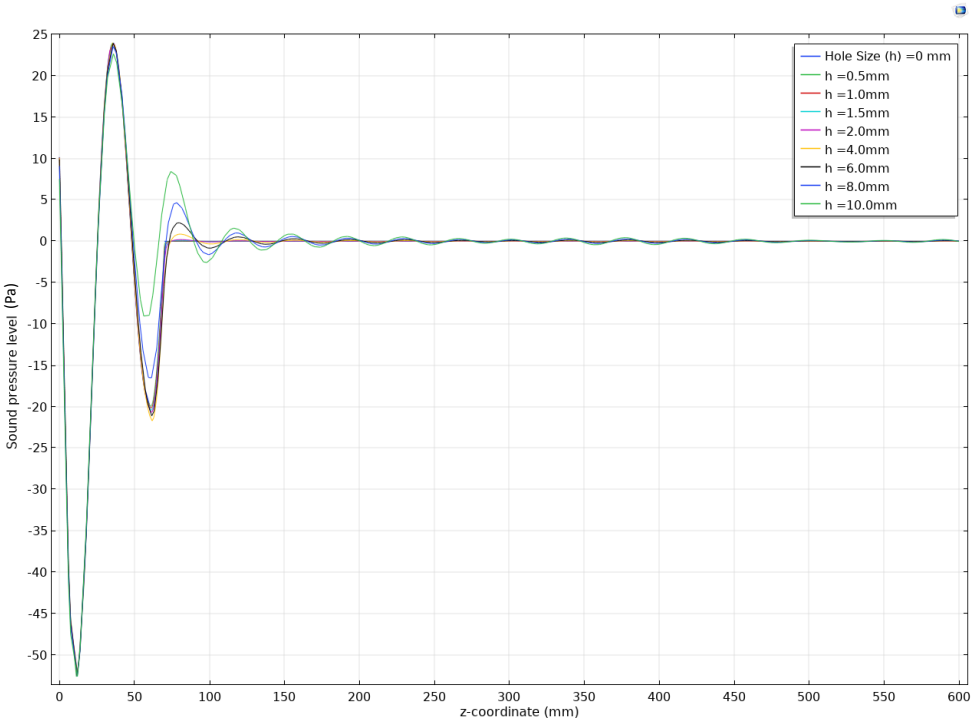

Fig. 4.35: Total acoustic pressure of 40 kHz through gap sizes from 0 to 10 mm in Pa.

As can be seen, as the hole size increases, so does the intensity of the waveform. This aligns with experimental data, however the simulation suggests that increasing distance does not equate to decreasing intensity. It is also noted that the variation between distance and gap size in Fig. 4.6 is not linear, which may also be suggested in Fig. 4.34 as there are various peaks an troughs throughout the plot. This is perhaps due to the additive and subtractive interference that the waveform experiences as it is refracted from the boundaries of the simulated plate.

4.6.2 Ultrasonic Waves through homogenous materials: Simulation

To simulate the ultrasonic waves through materials as discussed in Section. 4.4, a three-dimensional plate was constructed of 900 mm square, with a depth of 50 mm. The explicit geometry of the plate is unimportant, as the intention is to simulate an almost infinite plate size in order to find the extremities of the intensity decay.

A small circle of 10 mm radius was also constructed that would simulate the placement of an ultrasonic emitter (small circle at top of figure in Fig. 4.36). With initial values of 0 Pa and a normal acceleration in all directions as in Section. 4.6.1. Unless otherwise stated, a mesh size of “Extra Fine” was used.

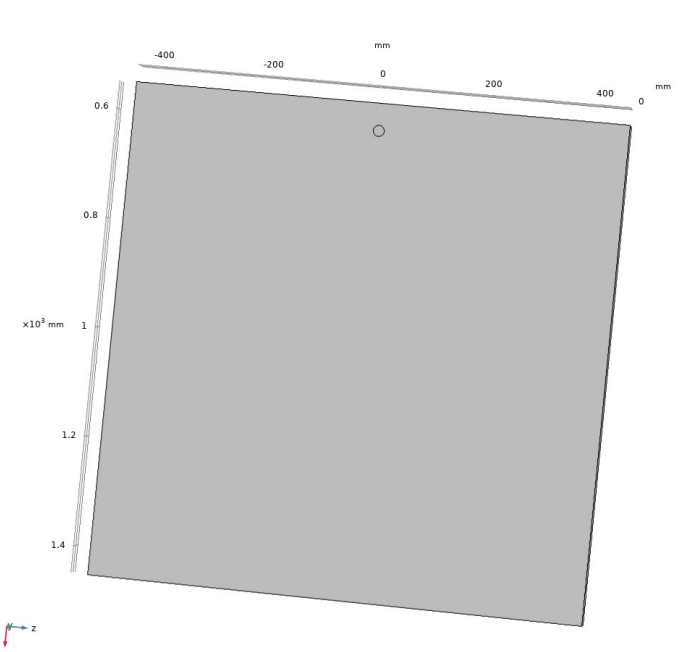

Fig. 4.36: Geometry of virtual chamber. Note small circle of 10 mm at top of plate denoting placement of emitter is of the same material as the remainder of the plate and would not impact the emitted waveform.

A "snapshot" of the pressure was evaluated over a cut line that bisected the ultrasonic emitter placement, offset into the plate by 25 mm. The material used both steel (Steel AlSl4340 from the built-in tree) and aluminium (from the built-in tree) at a frequency of 40 kHz and 400 kHz to align with the experimental process. For aluminium, the speed of sound was set to 6320 m/s [82], and for steel, the speed of sound for steel was taken to be 5920 m/s [83]. The total acoustic pressure (Pa) was evaluted for 40 kHz in steel and aluminium (Fig. 4.37 and 4.38 respectively), and for 400 kHz in steel and aluminium (Fig. 4.39 and 4.41 respectively). From Fig. 4.39, unexpected sharp features are seen, therefore the mesh size was changed to Extremely Fine, the output of which is smoother in Fig. 4.41. This change is likely due to the sharp changes in the waveform that a lower resolution of mesh is unable to distinguish. This smaller mesh side was also used to produce the 400 kHz plot in aluminium (Fig. 4.40).

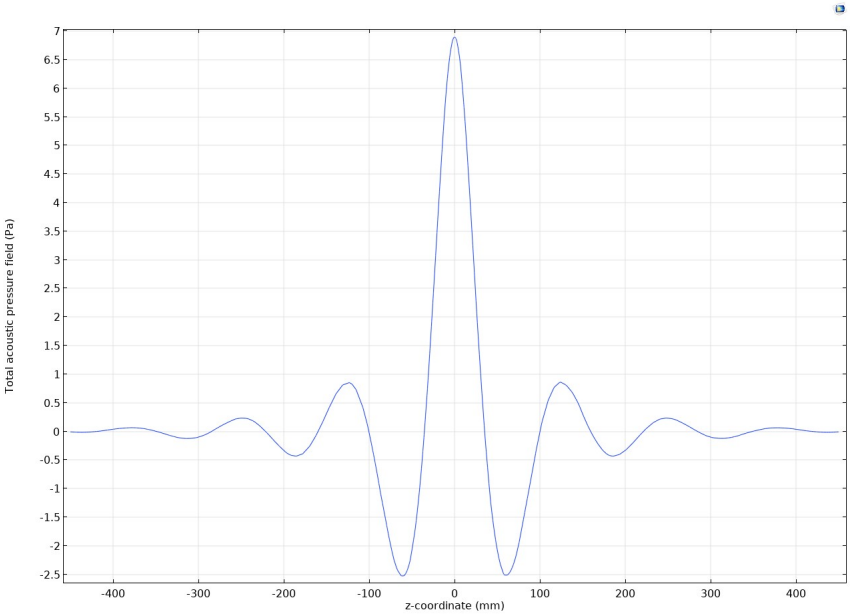

Fig. 4.37: Total acoustic pressure in Pa of 40 kHz within homogenous steel plate. Source is centered around $z = 0$.

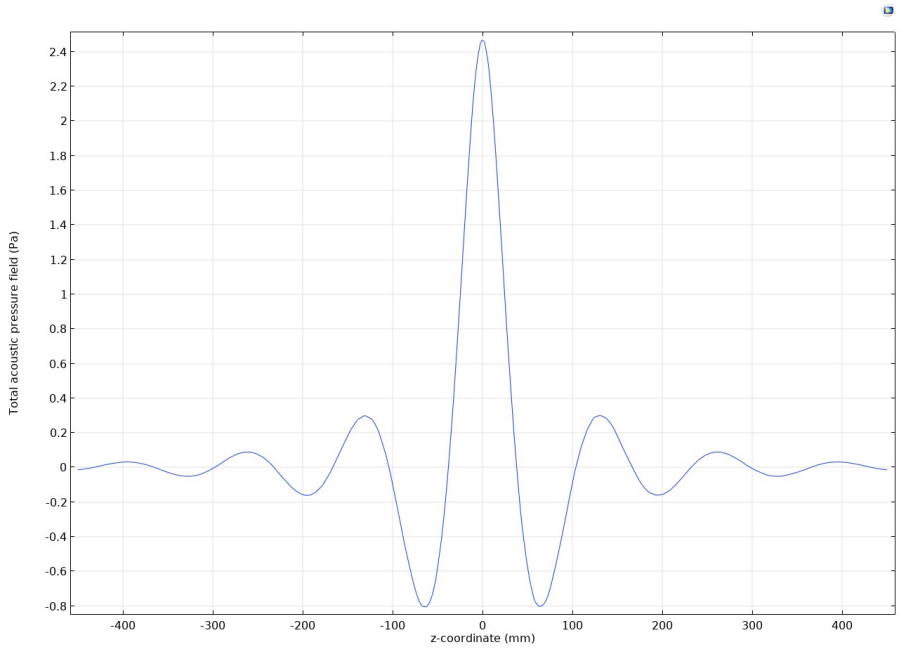

Fig. 4.38: Total acoustic pressure in Pa of 40 kHz within homogenous aluminium plate. Source is centered around $z = 0$.

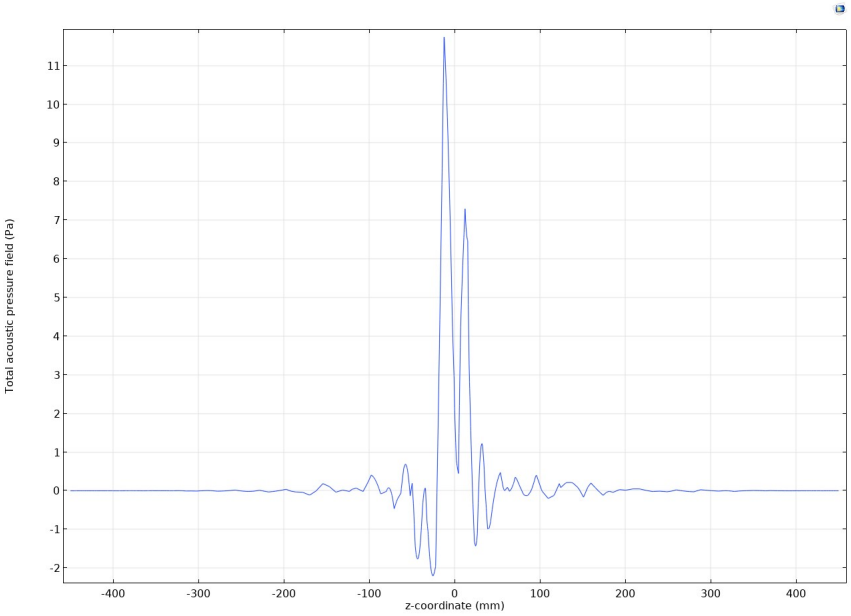

Fig. 4.39: Total acoustic pressure in Pa of 400 kHz within homogenous steel plate. Source is centered around $z = 0$. Note sharper features than in Fig. 4.41.

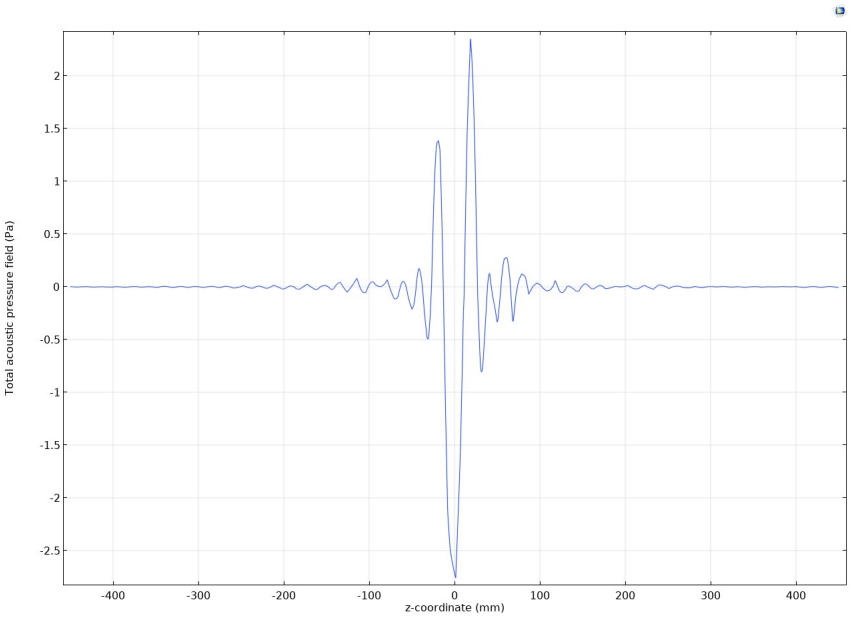

Fig. 4.40: Total acoustic pressure in Pa of 400 kHz within homogenous aluminium plate. Source is centered around $z = 0$.

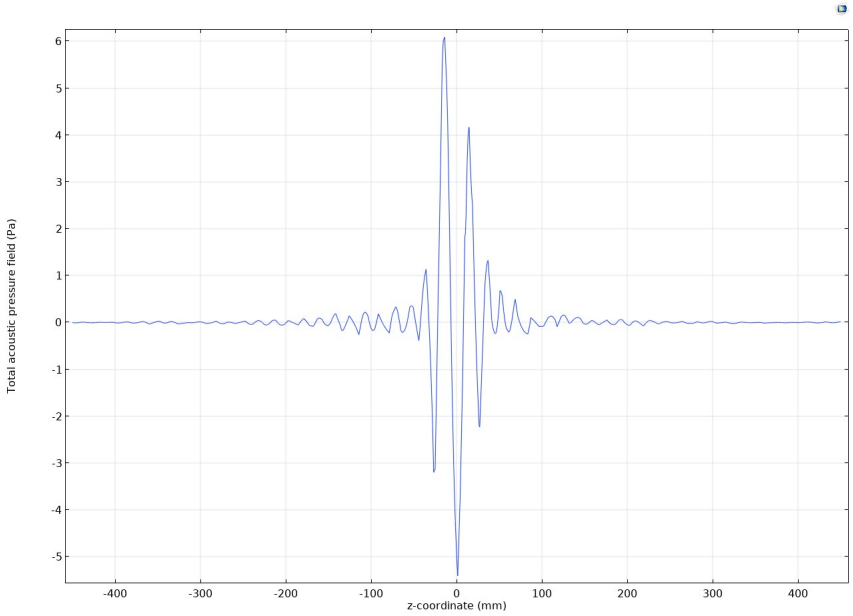

Fig. 4.41: Total acoustic pressure in Pa of 400 kHz within homogenous steel plate. Source is centered around $z = 0$. Note smoother features than in Fig. 4.39.

A difference in peak intensity is also seen between 40 and 400 kHz where 400 kHz has a higher initial intensity (Fig. 4.41 and 4.40) than the 40 kHz signal (Fig. 4.37 and 4.38), however this is not in agreement with experimental results found in Section 4.4.2, which show higher overall intensities from 40 kHz signals. As the simulated environment is an isolated one (where only the plate is modelled), this would not consider the space between the plate and the transducers, or the inhomogeneous composition of the materials, all of which contribute to the attenuation of the signal, which only increases with frequency. This may be responsible for the discrepancy between simulated and experimental results.

It is also noted that in all cases the intensity of the waveform decreases rapidly, falling below half the initial intensity before 100 mm from source. This is not in agreement with the experimental results found in Section 4.4, which found minimal decay up to 400 mm from source. As the boundaries of the simulation are assumed to be purely absorptive rather than reflective, this may have prevented the standing wave shown in Section 4.4. To validate this conclusion, the same simulation of 40 kHz traversing aluminium was used, changing the boundaries of the geometry to a purely reflective surface, the evaluated total

acoustic pressure (Pa) (Fig. 4.42), clearly shows a standing wave, which is in agreement with the conclusions drawn in Section 4.4.

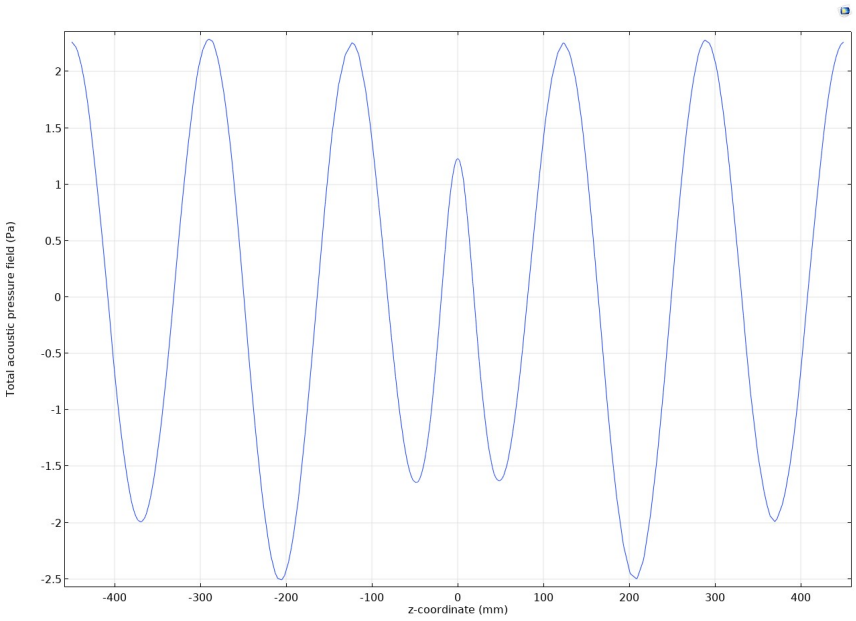

Fig. 4.42: Total acoustic pressure in Pa of 40 kHz within homogenous aluminium plate. Source is centered around $z = 0$. Note standing wave occurs as a result of reflective boundaries.

4.6.3 Rayleigh-Lamb Waves through composites: Simulation

To simulate the ultrasonic waves through Steel-Rubber and Aluminium-Rubber composites as investigated in Section 4.5, a two dimensional geometry was modelled of 100 mm plates of metal and rubber of thicknesses 6.24 mm and 3.24 mm respectively, with two trapezium shapes with lower width of 10 mm and upper width of 15 mm (see Fig. 4.43). These trapezia will be water, to illustrate transducer coupling to plate surface, although in practice this will be the air. As discussed in Section 3.3, water showed excellent illustrative results, and are more appropriate for qualitative comparison.

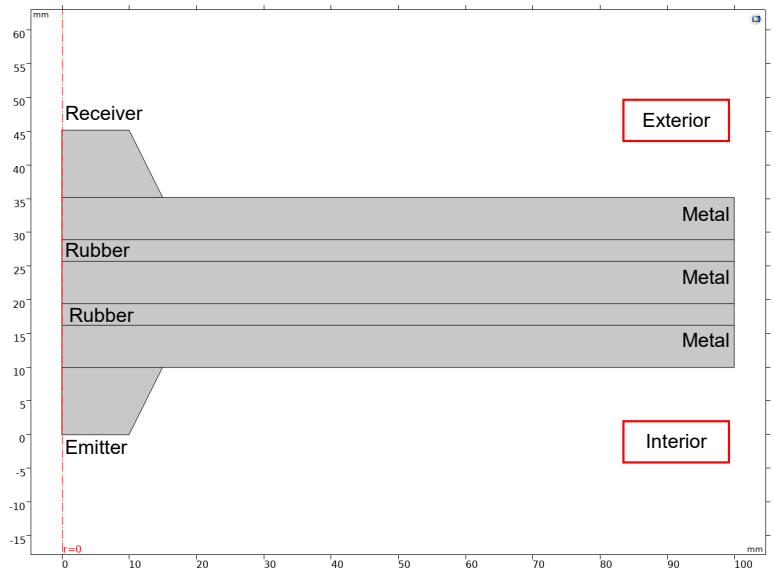

Fig. 4.43: 2D layout of composite material. 3D figure will be rotated about $r = 0$ axis. Note top and bottom trapezium will be water to illustrate transducer coupling to plate surface, and spacers will be placed between rubber and metal plates.

To create a defect, a geometry of 100 mm in length and 7.74 mm in thickness was added in the appropriate position to represent an air spacer (e.g. for a single air spacer present, this geometry may be placed between any metal or rubber plates shown in Fig. 4.43). These specific thicknesses were used as these are the same size as of metal, rubber, and air spacers used in experimentation, however the material chosen is water for illustrative purposes as discussed in Section 3. The initial values of pressure of the component was set to 0 Pa and a decreasing normal acceleration in all directions as in Section 4.6.1 was transmitted from the shortest width of one trapezium (lower edge of Fig.4.43). The mesh chosen was “Extremely Fine”.

In the COMSOL built-in tree, no options were available for rubber, therefore the relevant properties of rubber taken from online resources were set to the following;

- Density (ρ) = 2.3·10^{-6} [82],
- Speed of Sound (v) = 60 m/s [84],
- Poisson's Ratio (υ) = 0.49 [84],
- Young's Modulus (Y) = 5·10^{7} [84].

As from Section 4.6.2, the speed of sound for steel was taken to be 5920 m/s [83]. The waveform was evaluated across r = 0 (see Fig. 4.43) from the shortest edge of each trapezium. Using Aluminium-Rubber composites, the non defected seal (Fig. 4.44) was then compared to a single spacer in all orientations (Figs. 4.45, 4.46, 4.47, and 4.48).

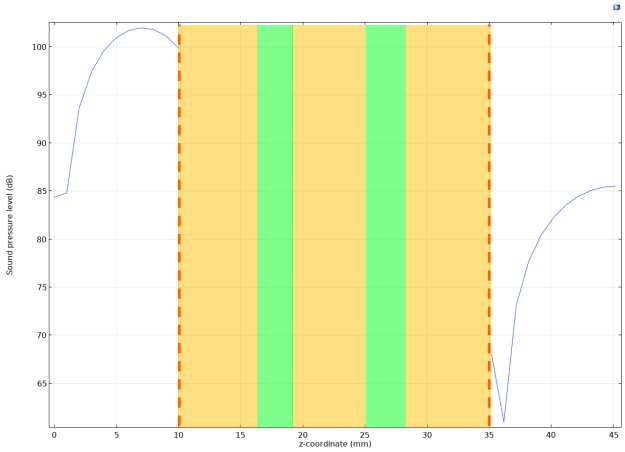

Fig. 4.44: Total acoustic pressure in dB of 40 kHz signal travelling from left to right through Aluminium - Rubber - Aluminium - Rubber - Aluminium composite. Note dashed red line shows where solid plates begin or end, with the orange and green shaded regions representing the aluminium and rubber respectively.

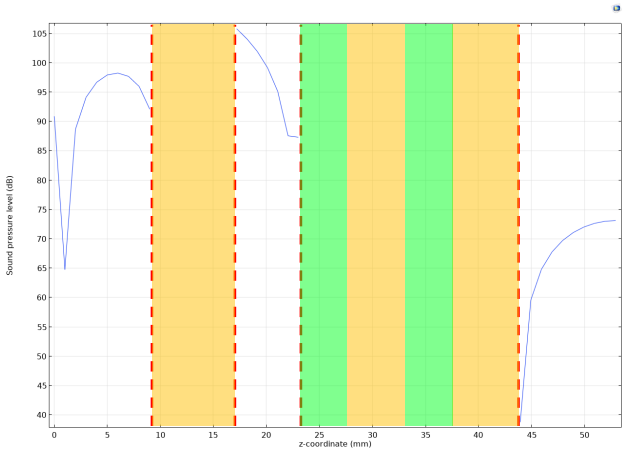

Fig. 4.45: Total acoustic pressure in dB of 40 kHz signal travelling from left to right through Aluminium - Spacer - Rubber - Aluminium - Rubber - Aluminium composite. Note dashed red line shows where solid plates begin or end, with the orange and green shaded regions representing the aluminium and rubber respectively.

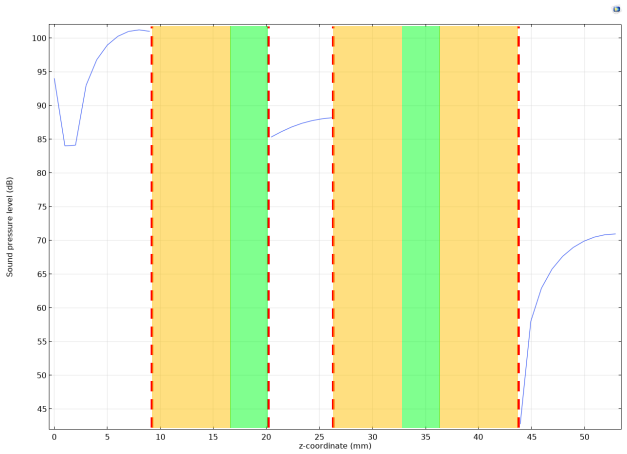

Fig. 4.46: Total acoustic pressure in dB of 40 kHz signal travelling from left to right through Aluminium - Rubber - Spacer - Aluminium - Rubber - Aluminium composite. Note dashed red line shows where solid plates begin or end, with the orange and green shaded regions representing the aluminium and rubber respectively.

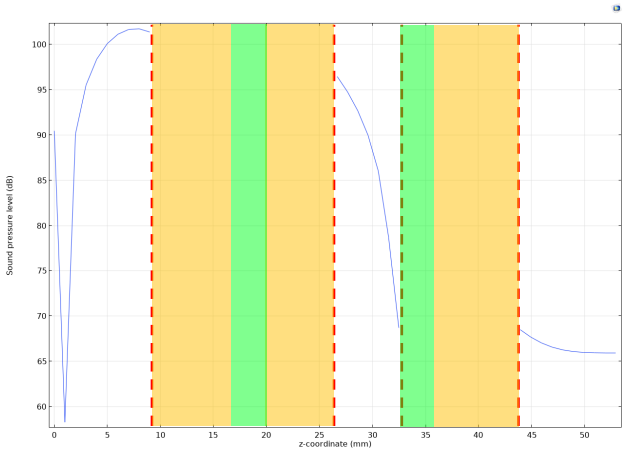

Fig. 4.47: Total acoustic pressure in dB of 40 kHz signal travelling from left to right through Aluminium - Rubber - Aluminium - Spacer - Rubber - Aluminium composite. Note dashed red line shows where solid plates begin or end, with the orange and green shaded regions representing the aluminium and rubber respectively.

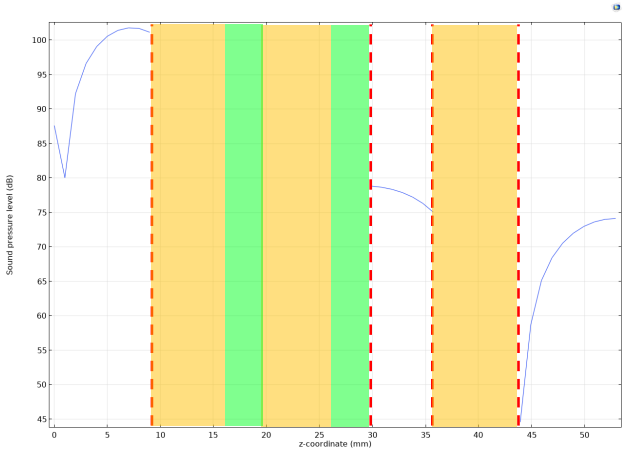

Fig. 4.48: Total acoustic pressure in dB of 40 kHz signal travelling from left to right through Aluminium - Rubber - Aluminium - Rubber - Spacer - Aluminium composite. Note dashed red line shows where solid plates begin or end, with the orange and green shaded regions representing the aluminium and rubber respectively.

Firstly, it is noted that the acoustic waveform is not shown during transit through the material, but shown through pockets of water in modelled spac-

ers, as well as prior to (left) and after (right) transmission through material. Although various methods were employed in an attempt to model both within the materials and the surrounding water at the same time, this was not possible using the COMSOL software. Comparing the non-defected and defected composite, an intensity reduction is noted of between 10 to 20 dB. There are also some qualitative similarities noted in the wave shape between each position of air spacer, however the waveform shape changes in Fig. 4.47, suggesting as discussed in Section 4.5, that the not only the number of air spacers, but also their location are variables that considerably change the intensity of the signal as it passes through the composite.

Additional spacers were added from the side closest to the emitter for two spacers (Fig. 4.49), three spacers (Fig. 4.50), and four spacers (Fig. 4.49).

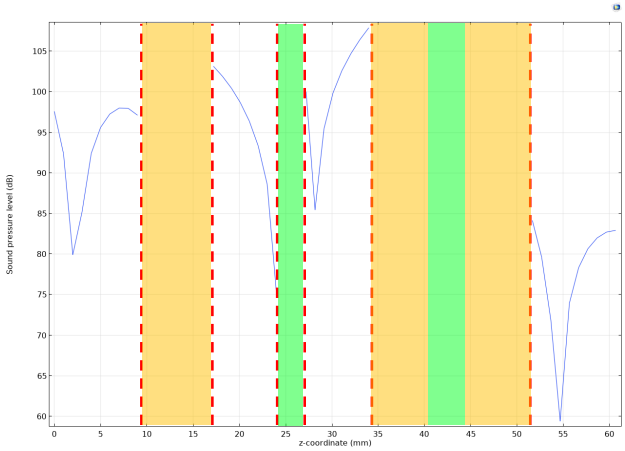

Fig. 4.49: Total acoustic pressure in dB of 40 kHz signal travelling from left to right through Aluminium - Spacer - Rubber - Spacer - Aluminium - Rubber - Aluminium composite. Note dashed red line shows where solid plates begin or end, with the orange and green shaded regions representing the aluminium and rubber respectively.

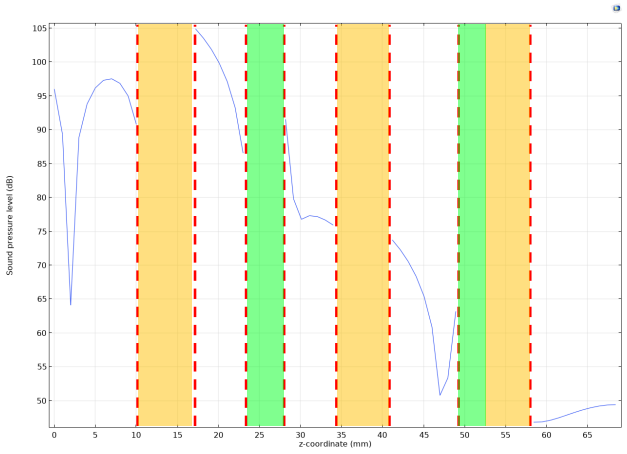

Fig. 4.50: Total acoustic pressure in dB of 40 kHz signal travelling from left to right through Aluminium - Spacer - Rubber - Spacer - Aluminium - Spacer - Rubber - Aluminium composite. Note dashed red line shows where solid plates begin or end, with the orange and green shaded regions representing the aluminium and rubber respectively.

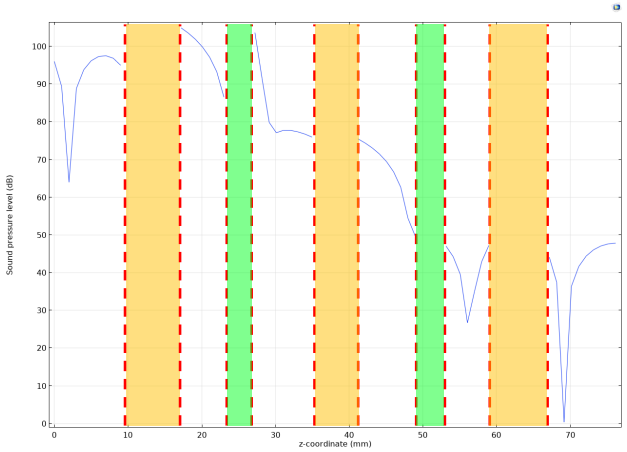

Fig. 4.51: Total acoustic pressure in dB of 40 kHz signal travelling from left to right through Aluminium - Spacer - Rubber - Spacer - Aluminium - Spacer - Rubber - Spacer - Aluminium composite. Note dashed red line shows where solid plates begin or end, with the orange and green shaded regions representing the aluminium and rubber respectively.

Here it is noted that the intensity of the waveform does decrease by up to 35 dB from a non-defected seal, however the decay is not noted to be linear,

but rather sharp sudden reductions in intensity. This is not in agreement with the results of Section 4.5 which showed no deviation from a constant, however as the placement of the spacer appeared to alter the reduction in intensity as shown for a single air spacer (Figs. 4.45, 4.46, 4.47, and 4.48), this effect also appeared to hold for additional spacers.

Comparing the same increase in quantity of air spacers present was repeated for steel comparing a non-defected composite (Fig. 4.52), with one (Fig. 4.53), two (Fig. 4.54), three (Fig. 4.55), and four spacers (Fig. 4.56).

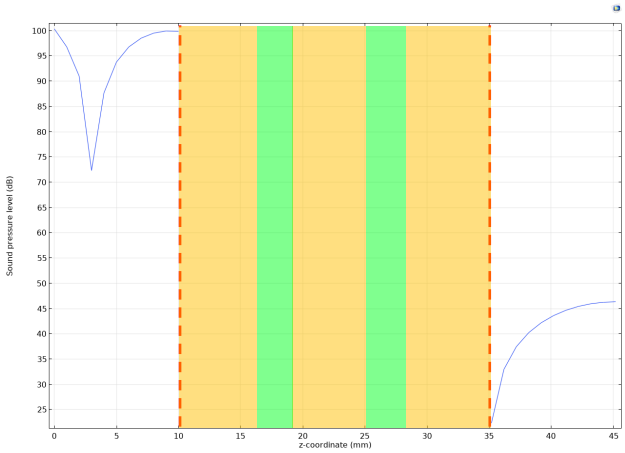

Fig. 4.52: Total acoustic pressure in dB of 40 kHz signal travelling from left to right through Steel - Rubber - Steel - Rubber - Steel composite. Note dashed red line shows where solid plates begin or end, with the orange and green shaded regions representing the steel and rubber respectively.

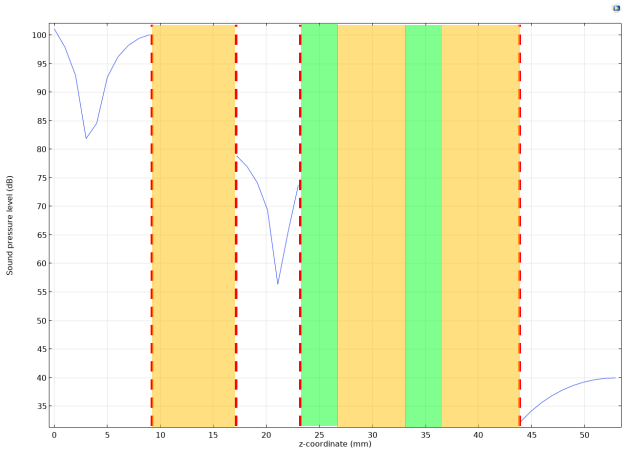

Fig. 4.53: Total acoustic pressure in dB of 40 kHz signal travelling from left to right through Steel - Spacer - Rubber - Steel - Rubber - Steel composite. Note dashed red line shows where solid plates begin or end, with the orange and green shaded regions representing the steel and rubber respectively.

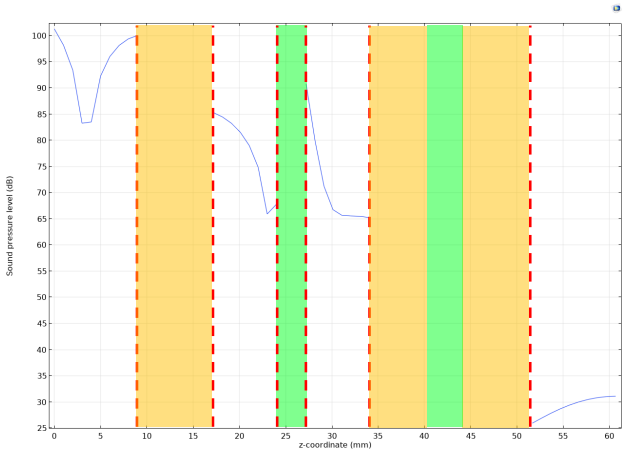

Fig. 4.54: Total acoustic pressure in dB of 40 kHz signal travelling from left to right through Steel - Spacer - Rubber - Spacer - Steel - Rubber - Steel composite. Note dashed red line shows where solid plates begin or end, with the orange and green shaded regions representing the steel and rubber respectively.

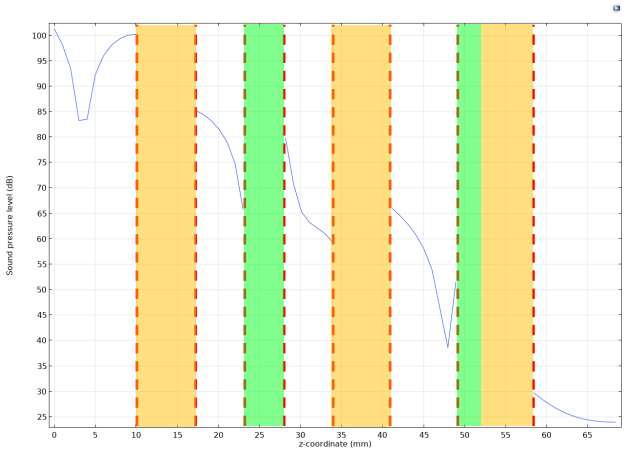

Fig. 4.55: Total acoustic pressure in dB of 40 kHz signal travelling from left to right through Steel - Spacer - Rubber - Spacer - Steel - Spacer - Rubber - Steel composite. Note dashed red line shows where solid plates begin or end, with the orange and green shaded regions representing the steel and rubber respectively.

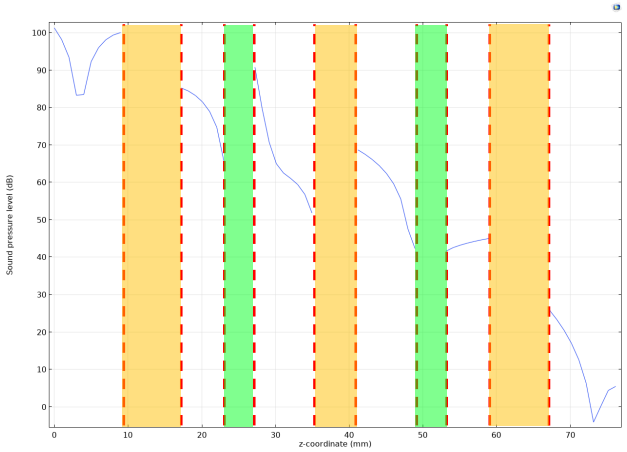

Fig. 4.56: Total acoustic pressure in dB of 40 kHz signal travelling from left to right through Steel - Spacer - Rubber - Spacer - Steel - Spacer - Rubber - Spacer - Steel composite. Note dashed red line shows where solid plates begin or end, with the orange and green shaded regions representing the steel and rubber respectively.

Here it is noted the immediate decay in intensity between aluminium and steel between Fig. 4.44 and 4.52, of 40 dB, which is a direct result of the dif-

ferences between attenuation coefficient, allowing for a greater transmission of signal within aluminium than steel. As found previously, the intensity reduces with an increasing number of air spacers present; however, it is also non-linear.

Calculating the wavelength of the 40 kHz signal, these range between 14 and 15 cm for rubber, steel, and aluminium, which is considerably larger when compared to the wavelength in air of 0.8 cm. Depending on the placement of the air spacer(s), this could cause standing waves nodes in some simulations, but not others, causing non-linear results.

The same Steel - Rubber composite used was repeated for 400 kHz to find qualitative differences betwen intensity reductions. The results are shown below for a non-defected seal (Fig. 4.57), and one (Fig. 4.58), two (Fig. 4.59), three (Fig. 4.60), and four spacers (Fig. 4.61).

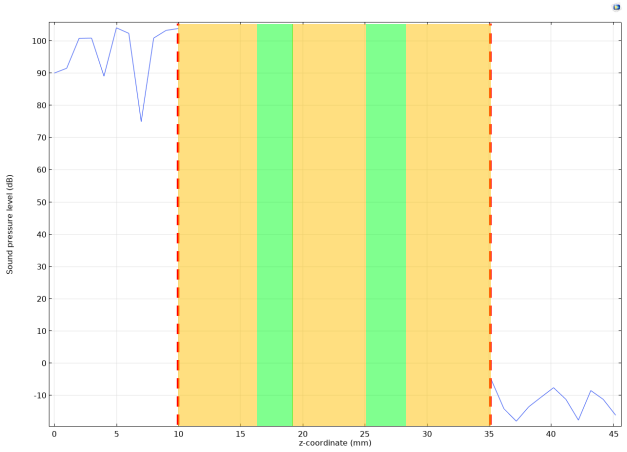

Fig. 4.57: Total acoustic pressure in dB of 400 kHz signal travelling from left to right through Steel - Rubber - Steel - Rubber - Steel composite. Note dashed red line shows where solid plates begin or end, with the orange and green shaded regions representing the steel and rubber respectively.

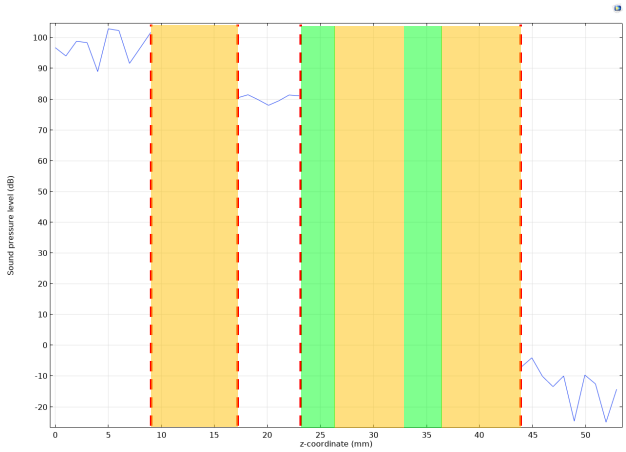

Fig. 4.58: Total acoustic pressure in dB of 400 kHz signal travelling from left to right through Steel - Spacer - Rubber - Steel - Rubber - Steel composite. Note dashed red line shows where solid plates begin or end, with the orange and green shaded regions representing the steel and rubber respectively.

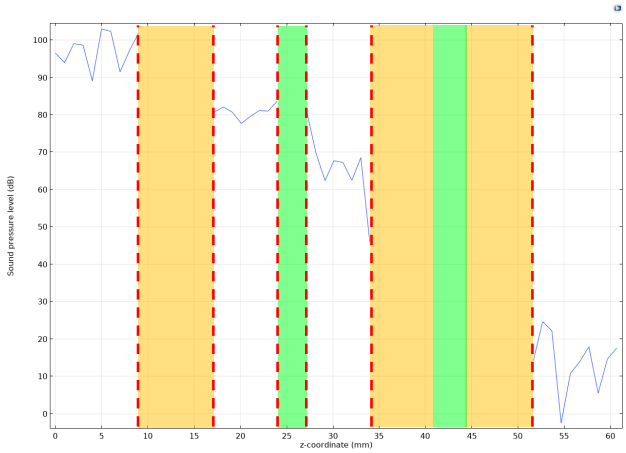

Fig. 4.59: Total acoustic pressure in dB of 400 kHz signal travelling from left to right through Steel - Spacer - Rubber - Spacer - Steel - Rubber - Steel composite. Note dashed red line shows where solid plates begin or end, with the orange and green shaded regions representing the steel and rubber respectively.

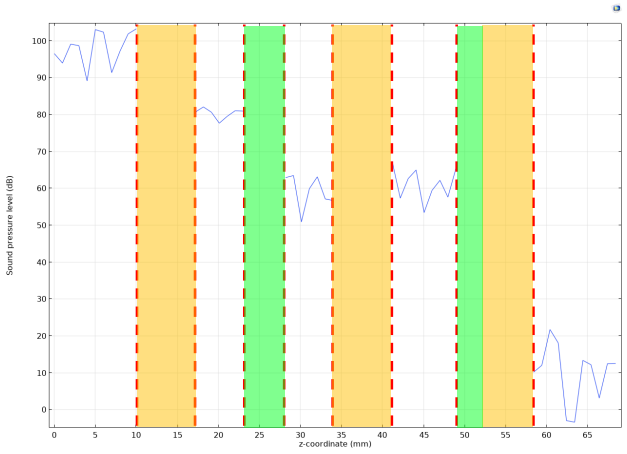

Fig. 4.60: Total acoustic pressure in dB of 400 kHz signal travelling from left to right through Steel - Spacer - Rubber - Spacer - Steel - Spacer - Rubber - Steel composite. Note dashed red line shows where solid plates begin or end, with the orange and green shaded regions representing the steel and rubber respectively.

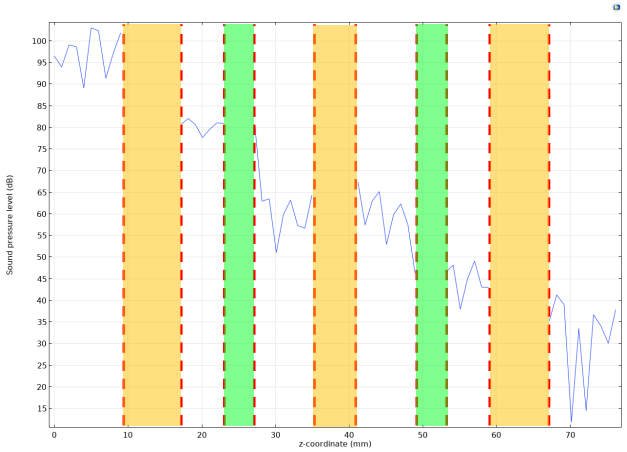

Fig. 4.61: Total acoustic pressure in dB of 400 kHz signal travelling from left to right through Steel - Spacer - Rubber - Spacer - Steel - Spacer - Rubber - Spacer - Steel composite. Note dashed red line shows where solid plates begin or end, with the orange and green shaded regions representing the steel and rubber respectively.

Here, a stready increase is noted in the intensity after the composite with increasing number of air spacers ranging from -5 dB to around 40 dB.

Qualitatively, change was noted between intensity and quantity of air spacers (i.e. a non-linear increase or decrease in final intensity with increasing air spacers), which differs from experiment, where no deviation from constant was seen in the majority of specimens.

As it was noted that thickness of plates and location of air spacers appeared to have an effect on the intensity of ultrasonic signal, a test geometry as in Fig. 4.43 was created, however the properties of the rubber were instead changed to simulate a degradation of rubber instead of inserting air spacers. As in Section 2.1, degraded rubber, whether hardened or softened will change the mechanical properties. Therefore the Young's Modulus was chosen to represent this degradation and increased by 20% to represent a hardening. This degraded rubber replaced the first incident rubber plate only, then the second incident rubber plate only, before replacing both plates of rubber. The results of these simulations are found in Fig. 4.62, 4.63, and 4.64 respectively.

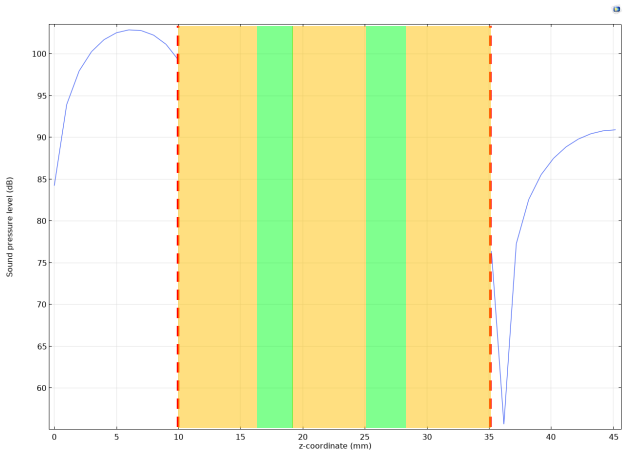

Fig. 4.62: Total acoustic pressure in dB of 40 kHz signal travelling from left to right through Aluminium - Degraded Rubber - Aluminium - Rubber - Aluminium composite. Note dashed red line shows where solid plates begin or end, with the orange and green shaded regions representing the aluminium and rubber respectively.

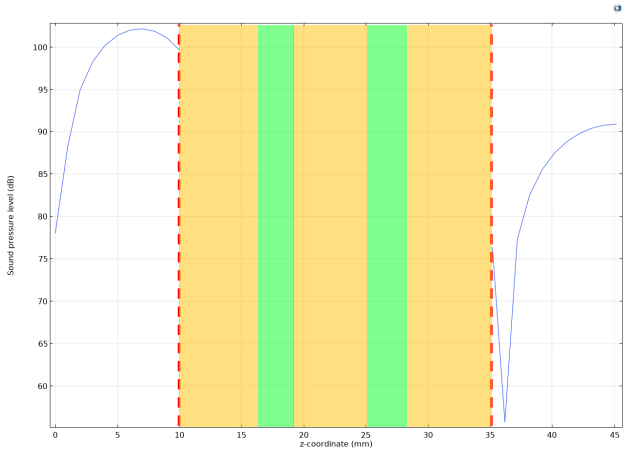

Fig. 4.63: Total acoustic pressure in dB of 40 kHz signal travelling from left to right through Aluminium - Rubber - Aluminium - Degraded Rubber - Aluminium composite. Note dashed red line shows where solid plates begin or end, with the orange and green shaded regions representing the aluminium and rubber respectively.

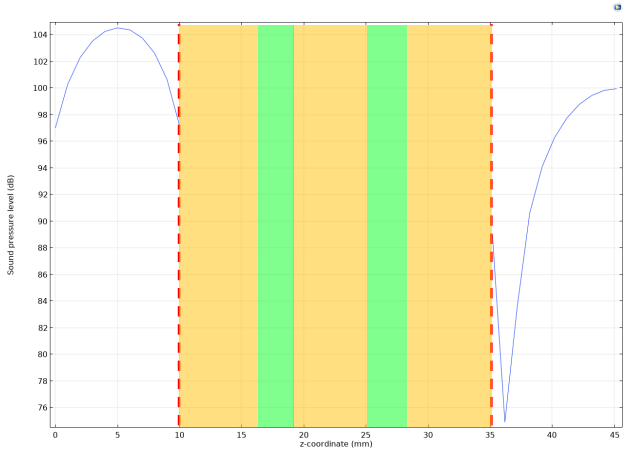

Fig. 4.64: Total acoustic pressure in dB of 40 kHz signal travelling from left to right through Aluminium - Degraded Rubber - Aluminium - Degraded Rubber - Aluminium composite. Note dashed red line shows where solid plates begin or end, with the orange and green shaded regions representing the aluminium and rubber respectively.

Here it can be clearly seen that the placement of degraded rubber does not change the shape or intensity of the waveform, and that an increase in number

of degraded plates of rubber that replace their non-degraded counterparts shows changes in intensity that appear linear (i.e. from an initial reduction to 85 dB, this changes to 90 dB for one plate of degraded rubber and 100 dB for two plates of degraded rubber, which suggests a linear change in sound pressure).

As the conclusions from degraded rubber plates are not in agreement with experimental results seen in composites (Section 4.5) or FEA seen previously in Figs. 4.44 to 4.61, it is believed that including an spacer fundamentally changes the waveform and needs to be investigated further. It is advised that following the results of FEA, it would be appropriate to conduct experiments on degraded pieces of rubber as opposed to placement of air spacers and compare experimental results to these findings. This has been preliminarily investigated in Section 5.

4.7 Summary

Using FEA, it has been possible to qualitatively compare computational simulations to experimental results in order to validate the experimental practice used and guide future experimentations.

In Section 4.6.1, it was shown that simulated results were in agreement with experimental data, and conclusions regarding anomalous intensity spikes which could be a result of refracted waveforms causing constructive or destructive interference. In Section 4.6.2, the simulated analysis which found a rapid intensity decay between 0 and 100 mm was not in agreement with experimental data, which showed consistent intensity up to 400 mm. A purely reflective boundary of the geometry used showed that, similar to the experimental results, standing waves were created within the bar or plate which showed little deviation from a constant value.

Finally in Section 4.6.3, it was shown that location of spacers appeared to have an effect on measured intensity, and that additional spacers appear to have a non-linear impact on the measured intensity. Although this was not in agreement with experimental results, it served to highlight the highly variable impact that the number and location of spacers have on the waveform. This led to a preliminary FEA simulation using degraded rubber plates as opposed to spacers, which showed not only that position of degraded rubber plates did

not significantly change the measured intensity, but also distinct linear rise in intensity occured with increased degraded rubber plates, aligning with the conclusions derived from Section 2.4 that Rayleigh-Lamb waves can be used in defect detection. Preliminary experiments of this were therefore carried out in Section 5.

5. FURTHER EXPERIMENTATION

As a result of simulations in Section 4.6.3 that suggested that the use of degraded rubber plates (in place of non-degraded rubber plates) as opposed to inserted air spacers showed a linear increase in intensity with quantity of non-degraded rubber plates present, a preliminary experiment was carried out to confirm these simulations.

5.1 Method

Using the same vertical plate apparatus, steel plates, and rubber plates used in Section 4.5, a non-adhered steel-rubber composite was constructed:

Steel-Rubber-Steel-Rubber-Steel.

This was placed within the anechoic chamber with the 400 kHz emitter and receiver placed on opposite ends of the composite orientated such that the direction of propogation travels through the centre of the composite.

However, where previously an air spacer was placed into the composite to simulate a defect, separate rubber plates were degraded over time. Conforming to standards [14], two plates of rubber were submerged in sea water and placed within a Binder MK 115 temperature chamber [85] over a period of 72 hours with a temperature cycling between -2^{o}C and 40^{o}C over an 8 hour period (i.e. 9 temperature cycles). These plates (now referred to as "degraded rubber") were then removed and dried by hand.

The degraded rubber plates were then used to replace the non-degraded rubber ("rubber") plates in turn:

Steel-Degraded Rubber-Steel-Rubber-Steel, and

Steel-Rubber-Steel- Degraded Rubber-Steel,

these shall be referred to as the degraded rubber plates in position 1 and 2 respetively.

Both non-degraded rubber plates were then replaced with the degraded rubber:

Steel-Degraded Rubber-Steel-Degraded Rubber-Steel.

A background measurement was also be taken and subtracted from each measurement. To provide statistically significant results, each composite was measured in triplicate.

5.2 Results and Discussion

To quantify the level of decay, as in Section 4.5, a FFT was performed on each measurement and the subsequent frequency spectrum was integrated using the trapezium method. The results of non-degraded and degraded rubber plates only are shown in Table 5.1, and the mix of degraded and non-degraded rubber in positions 1 and 2 (see Section 5.1) are shown in Table 5.2.

Table 5.1: Integrated power spectrum density of 40 kHz ultrasonic signal measured through steel-rubber composite enitrely non-degraded and entirely degraded rubber plates only. Each measurement was performed in triplicate, averaged, and the standard error in the mean calculated.

Non-Degraded Rubber Only		**Degraded Rubber Only**	
Power Spectrum Density (dB/Hz)	**Uncertainty (dB/Hz)**	**Power Spectrum Density (dB/Hz)**	**Uncertainty (dB/Hz)**
$2.1{\cdot}10^{-5}$	$0.1{\cdot}10^{-5}$	$2.0{\cdot}10^{-5}$	$0.04{\cdot}10^{-5}$

Table 5.2: Integrated power spectrum density of 40 kHz ultrasonic signal measured through steel-rubber composite with both degraded rubber and non-degraded rubber present in first and second positions. Each measurement was performed in triplicate, averaged, and the standard error in the mean calculated.

Degraded Rubber, Position 1		**Degraded Rubber, Position 2**	
Power Spectrum Density (dB/Hz)	**Uncertainty (dB/Hz)**	**Power Spectrum Density (dB/Hz)**	**Uncertainty (dB/Hz)**
$1.9{\cdot}10^{-5}$	$0.04{\cdot}10^{-5}$	$1.9{\cdot}10^{-5}$	$0.04{\cdot}10^{-5}$

As can be seen from Table 5.2, the positions of degraded rubber plates does not have a significant impact on the measured intensity of the ultrasonic signal, and is partially distinct from the values of enitrely non-degraded or degraded rubber shown in Table 5.1, within error. This is in strong qualitative agreement with the simulated results found in Section 4.6.3. Discrepancy from simulated results do occur for entirely degraded rubber (i.e. that deviation from enitrely non-degraded rubber is expected from simulation, but does not appear in experimentation), however the cause of this is unclear.

This shows that, as originally hypothesised, non-modal Rayleigh-Lamb waves can be used to detect a defect within layered composites should the focus be on the properties of the rubber as degradation occurs, as opposed to attempting to detect holes within the composite structure. However as the enitrely degraded and non-degraded specimens are in agreement with each other, further study should be undertaken to fully characterise how the degradation life cycle of rubber affects the measured signal.

6. DISCUSSION

The findings of Sections 4, 4.6, and 5 will be discussed below, and recommendations will be made towards improvements upon the current generation of leak detection system developed by Coltraco.

Standard ultrasonic leak detection systems rely on detecting leaking ultrasonic signals through hatch seals. However, not only was it established that ultrasonic signals could escape from a sealed hatch, leading to false positive results in Section 2.1, but as a result of experimental work shown in Section 4.2, the detection of defects within hatch seal and the ability to distinguish between size of defects becomes difficult at relatively short distances of around 50 cm from the source. For this reason, it is recommended that a different methodology is used when using ultrasonic detection where the ultrasonic signal is transmitted through the hatch seal. The transmitted ultrasonic signals were defined as Rayleigh-Lamb waves.

Using Rayleigh-Lamb waves as a defect detection system requires surface coupling to the hatch, which is not currently used in standard ultrasonic detection. Although in Sections 4.4, 4.5, and 5, the surface coupling was made with the material surface, further improvements could be made to the coupling methodology to more accurately define defect size within a hatch seal. Szilard [86] discusses using rubber as a coupling material as this soft material can mold around the variable surface of an object. Whilst there are many practical advantages to the use of rubber, it is limited in the methodology used for testing, for example the Pulse-Echo method in Section 2.5.1. Alternatively, further research could be conducted into the use of other acoustic generation techniques such as an electromagnetic acoustic transducer (EMAT) which would remove the need for a coupling medium [87].

When considering surface coupled ultrasonic emitters and receivers, simulations conducted in Section 4.4 showed that the intensity will reduce by half at

distances of less than 10 cm from the source, implying that should a consistent signal intensity be required, additional emitters and receivers should be placed at intervals of 10 cm or less. This was not in agreement with experimental results in Section 4.6.2, which showed no decay for distances of 35 cm from source. This was shown both experimentally and through simulation to be a result of a standing wave that was formed within the material. Establishing a standing wave is not advisable for defect detection as the consistent intensity would not be able to identify defects present. For this reason, it is recommended that, should a surface coupled permanent system be implemented on board ships, a pulsed signal should be used.

When considering the reduction of noise, in a practical setting such as on-board ship, is it not possible to isolate the hatch from the environment. As seen in Section 4.5, the output of the whole spectrum may show a slight reduction in the measured uncertainty, therefore further work on suitable filtration units that remove noise (such as adaptive filters) rather than isolate frequency bandwidths (such as a high-pass filter) as discussed in Section 2.7 could be investigated and incorporated into the receiving device.

The work conducted in Section 4.5 does not support previous findings that utilise Lamb Waves to evaluate defects [41, 43, 45, 46, 63]. This may be due to the anti-symmetric and symmetric modes of propagation for a Lamb Wave, which vary depending on plate thickness [43]. Although modal Lamb waves were not intentionally propagated, these could still occur naturally. As the experimentation carried out in Section 4.5 varied the number of air spacers, this changed the total thickness of the composite, which affects Eqns. 2.9 and 2.10. As such, the resulting change of thickness would change the Lamb wave mode and therefore change the intensity of the signal, and subsequently the intensity measured. Depending on how the intensity varied between air spacers, this could result in the inability to detect defects effectively.

From the comparative simulations conducted in Section 4.6, strong qualitative agreement was seen between FEA and experimental results. In addition, FEA was then used to simulate a test environment using degraded rubber instead of air spacers, which showed that location of degradation did not change the measured intensity and also showed distinct deviation from enitrely

non-degraded rubber within metal-rubber composites. As a result, preliminary experiments were conducted replacing the non-degraded rubber plates with artificially aged rubber. The results of this (Section 5.2) showed that the location of the degraded plate of rubber did not alter the measured intensity, and was distinct from non-degraded rubber within steel-rubber composites, aligning with simulated results. Although when using entirely degraded rubber within a steel-rubber composite, it was found that the measured intensity did not deviate from the measured values using enitrely non-degraded rubber, this method would still provide applications for the detection of degradation within rubber and, therefore, hatch seals.

If a system is to be installed that measures the intensity of an ultrasonic signal through the hatch seal over time, it is possible to plot the level of degradation of rubber within the seal over time. This could be investigated further, using rubber plates of varying degrees and types of degradation (e.g. more temperature cycles as used in Section 5 or applying stresses to the rubber plates) to see how these affect the measured intensity.

7. CONCLUSION

An investigation into the feasibility of using ultrasonic non-modal Rayleigh-Lamb waveforms to detect defects and holes within hatch seals both through air and using surface coupled transducers was conducted.

Through a review of the literature in Section 2.1, the importance of weather- and water-tightness in hatch covers on board ships was discussed as well as the current tightness tests that are conducted along with their particular advantages or disadvantages. In Section 2.2, the underlying physics of ultrasonic detection were covered, including ultrasonic theory, and how an emitted ultrasonic waveform interacts with the environment and materials. This was followed with a description of how the ultrasonic waveform traverses through a material using Rayleigh and Lamb Waves, in Section 2.4.

The current detection methodologies were then reviewed in Section 2.5, before finally discussing noise and the filters and computations that can be utilised in order to receive a more accurate signal in Section 2.6.

In Section 3, an overview of the current generation of simulation software that can be utilised to both model an environment and qualitatively compare with experimental data to was given and the modelling of a typical environment was described in Section 3.2. An example of this, simulating a simple 2D ultrasonic waveform, was shown in Section 3.3.

The experimental work conducted was described in Section 4. Firstly, an anechoic chamber was constructed in order to isolate the emitted ultrasonic signal from the environment (Section 4.1). The chamber walls were found to reduce reflected sound levels of a 40 kHz signal by 34.3 dB, which is a greater reduction than an open space reduction of 20.2 dB.

In Section 4.2, an investigation into how effectively a varying hole size within a metal plates could be detected using 40 kHz ultrasonic signals that would replicate a non weather- and water-tight seal. It was found that even at small

distances from a hatch seal, using ultrasonic detection becomes unreliable.

The decay of 40 kHz and 400 kHz ultrasonic signals were then measured as they travelled through homogenous aluminium and steel metals in order to recommend a suitable number of emitters and receivers that would be required to maintain a consistent signal intensity (Section 4.4). For 40 cm distances in aluminium and 35 cm for steel, the signal did not decay significantly, therefore suggesting that the distance required between each subsequent receiver and emitter is greater than 40 or 35 cm depending on material used.

An investigation was then conducted into how a 40 kHz and 400 kHz ultrasonic waveform transmitted through aluminium-rubber and steel-rubber non-adhered composites and compared to composites with a varying number of air spacers present (which represent a defect within a seal) in Section 4.5. Although there was no statistically significant evidence to show that it is possible to distinguish between the increasing number of air spacers, it was established that a 400 kHz signal provided more consistent measurements than 40 kHz which agrees with the literature [37] and therefore 400 kHz is recommended for ultrasonic testing of defects.

In Section 4.6, finite element analysis was undertaken and compared to experimental results. In some cases, the analysis showed qualitative agreement with the findings. Where discrepancies occured, these findings were compared and reviewed for possible conclusions. These were then used to guide future experimentation where the degraded plates of rubber as opposed to placement of spacers showed effective defect detection in FEA. Experiments using artifically degraded rubber and a 400 kHz ultrasonic signal were conducted in Section 5, and showed that the location of single degraded rubber plates within steel-rubber composites did not affect the measured intensity, as well as a linear decay from non-degraded rubber composites. This implies that Rayleigh-Lamb waves could be effectively used as an early warning system to indicate the progress of degradation within hatch seals.

Within this project, it has been shown that the current method of ultrasonic leak detection becomes unreliable at short distances of around 50 cm, and is often unable to distinguish between holes present within materials, potentially compromising seafaring vessel cargo, and that more accurate results can be ob-

tained through the increase of signal frequency. It has also been shown that using a surface coupled system is an effective way of measuring defects within hatch seals and, whilst the decay of ultrasonic signals through materials was inconclusive, simulations suggest that the distance between this permanent array of emitter and receiver pairs should be around 10 cm. Whilst anechoic chambers cannot be used in practice, more research should be conducted into the use of filters or different methods of ultrasonic signal generation, which would increase the accuracy of measurements.

REFERENCES

[1] J. Blitz. *Fundamentals of Ultrasonics*. Second. London: Butterworth & Co. Ltd., 1967.

[2] P. J. Highmore. "The depth location of non-bonds in multi-layered media". *Non-Destructive Testing* 7 (1974), pp. 327–330.

[3] W. Wersing and R. Lerch. "Ultrasonic Imaging". In: *Piezoelectricity: Evolution and Future of a Technology*. Berlin, Heidelberg: Springer, 2008, pp. 199–221.

[4] The Standard Club. *A Master's Guide to Hatch Cover Maintenance*. London:Witherby & Co. 2002.

[5] Coltraco Ltd. *About Us*. `http://www.coltraco.com/aboutus/`. Accessed: 16/03/2018.

[6] Coltraco Ltd. *Portascanner^{TM} Watertight*. `http://www.coltraco.com/portascanner-watertight`. Accessed: 16 March 2018.

[7] Coltraco Ltd. *Portascanner^{TM} II User Manual*.

[8] BenFrantzDale. *Dogs on a door of the R/V Knorr*. `https://commons.wikimedia.org/wiki/File:Door_dogs.jpg`. Accessed: 16 August 2019. Aug. 2007.

[9] Pacific Marine & Industrial. *Quick Acting Cleats*. `https://www.pacificmarine.net/marine-deck/hatch-cover-spare-parts/13-00-ship-quick-acting-cleat-hatch.htm`. Accessed: 16 August 2019.

[10] Zhiyou Marine. *Marine Oil-tight Hatch Cover*. `https://www.zhiyoumarine.com/marine-manhole-and-hatch-cover/marine-oil-tight-hatch-cover.html`. Accessed: 16 August 2019.

[11] Polymer Properties Database. *Thermal-Oxidative Degradation of Rubber*. http://polymerdatabase.com/polymer\%20chemistry/Thermal\%20Degradation\%20Elastomers.html. Accessed: 23 August 2019.

[12] The Swedish Club. *P&I Claims Analysis*. https://www.swedishclub.com/media_upload/files/Publications/P\%26I\%20Claims\%20Analysis\%20web.pdf. Accessed: 29 March 2019. 2016.

[13] The Swedish Club. *Risk Focus: Hatch Cover*. https://www.ukpandi.com/fileadmin/uploads/uk-pi/Documents/2017/Loss_Prevention/UK_Risk_Focus_-_Hatch_Covers_WEB.pdf. Accessed: 29 March 2019. 2017.

[14] *BS ISO 23529:2016: General procedures for preparing and condition test pieces for physical test methods*. The British Standards Institution. 2018.

[15] Met Office. *Fact Sheet No. 3 - Water in the atmosphere*. https://www.electronics-notes.com/articles/radio/pll-phase-locked-loop/tutorial-primer-basics.php. Accessed: 28 March 2019. 2011.

[16] Det Norske Veritas. *Standard for Certification - No. 2.9: Service Suppliers Performing Tightness Testing of Hatches With Ultrasonic Equipment on Ships, High Speed and Light Craft and Mobile Offshire Units*. Aug. 2013.

[17] The North of England P & I Association. *Hatch Cover Testing*. http://www.nepia.com/media/869543/Hatch-Cover-Testing-LP-Briefing.PDF. Accessed: 02 May 2019. Sept. 2015.

[18] A. Saw. *Personal Communication*. Apr. 2019.

[19] E. G. Richardson. *Ultrasonic Physics*. London: Cleaver-Hume Press, 1952.

[20] J. Daintith and E. Martin, eds. *Dictionary of Science*. Sixth. New York: Oxford University Press, 2010.

[21] J. van Randeraat and R. E. Setterington, eds. *Piezoelectric ceramics*. London: Mullard Limited, 1974.

[22] R. B. Lindsay and R. T. Beyer. "A Physicist's Desk Reference: The Second Edition of Pysics Vade Mecum". In: ed. by H. L. Anderson. Second. New York: American Institute of Physics, 1989. Chap. Acoustics, pp. 52–64.

[23] J. Krautkrämer and H. Krautkrämer. *Ultrasonic Testing of Materials*. Germany: Springer-Verlag, 1990.

[24] A. B. Pippard. "Theory of Ultrasonic Attenuation in Metals and Magneto-Acoustic Oscillations". *Proceedings of the Royal Society of London. Series A, Mathematical and Physical Sciences* 257.1289 (1960), pp. 165–193.

[25] A. Granato and K. Lücke. "Application of Dislocation Theory to Internal Friction Phenomena at High Frequencies". *Applied Physics* 27.7 (1956), pp. 789–805.

[26] P. Lukáš and M. Klesnil. "Cyclic Stress-Strain Response and Fatigue Life of Metals in Low Amplitude Region". *Materials Science and Engineering* 11 (1973), pp. 345–356.

[27] Copper Development Association Inc. *Fatigue Strength*. `https://www.copper.org/applications/industrial/DesignGuide/performance/fatigue03.html`. Accessed: 06 March 2020.

[28] ASM International. *Fatigue*. `https://www.asminternational.org/documents/10192/1849770/05224G_Chapter14.pdf`. Accessed: 06 March 2020.

[29] S. E. Stanzl-Tschegg and H. Mayer. "Fatigue and fatigue crack growth of aluminium alloys at very high numbers of cycles". *Internation Journal of Fatigue* 23 (2001), pp. 231–237.

[30] M. Milad, N. Zreiba, F. Elhalouani, and C. Baradai. "The effect of cold work on structure and properties of AISI 304 stainless steel". *Journal of Materials Processing Technology* 203 (2008), pp. 80–85.

[31] J. Szilard. "Ultrasonic Testing". In: ed. by J. Szilard. New York: John Wiley & Sons Inc., 1982. Chap. Physical principles of ultrasonic testing, pp. 1–23.

[32] L. Rayleigh. "On Waves Propagated along the Plane Surface of an Elastic Solid". *Proceedings of the London Mathematical Society* s1-17.1 (1885), pp. 4–11.

[33] V. Rajendran. *Engineering Physics*. New Delhi: Tata McGraw-Hill Publishing Company Limited, 2009.

[34] I. A. Viktorov. *Rayleigh and Lamb Waves: Physical Theory and Applications*. New York: Plenum Press, 1967.

[35] H. Lamb. "On Waves in an Elastic Plate". *Proceedings of the Royal Society A: Mathematical, Physical and Engineering Sciences* 93.648 (1917), pp. 114–128.

[36] S. Pant, J. Laliberte, M. Martinez, and B. Rocha. "Derivation and experimental validation of Lamb wave equations for an n-layered anisotropic laminate". *Composite Structures* 111 (2014), pp. 566–579.

[37] T. Ghosh, T. Kundu, and P. Karpur. "Efficient use of Lamb modes for detecting defects in large plates". *Ultrasonics 36* (1998), pp. 791–801.

[38] P. Gabriels, R. Snieder, and G. Nolet. "In Situ Measurements of Shear-Waves Celovity in Sediments with Higher-Mode Rayleigh Waves". *Geophysical Prospecting* 35.2 (1987), pp. 187–196.

[39] M. Matsushita, N. Mori, and S. Biwa. "Transmission of Lamb waves across a partially closed crack: Numerical analysis and experiment". *Ultrasonics 92* (2019), pp. 57–67.

[40] T. Stratoudaki, M. Clark, and P. Wilcox. "Full matrix capture and the total focusing imaging algorithm using laser induced ultrasonic phased arrays". *AIP Conference Proceedings* 1806.1 (2017), p. 020022.

[41] H. Kim, K. Jhang, M. Shin, and J. Kim. "A noncontact NDE method using a laser generated focused-Lamb wave with enhanced defect-detection ability and spatial resolution". *NDT&E International 39* (2006), pp. 312–319.

[42] J. J. Ditri, J. L. Rose, and C. Guixiang. "Mode selection criteria for defect detection optimization using Lamb waves". *Review of progress in quantitative nondestructive evaluation* 11B (1991), pp. 2109–2115.

[43] U. Bork and R. E. Challis. "Non-destructive evaluation of the adhesive fillet size in a T-peel joint using ultrasonic Lamb Waves and a linear network for data discrimination". *Meas. Sci. Technol* 6.72 (1995), pp. 72–84.

[44] D. M. Benson, P. Karpur, T. E. Matikas, and T. Kundu. "Experimental Generation of Lamb Wave Dispersion using Fourier Analysis of Leaky Modes". *Review of progress in quantitative nondestructive evaluation* 14 (1995), pp. 187–194.

[45] H. Lu, Z. Wang, and Y. Han. "The Ultrasonic NDT Technique Utilizing the Longitudinal or Transverse Waves Induced by Lamb Wave in Thin Plate". *IEEE Instrumentation and Measurement Technology Conference* (1994), pp. 1195–1197.

[46] D. N. Alleyne and P. Cawley. "The Interaction of Lamb Waves with Defects". *IEEE Transactions on Ultrasonics, Ferroelectrics, and Frequency Control* 39.1 (1992), pp. 381–397.

[47] J. L. Rose. *Ultrasonic Waves in Solid Media*. Cambridge: Cambridge University Press, 2004.

[48] R. Raišutis, R. Kažys, and L. Mažeika. "Application of the ultrasonic pulse-echo technique for quality control ofthe multi-layered plastic materials". *NDT&E International* 41 (2008), pp. 300–311.

[49] Omega. *Differentiating Between Doppler & Transit Time Ultrasonic Flow Meters*. `https://www.omega.com/en-us/resources/dif-between-doppler-transit-time-ultrasonic-flow-meters`. Accessed: 22 August 2019. 2018.

[50] N. Netshidavhini. "Detection of defects in aerostructures using non-contact ultrasonic transducers". *Proc. Mtgs. Acoust.* 19 (2013).

[51] R. Sicard, J. Goyette, and D. Zellouf. "A numerical dispersion compensation techniques for time recompression of Lamb wave signals". *Ultrasonics 40* (2002), pp. 727–732.

[52] D. N. Alleyne and P. Cawley. "The Measurement and Prediction of Lamb Wave Interaction with Defects". *Ultrasonics Symposium* (1991), pp. 855–857.

[53] T. Jenny and B. E. Anderson. "Ultrasonic anechoic chamber qualification: Accounting for atmospheric absorption and transducer directivity". *The Journal of the Acoustical Society of America* 130.2 (2011), EL69–EL75.

[54] L. L. Beranek and H. P. Sleeper Jr. "The Design and Construction of Anechoic Sound Chambers". *The Journal of the Acoustical Society of America* 18.1 (1946), pp. 140–150.

[55] B. Widrow, J. R. Glover, J. M. McCool, J. Kaunitz, C. S. Williams, R. H. Hearn, J. R. Zeidler, E. Dong, and R. C. Goodlin. "Adaptive Noise Cancelling: Principles and Applications". *Proceedings of the IEEE* 63.12 (1975), pp. 1692–1716.

[56] G. Garner III, J. Wilkerson, M. Skeen, D. Patrick, R. Hodges, R. Schimizzi, S. Vora, Z. Feng, K. Gard, and M. Steer. "Acoustic-RF Anechoic Chamber Construction and Evaluation". *IEEE Radio Wireless Symposium Proceedings* (2008), pp. 331–334.

[57] F. Forouharmajd and Z. Mohammadi. "Assessment of normal incidence absorption performance of sound absorbing materials". *Int J Env Health Eng* (2016), pp. 5–10.

[58] K. U. Simmer, J. Bitzer, and C. Marro. "Microphone Arrays: Signal Processing Techniques and Applications". In: ed. by M. Ward D. Brandstein. Germany: Springer-Verlag, 2001. Chap. Post-Filtering Techniques, pp. 39–60.

[59] P. F. Adams, C. F. N. Cowan, E. R. Ferrara Jr., B. Friedlander, P. M. Grant, Treichler J. R., and J. M. Turner. *Adaptive Filters*. Ed. by C. F. N. Cowan and P. M. Grant. Prentice-Hall Signal Processing Series. New Jersey: Prentice-Hall, Inc., 1985.

[60] W. F. Egan. *Phase-Lock Basics*. New Jersey: Wiley-IEEE Press, 2008.

[61] Electronics Notes. *PPL Phase Locked Loop Tutorial & Primer*. `https://www.electronics-notes.com/articles/radio/pll-phase-locked-loop/tutorial-primer-basics.php`. Accessed: 15 February 2019.

[62] A. I. Zverev. *Handbook of Filter Synthesis*. New York: John Wiley and Sons, Inc., 1967.

[63] C. T. Ng and M. Veidt. "A Lamb-wave-based technique for damage detection in composite laminates". *Smart Mater. Struct.* 18.074006 (2009).

[64] K. Schwertz and J. Burge. "Field Guide to Optomechanical Design and Analysis". In: SPIE Press, 2012. Chap. Finite Element Analysis, pp. 90–93.

[65] I. Holland. "Fundamentals of the finite element method". *Computer & Structures* 4 (1974), pp. 3–15.

[66] COMSOL. *Finite Element Mesh Refinement*. `https://uk.comsol.com/multiphysics/mesh-refinement`. Accessed: 20 September 2019. Feb. 2017.

[67] SimWiki. *What is FEA — Finite Element Analysis?* `https://www.simscale.com/docs/content/simwiki/fea/whatisfea.html`.

[68] Andrew Griesmer. *What Is COMSOL Multiphysics*. `http://uk.comsol.com/blogs/what-is-comsol-multiphysics/`. Accessed: 01 March 2019. Mar. 2013.

[69] COMSOL. *Understand, Predict, and Optimize Physics-Based Designs and Processes with COMSOL Multiphysics*. `http://www.comsol.com/comsol-multiphysics`. Accessed: 01 March 2019.

[70] Amelia Halliday. *Creating a Model Geometry in COMSOL Multiphysics*. `http://uk.comsol.com/blogs/creating-a-model-geometry-in-comsol-multiphysics/`. Accessed: 01 March 2019. June 2017.

[71] COMSOL. *Introduction to COMSOL Multiphysics*. `http://cdn.comsol.com/documentation/5.3.0.316/IntroductionToCOMSOLMultiphysics.pdf`. Accessed: 01 March 2019. 2017.

[72] JCW Acoustic Supplies. *Absorption Coefficient Chart*. `https://www.acoustic-supplies.com/absorption-coefficient-chart/`. Accessed: 16 March 2018.

[73] M. Bannon and F. Kaputa. *Decibel drop and noise reduction coefficient for material combinations*. `https://www.thermaxxjackets.com/noise-reduction-coefficients-and-decibel-drop/`. Accessed: 15 August 2019.

[74] Department for Communities and Local Government. *Resistance to the passage of sound: Approved Document E*. https://www.gov.uk/government/publications/resistance-to-sound-approved-document-e. 2015.

[75] C. Wassilieff. "Sound Absorption of Wood-Based Materials". *Applied Acoustic* 48.4 (1996), pp. 339–356.

[76] Woodfit Acoustics. http://www.woodfitacoustics.com. Accessed: 13 March 2018. 2016.

[77] Stil Acoustics. http://www.stil-acoustics.co.uk. Accessed: 13 March 2018. 2017.

[78] I. G. Hughes and T. P. A. Hase. *Measurements and their Uncertainties: A Practical Guide to Modern Error Analysis*. New York: Oxford University Press, 2010.

[79] Pico Technology. *Pico Oscilloscope Range*. https://www.picotech.com/products/oscilloscope. Accessed: 02 September 2019.

[80] MathWorks. *MATLAB*. https://www.mathworks.com/products/matlab.html.

[81] Cargo Care Solutions. *Hatch cover rubber packing*. http://www.cargocaresolutions.com/products/hatch-cover-rubber-packing.aspx. Accessed: 06 December 2018.

[82] NDT Resource Center. *The Speed of Sound in other Materials*. https://www.nde-ed.org/EducationResources/HighSchool/Sound/speedinmaterials.htm. Accessed: 20 August 2019.

[83] Class Instrumentation Ltd. *Class Instrumentation Ltd Ultrasonic Sound Velocity Table*. http://www.classltd.com/sound_velocity_table.html. Accessed: 20 August 2019.

[84] AZo Materials. *Silicone Rubber*. https://www.azom.com/properties.aspx?ArticleID=920. Accessed: 20 August 2019.

[85] BINDER. *Model MK 115*. https://www.binder-world.com/en/products/dynamic-climate-chambers/series-mk/mk-115. Accessed: 20 September 2019.

[86] J. Szilard. “Ultrasonic Testing”. In: ed. by J. Szilard. New York: John Wiley & Sons Inc., 1982. Chap. Techniques using dry coupling or non-contact coupling, pp. 381–409.

[87] R. B. Thompson. “Ultrasonic Measurement Methods”. In: ed. by R. N. Thurston and A. D. Pierce. London: Academic Press Limited, 1990. Chap. Physical Principles of Measurements with EMAT Transducers, pp. 157–199.